AGU ADVANCING EARTH AND SPACE SCIENCES

Reviews of Geophysics®

REVIEW ARTICLE
10.1029/2022RG000800

Minhan Dai and Ya-Wei Luo contributed equally to this work.

Key Points:

- Subtropical gyres display larger spatiotemporal dynamics in biogeochemical properties than previously considered
- An improved two-layer framework is proposed for the study of nutrient-driven and biologically mediated carbon export in the euphotic zone
- Future research will benefit from high-resolution samplings, improved sensitivity of nutrient analyses, and advanced modeling capabilities

Supporting Information:

Supporting Information may be found in the online version of this article.

Correspondence to:

M. Dai and Y.-W. Luo,
mdai@xmu.edu.cn;
ywluo@xmu.edu.cn

Citation:

Dai, M., Luo, Y.-W., Achterberg, E. P., Browning, T. J., Cai, Y., Cao, Z., et al. (2023). Upper ocean biogeochemistry of the oligotrophic North Pacific Subtropical Gyre: From nutrient sources to carbon export. *Reviews of Geophysics*, *61*, e2022RG000800. https://doi.org/10.1029/2022RG000800

Received 24 OCT 2022
Accepted 16 MAY 2023
Corrected 15 JUL 2023

This article was corrected on 15 JUL 2023. See the end of the full text for details.

Author Contributions:

Conceptualization: Minhan Dai (lead), Ya-Wei Luo (equal)
Data curation: Ya-Wei Luo (equal), Matthew J. Church (supporting), Dongjian Ci (supporting), Zhendong Hu (supporting), Zhongping Lee (supporting), Weicheng Luo (lead), Feifei Meng (supporting), Shaoling Shang (supporting), Hiroaki Saito (supporting), Luping Song (supporting), Kuanbo Zhou (supporting)

Upper Ocean Biogeochemistry of the Oligotrophic North Pacific Subtropical Gyre: From Nutrient Sources to Carbon Export

Minhan Dai[1,2], Ya-Wei Luo[1,2], Eric P. Achterberg[3], Thomas J. Browning[3], Yihua Cai[1,2], Zhimian Cao[1,2], Fei Chai[1,2], Bingzhang Chen[4,5], Matthew J. Church[6], Dongjian Ci[1,2], Chuanjun Du[7], Kunshan Gao[1,2], Xianghui Guo[1,2], Zhendong Hu[1,2], Shuh-Ji Kao[1,2], Edward A. Laws[8], Zhongping Lee[1,2], Hongyang Lin[1,2], Qian Liu[9], Xin Liu[1,10], Weicheng Luo[1,2], Feifei Meng[1,2], Shaoling Shang[1,2], Dalin Shi[1,2], Hiroaki Saito[11], Luping Song[1,2], Xianhui Sean Wan[1,12], Yuntao Wang[13], Wei-Lei Wang[1,2], Zuozhu Wen[1], Peng Xiu[14,15], Jing Zhang[9,16], Ruifeng Zhang[17], and Kuanbo Zhou[1,2]

[1]State Key Laboratory of Marine Environmental Science, Xiamen University, Xiamen, China, [2]College of Ocean and Earth Sciences, Xiamen University, Xiamen, China, [3]GEOMAR Helmholtz Centre for Ocean Research Kiel, Kiel, Germany, [4]Department of Mathematics and Statistics, University of Strathclyde, Glasgow, UK, [5]Southern Marine Science and Engineering Guangdong Laboratory (Guangzhou), Guangzhou, China, [6]Flathead Lake Biological Station, University of Montana, Polson, MT, USA, [7]State Key Laboratory of Marine Resource Utilization in South China Sea, Hainan University, Haikou, China, [8]Department of Environmental Sciences, College of the Coast and Environment, Louisiana State University, Baton Rouge, LA, USA, [9]Frontiers Science Center for Deep Ocean Multispheres and Earth System, Key Laboratory of Marine Chemistry Theory and Technology, Ministry of Education, Ocean University of China, Qingdao, China, [10]College of Environment and Ecology, Xiamen University, Xiamen, China, [11]Atmosphere and Ocean Research Institute, The University of Tokyo, Chiba, Japan, [12]Department of Geosciences, Princeton University, Princeton, NJ, USA, [13]State Key Laboratory of Satellite Ocean Environment Dynamics, Second Institute of Oceanography, Ministry of Natural Resources, Hangzhou, China, [14]State Key Laboratory of Tropical Oceanography, South China Sea Institute of Oceanology, Chinese Academy of Sciences, Guangzhou, China, [15]Guangdong Key Laboratory of Ocean Remote Sensing, South China Sea Institute of Oceanology, Chinese Academy of Sciences, Guangzhou, China, [16]Faculty of Science, Academic Assembly, University of Toyama, Toyama, Japan, [17]School of Oceanography, Shanghai Jiao Tong University, Shanghai, China

Abstract Subtropical gyres cover 26%–29% of the world's surface ocean and are conventionally regarded as ocean deserts due to their permanent stratification, depleted surface nutrients, and low biological productivity. Despite tremendous advances over the past three decades, particularly through the Hawaii Ocean Time-series and the Bermuda Atlantic Time-series Study, which have revolutionized our understanding of the biogeochemistry in oligotrophic marine ecosystems, the gyres remain understudied. We review current understanding of upper ocean biogeochemistry in the North Pacific Subtropical Gyre, considering other subtropical gyres for comparison. We focus our synthesis on spatial variability, which shows larger than expected dynamic ranges of properties such as nutrient concentrations, rates of N_2 fixation, and biological production. This review provides new insights into how nutrient sources drive community structure and export in upper subtropical gyres. We examine the euphotic zone (EZ) in subtropical gyres as a two-layered vertically structured system: a nutrient-depleted layer above the top of the nutricline in the well-lit upper ocean and a nutrient-replete layer below in the dimly lit waters. These layers vary in nutrient supply and stoichiometries and physical forcing, promoting differences in community structure and food webs, with direct impacts on the magnitude and composition of export production. We evaluate long-term variations in key biogeochemical parameters in both of these EZ layers. Finally, we identify major knowledge gaps and research challenges in these vast and unique systems that offer opportunities for future studies.

Plain Language Summary Vast subtropical oceans feature basin-wide anticyclonic gyres, which restrict vertical supplies of nutrients, resulting in low surface nutrient concentrations and generally low rates of biological production. The subtropical gyres have therefore traditionally been regarded as ocean deserts. Through a comprehensive data re-analysis focusing on the North Pacific Subtropical Gyre, we find larger than expected spatiotemporal variability in biogeochemical properties in subtropical gyres, including the distribution of nutrients, N_2 fixation, and biological production. Such variations are most pronounced through the sunlit water column (euphotic zone [EZ]), including sharp gradients in nutrient concentrations and sources and microbial community structure. Based on analysis and synthesis conducted in this study, we show evidence

Funding acquisition: Minhan Dai (lead)
Investigation: Ya-Wei Luo (equal), Yihua Cai (supporting), Chuanjun Du (supporting), Zhendong Hu (equal), Zhongping Lee (supporting), Weicheng Luo (lead), Zuozhu Wen (supporting), Peng Xiu (equal), Kuanbo Zhou (equal)
Visualization: Ya-Wei Luo (equal), Dongjian Ci (supporting), Zhendong Hu (supporting), Zhongping Lee (supporting), Weicheng Luo (lead), Shaoling Shang (supporting), Luping Song (supporting), Kuanbo Zhou (supporting)
Writing – original draft: Minhan Dai (lead), Ya-Wei Luo (lead), Eric P. Achterberg (lead), Thomas J. Browning (equal), Yihua Cai (equal), Zhimian Cao (equal), Fei Chai (equal), Bingzhang Chen (equal), Matthew J. Church (equal), Dongjian Ci (equal), Chuanjun Du (lead), Kunshan Gao (equal), Xianghui Guo (equal), Zhendong Hu (equal), Shuh-Ji Kao (lead), Edward A. Laws (equal), Zhongping Lee (equal), Hongyang Lin (equal), Qian Liu (equal), Xin Liu (lead), Weicheng Luo (equal), Feifei Meng (equal), Shaoling Shang (lead), Dalin Shi (lead), Hiroaki Saito (lead), Luping Song (equal), Xianhui Sean Wan (lead), Yuntao Wang (equal), Wei-Lei Wang (equal), Zuozhu Wen (equal), Peng Xiu (equal), Jing Zhang (equal), Ruifeng Zhang (equal), Kuanbo Zhou (equal)
Writing – review & editing: Minhan Dai (lead), Ya-Wei Luo (lead), Eric P. Achterberg (equal), Thomas J. Browning (equal), Yihua Cai (equal), Zhimian Cao (lead), Fei Chai (equal), Bingzhang Chen (equal), Matthew J. Church (equal), Dongjian Ci (equal), Chuanjun Du (equal), Kunshan Gao (equal), Xianghui Guo (equal), Zhendong Hu (equal), Shuh-Ji Kao (equal), Edward A. Laws (equal), Zhongping Lee (equal), Hongyang Lin (equal), Qian Liu (equal), Xin Liu (equal), Weicheng Luo (equal), Feifei Meng (equal), Shaoling Shang (equal), Dalin Shi (equal), Hiroaki Saito (equal), Luping Song (equal), Xianhui Sean Wan (equal), Yuntao Wang (equal), Wei-Lei Wang (lead), Zuozhu Wen (equal), Peng Xiu (equal), Jing Zhang (equal), Ruifeng Zhang (equal), Kuanbo Zhou (equal)

for the functioning of a two-layer EZ habitat, with each layer differentiated primarily by inputs of sunlight and nutrients. Our understanding of long-term biogeochemical variability is relatively restricted, owing to a lack of reliable long-term observations at adequate spatial scales. We therefore urge the development and use of higher temporal and spatial resolution sampling strategies, for example, through the use of autonomous sampling platforms, that will allow for a greater understanding of biogeochemical processes and facilitate improvements in numerical modeling capabilities.

1. Introduction

The oceans cover ca. 71% of Earth's surface, including vast subtropical areas featuring basin-wide anticyclonic circulation or ocean gyres. Five major subtropical gyres are currently recognized: the North and South Pacific Subtropical Gyres (NPSG and SPSG, respectively; all the acronyms used in this article are listed in Appendix A), the North and South Atlantic Subtropical Gyres (the NASG and SASG, respectively), and the Indian Ocean Subtropical Gyre (IOSG) (Figure 1). The circulation of the subtropical gyres is a critical component of the thermohaline circulation, also known as the "ocean conveyor belt," which circulates ocean water around the planet and is essential for redistributing freshwater, salt, heat, carbon, oxygen, and nutrients. The subtropical gyres store a considerable amount of heat and carbon and therefore play an essential role in regulating the dynamics and functioning of Earth's system, including climate. They are also the largest continuous ecosystems on Earth; they are habitats for marine organisms that provide critical ecological services (Karl, 1999), sequester anthropogenic carbon dioxide (CO_2) (Iida et al., 2021), and support extended food chains typically with five or six trophic levels (Seki & Polovina, 2001). The biota of the gyres is a highly diverse community populated at the top trophic levels by large, pelagic organisms, such as billfish, tuna, sharks, and toothed marine mammals, with the lowest trophic levels dominated by small plankton. Moreover, several studies have argued that the permanently oligotrophic subtropical gyres are expanding at an accelerating rate in response to anthropogenic global warming (Irwin & Oliver, 2009). Stressors associated with climate change, such as warming, deoxygenation, and ocean acidification, have raised important concerns about the interactive roles of oligotrophic subtropical gyres in Earth's climate system (Kletou & Hall-Spencer, 2012).

One of the most prominent features of the subtropical ocean gyres is their permanent stratification. This is often explained by the subduction of surface waters from different latitudes and the formation of vertically averaged layers of differing densities, including the pycnocline, which acts as a barrier to the mixing of water between the surface and deeper ocean. The Trade Winds in the tropics and the Westerlies at mid-latitudes lead to Ekman convergence of subtropical gyres in the upper ocean, further depressing the pycnocline and hindering the upward movement of nutrients in these areas (Letscher et al., 2016). The permanent pycnocline in subtropical gyres is at a depth of approximately several hundred meters to 1 km (Feucher et al., 2019).

Because of their stratification and remoteness from land and hence great distance from land-derived nutrients, the subtropical gyres maintain extremely low concentrations of nutrients and biomass in the upper water column, making them historically regarded as the biological deserts of the ocean. However, they are home to abundant picoplankton (<2 μm), whose elevated surface-area-to-volume ratios make them uniquely adapted to the efficient acquisition of low concentrations of nutrients. These tiny cells, often too small to be ingested by copepods, are the basis of extended food webs that include microzooplankton (20–200 μm) and mesozooplankton (0.2–20 mm), some of which form large particle aggregates that are consumed by crustaceans and gelatinous zooplankton. The efficiency of energy transfer to higher trophic levels in these oligotrophic systems is therefore characteristically low (Kletou & Hall-Spencer, 2012). The significance of the microbial loop is greater in these oligotrophic systems due to the utilization of dissolved organic matter (DOM) by heterotrophic bacteria (e.g., Azam et al., 1983).

Partly inspired by the recognition that subtropical gyres are globally important ecosystems for the cycling and transformation of carbon, two representative time-series stations, the Hawaii Ocean Times-series (HOT; study site Station ALOHA) and the Bermuda Atlantic Time-series Study (BATS), were initiated in 1988 (Karl & Church, 2014; Karl & Michaels, 1996; Steinberg et al., 2001). These two time-series studies have greatly advanced our understanding of the biogeochemistry and functionality of subtropical gyre ecosystems. One striking observation from these time series is the unexpected temporal variation in the biogeochemical characteristics of these gyres at timescales from hours to decades (Karl, 1999; Karl & Church, 2014; Steinberg et al., 2001). At seasonal timescales, for example, from spring to autumn, surface dissolved inorganic carbon (DIC) is frequently

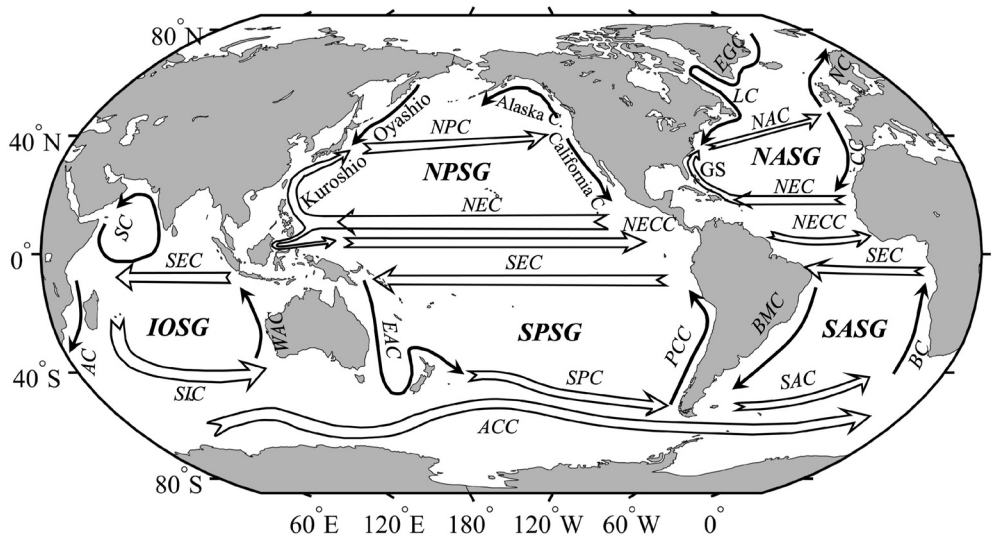

Figure 1. Long-term average patterns of the major global surface ocean currents and identification of the five subtropical gyres. NEC: North Equatorial Current; NPC: North Pacific Current; NECC: North Equatorial Countercurrent; SEC: South Equatorial Current; EAC: East Australian Current; SPC: South Pacific Current; PCC: Peru-Chile Current; GS: Gulf Stream; CC: Canary Current; NAC: North Atlantic Current; EGC: East Greenland Current; LC: Labrador Current; NC: Norwegian Current; BMC: Brazil-Malvinas Current; SAC: South Atlantic Current; BC: Benguela Current; AC: Agulhas Current; SIC: South Indian Current; WAC: West Australian Current; SC: Somali Current; and ACC: Antarctic Circumpolar Current.

drawn down, even when the upper ocean remains nitrate-depleted (Karl et al., 2003, 2012; K. Lee et al., 2002). At decadal timescales, phytoplankton communities in the NPSG appear to have increased biomass and productivity (Karl, Bidigare, & Letelier, 2001; Karl et al., 2021). This contrasts with suggested global trends of declining marine productivity (Boyce et al., 2010; Polovina et al., 2008). Extrapolating from these temporal observations to predict how the subtropical gyre systems will interact with future climate and environmental changes remains a considerable challenge. Undersampling throughout the vast subtropical gyres makes it unclear how representative BATS and Station ALOHA are of the larger subtropical gyres. International programs such as World Ocean Circulation Experiment (WOCE) and GEOTRACES—An International Study of the Marine Biogeochemical Cycles of Trace Elements and Their Isotopes—demonstrate that the spatial variability of nearly all biogeochemical properties in these ocean deserts is much larger than previously recognized (e.g., Ganachaud & Wunsch, 2002; Henderson, 2016). However, the mechanisms underlying these variations have not been well documented or investigated.

Historically, understanding of upper ocean biogeochemistry in these ecosystems hinged on the concept of mass-balance box models (e.g., Dugdale & Goering, 1967; Eppley & Peterson, 1979). Such models treated the sunlit surface waters (i.e., the euphotic zone [EZ]) as a single box where bioavailable "new" nutrients are supplied via deep mixing, riverine and atmospheric inputs, or in the case of nitrogen (N), from dinitrogen (N_2) fixation, to support primary production (hence such part of primary production is also termed "new" production). Following transfer to higher trophic levels, nutrients undergo remineralization, making them available for reuse by phytoplankton, supporting "regenerated" production. Eventually, a portion of the organic matter is exported out of the EZ in both particulate and dissolved phases. These processes constitute a biologically mediated pathway, the so-called biological carbon pump, that transports carbon from the surface to the deep ocean (e.g., Ducklow et al., 2001). Under steady-state conditions, the organic matter that is exported out of the EZ (i.e., export production) is balanced by new production supported by the influx of new nutrients into the EZ (e.g., Eppley & Peterson, 1979).

During the development of the production–export production paradigm, it was recognized that there are two distinct regimes in terms of nutrient and light limitation occurring in the EZ. A theoretical model separated the EZ into two layers: (a) an upper EZ where there was adequate light for photosynthesis but nutrient concentrations were low and limited phytoplankton growth and (b) a lower EZ where light limited phytoplankton production (Dugdale, 1967). Subsequently, Eppley et al. (1973) and Small et al. (1987) viewed the upper euphotic layer as

identical to the surface mixed layer (SML), while the lower euphotic layer was light-limited. Dore et al. (2008) argued that the lower EZ was located at the top of the nutricline, where nutrients were more readily available, but photosynthesis was light-limited. More recently, Du et al. (2017) explicitly divided the EZ into a nutrient-depleted layer (NDL), extending from the surface to the top of the nutricline, and a nutrient-replete layer (NRL), extending across the nutricline to the base of the EZ.

We highlight two important considerations in characterizing the euphotic ocean as a two-layer system. (a) It is important to understand the processes well enough to model them and (b) the upper part of the EZ is more directly impacted by, and possibly more sensitive to, regional climate change. In this two-layer view of the EZ, it was traditionally believed that biological production in the NDL was essentially sustained by regenerated rather than new nutrients, resulting in little export to deeper waters (Goldman, 1984). The origin of nearly all the particulate organic matter (POM) exported from the EZ would therefore be the NRL, while the NDL would be sustained by regenerated nutrients (Coale & Bruland, 1987; Goldman, 1984). However, significant POM export or net community production (NCP) has been observed to be derived from the NDL at BATS and Station ALOHA (Dore et al., 2002; Emerson, 2014; Ferrón et al., 2021; K. S. Johnson et al., 2010; Michaels et al., 1994). It is therefore important to ask where the "new" nutrients come from that fuel export production from the NDL (e.g., Williams & Follows, 2011).

To provide insight into how coupled physicochemical processes modulate carbon and nutrient biogeochemistry under changing climatic and environmental conditions in subtropical gyres, this review assesses our current understanding of both macro- and micro-nutrient cycling and how they sustain new and export production in the subtropical gyres. Special attention is given to the NPSG, but other gyres are also examined to provide context and to serve as references for comparisons. We advocate for an improved two-layered model of upper gyre biogeochemistry centered on *nutrient sources* in the EZ. Additionally, we show how differently sourced nutrients could drive changes in biological production, ecosystem structure, and carbon cycling, particularly *POM export and/or new production*. Finally, we identify major research and knowledge gaps challenging our understanding of these unique, vast ecosystems that provide promising opportunities for future studies.

2. General Characteristics of Subtropical Gyres

2.1. Gyre Physics

An ocean gyre is a large system confined by circular ocean currents driven by a combination of wind stress, Earth's rotation, and landmasses ((i.e., continents, islands). The frictional force of the wind blowing over the ocean's surface causes water to move in the direction of the wind. Earth's rotation redirects these wind-driven currents, causing the currents to be deflected to the right in the Northern Hemisphere and the left in the Southern Hemisphere. The Coriolis force caused by Earth's rotation maintains the stability of gyres.

There are three major types of ocean gyres: subpolar, tropical, and subtropical. Subpolar gyres form at high latitudes near the polar regions of the planet. Tropical gyres are formed between the equator and the North or South Equatorial Current (NEC or SEC).

Subtropical gyres are located between the subpolar and tropical gyres and lie beneath regions of high atmospheric pressure. They occupy a much larger area of the world's ocean than the other two gyres. The circulation of subtropical gyres is anticyclonic (i.e., clockwise in the Northern Hemispheres and counterclockwise in the Southern Hemisphere). All the subtropical gyres are encircled by four linked currents: two roughly meridional boundary currents at their eastern and western margins, and two zonal currents at the northern and southern boundaries of the gyres (Figure 1). For example, the NPSG is confined by the North Pacific Current to the north, the California Current, an Eastern Boundary Current (EBC) to the east, the NEC to the south, and the Kuroshio Current (a Western Boundary Current [WBC]) to the west. Although all gyres are characterized by general circulation patterns as described above, the flow intensity (speed and volume of transport) and the size of individual gyres vary over time at local and regional scales. These variabilities are caused by seasonal changes in the spatial distribution of solar insolation on Earth's surface, which may lead to differences in the temperature of the land and oceans and thus variability in winds.

2.1.1. Subtropical Gyre Circulation Patterns

Although gyres are encircled by linked currents, the Coriolis force increases with latitude, resulting in a westward intensification of gyre currents and hence a westward shift of the center of subtropical gyres, typically narrow and intense poleward WBCs and weaker and much wider equatorward EBCs. WBCs play an important role in global meridional heat transport, carrying warm water from the tropics to higher latitudes and releasing a large proportion of the heat to the atmosphere (e.g., Kwon et al., 2010), while the remainder might be trapped via recirculation in the interior waters of subtropical gyres. The interior equatorward currents across the basin serve as subsurface return flows of water masses and possibly heat. Since this return flow starts from the mid-latitudes, where nutrient concentrations are higher, such a basin-crossing equatorward flow may interact with the upper sunlit ocean and interfere with the vertical connectivity between surface and subsurface waters (Y. Luo et al., 2009; Palter et al., 2005).

The depth of subtropical gyres varies with location and season. Subtropical gyres weaken and shrink with increasing depth, with the gyre centers shifting westward and poleward (Talley et al., 2011). Generally, subtropical gyres extend from the surface to a depth of approximately 1,000 m, but can almost reach the ocean bottom near WBCs and their extensions due to their relatively strong barotropicity (Reid, 1997).

The subtropical gyres are also home to the Subtropical Mode Water (STMW), which develops in the WBC extensions in winter due to substantial buoyancy loss and then subducts equatorward along tilting isopycnals (Qiu & Chen, 2006). The nutrient concentrations are relatively low within the STMW (Palter et al., 2005), which is situated between the seasonal and permanent pycnoclines and, via wind- or eddy-driven vertical transport, could further affect the vertical and horizontal distributions of nutrients in the upper water column of subtropical gyres.

2.1.2. Currents From Gyre Boundaries to Gyre Centers

Although subtropical gyres are generally considered to be bounded by continents at their western and eastern boundaries, not all water parcels travel along the outermost boundaries of the gyres. Instead, a gyre may be more appropriately considered to be composed of numerous, nested sub-gyres with different eastern boundaries because Sverdrup transport spans the vast basin interior up to the eastern, solid boundary. The implication is that there is significant water exchange between the boundaries and centers of a gyre.

In the NPSG, for example, water parcels in the Kuroshio Current separate from the Japanese coast at approximately 35°N and enter the Kuroshio Extension region. During the eastward movement of the water parcels at mid-latitudes, the Coriolis force turns the water to the right more easily than the relatively weak Coriolis force at the low latitudes of the NEC. In addition to the prominent anticyclonic recirculation south of the Kuroshio Extension jet, numerous southward-flowing branches are formed that transport water parcels from the northern boundary of the NPSG into its interior.

Zonal transport also promotes material exchanges between the gyre boundaries and gyre centers. In the NPSG, there is a relatively weak mean eastward current roughly from east of the Luzon Strait to the west of the Hawaiian Islands, that is, the subtropical countercurrent (STCC), several segments of which have been reported (Kobashi & Kubokawa, 2012). Instantaneous snapshots show that the STCC region is full of westward-propagating mesoscale eddies, but the long-term average flow indicates a weak mean current from the western boundary of the NPSG toward its center (Qiu, 1999). Observations and numerical simulations have also demonstrated the existence of multiple zonal jets in the NPSG (e.g., Maximenko et al., 2005), which can presumably enhance the exchange of water between the gyre boundaries and gyre centers.

Hence, although subtropical gyres are maintained by geostrophic currents that form a topographic high with warm, thick water masses converging in their interiors, they are not isolated systems. Understanding how physical processes work together spatiotemporally to control biogeochemical processes in such unique oligotrophic environments will facilitate articulation of the role of the gyres in ocean basins and thus a better understanding of the ocean as a whole from an Earth system perspective.

2.1.3. Range of Subtropical Gyres

The areal extent of subtropical gyres has never been clearly defined. Here, we first use a climatological absolute dynamic topography (ADT, a satellite product used to derive geostrophic ocean currents) of 76 cm to identify the spatial extent of the NPSG, SPSG, and IOSG and 35 cm to define that of the NASG and SASG. These

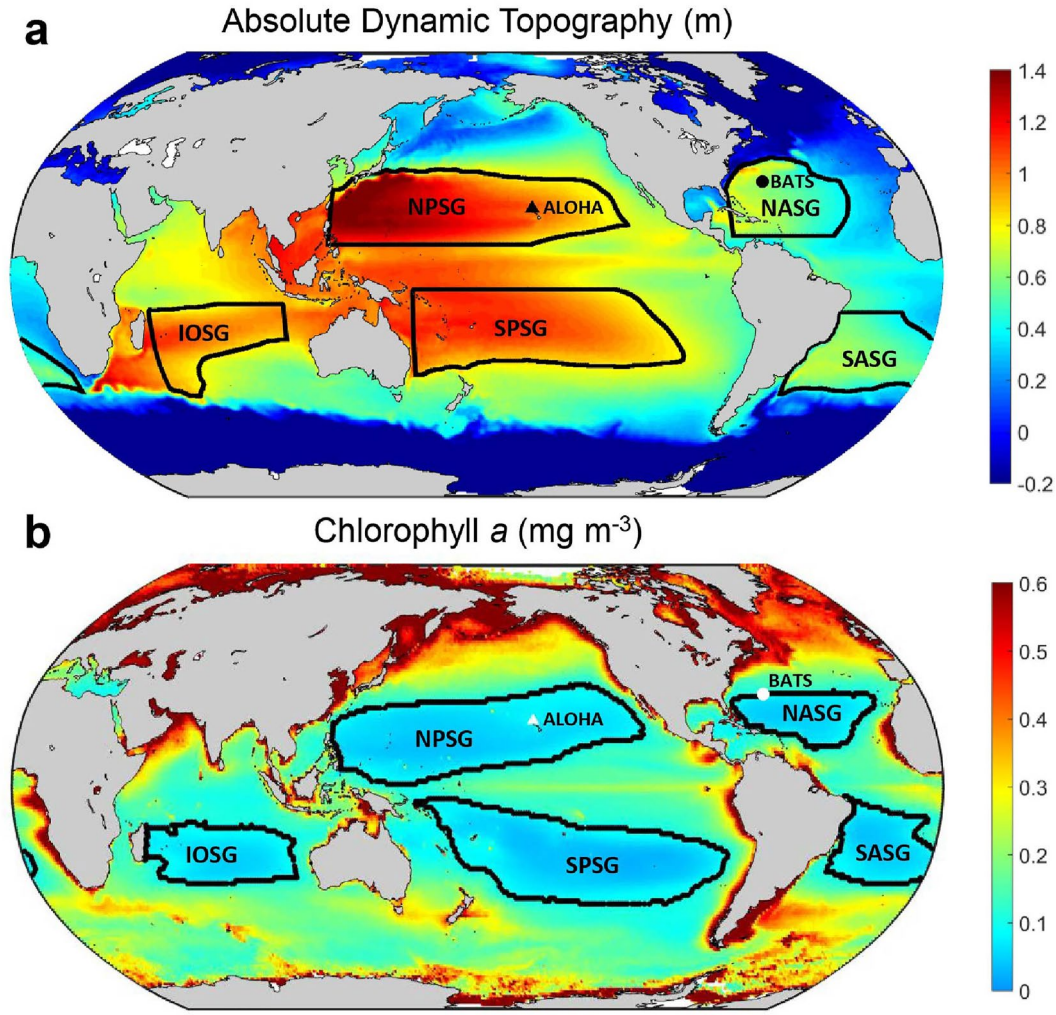

Figure 2. Ranges of the subtropical gyres based on (a) climatological sea surface absolute dynamic topography (ADT) of >0.76 m for the North Pacific Subtropical Gyre, South Pacific Subtropical Gyres, and Indian Ocean Subtropical Gyre, and >0.35 m for the North Atlantic Subtropical Gyres and South Atlantic Subtropical Gyres, and (b) using surface Chl-*a* concentrations of <0.1 mg m^{-3} (black line). ADT is a satellite-based product (https://doi.org/10.24381/cds.4c328c78). Chlorophyll-*a* concentrations are an ensemble product from Ocean-Colour Climate Change Initiative using multiple satellite sensors, including MERIS, SeaWiFS, MODIS-Aqua, and VIIRS from 1997 to 2019 (https://www.oceancolour.org/) (Sathyendranath et al., 2019).

dynamics-based criteria have been used to ensure that the isolines approximately follow the inside edges of the western and northern boundary currents (Figure 2a). We further constrain the Northern Hemisphere gyres (i.e., NPSG and NASG) by requiring that they lie to the north of 10°N to avoid overlapping with the equatorial upwelling zone (Kavanaugh et al., 2018). These criteria imply that the subtropical gyres occupy 28.8% of the global ocean surface (Table 1). The errors associated with the ADT products are generally low, with their root mean squared errors in the open ocean varying between approximately 1.2 in low-variability areas and 5.3 cm in high-variability areas (Pujol et al., 2016, 2022).

We then assess the areal extent of the gyres based on annual averages of surface-ocean chlorophyll-*a* (Chl-*a*) concentrations, which were generated by the Ocean-Colour Climate Change Initiative (OC-CCI) (Sathyendranath et al., 2019). The algorithm employed for the estimation of Chl-*a* concentrations followed the band-difference approach (Hu et al., 2012), an innovative algorithm specifically designed for the remote sensing of Chl-*a* over clear oceanic waters (Chl-*a* concentration <0.25 mg m^{-3}), which achieved an unbiased relative difference of ∼16.5% between ocean color inversion and in situ measurements (Hu et al., 2012). Following the scheme reported in literature (e.g., Dave et al., 2015), the criterion for gyre waters is that Chl-*a* concentrations should

Table 1
Ranges of Subtropical Gyres Based on Different Criteria (See Texts for Details)

	Global ocean	NPSG	SPSG	IOSG	NASG	SASG	Subtropical gyres total
Absolute dynamic topography (ADT)-based							
Area (10^6 km^2)	361.9	29.1	29.7	11.6	12.1	14.3	96.8
Percentage of the global ocean		8.0%	8.2%	3.2%	3.4%	3.9%	28.8%
Chl-a concentrations <0.1 mg m^{-3}							
Area (10^6 km^2)		31.8	30.8	12.2	8.8	10.3	93.9
Percentage of the global ocean		8.8%	8.5%	3.4%	2.4%	2.8%	25.9%
Chl-a concentrations <0.07 mg m^{-3}							
Area (10^6 km^2)		20.2	18.9	5.3	5.5	6.2	56.1
Percentage of the global ocean		5.6%	5.2%	1.5%	1.5%	1.7%	15.5%

not exceed 0.1 mg m^{-3}, with the annual mean state shown in Figure 2b. In contrast to the areal extent estimated based on ADT (Figure 2a), the area based on Chl-*a* concentrations stretched further eastward and poleward on the eastern side of each gyre and closer to the equator on the western side in all ocean basins except the Atlantic Ocean (Figure 2b). The total area of the subtropical gyres based on the Chl-*a* criterion is 25.9% of the global ocean and close to the estimate of 28.8% based on physical dynamics. For comparison, the ultra-oligotrophic area of the subtropical gyres, which is characterized by Chl-*a* concentrations no greater than 0.07 mg m^{-3} (McClain et al., 2004; Polovina et al., 2008), is only 15.5% of the global ocean. The NPSG and SPSG are the two subtropical gyres with the largest areas based on either the dynamic or Chl-*a* criteria (Table 1).

We obtain smaller total surface areas of the subtropical gyres than some previous reports that estimated that the gyres comprised up to 40% of the world's ocean surface (Hoegh-Guldberg et al., 2014). This difference is mainly because the previous results overestimated the surface area of the IOSG by including the northern part of the Indian Ocean, whereas the boundary currents indicate that it should not be included in the IOSG (Figures 1 and 2). Our conservative estimate, supported by the dynamics-based criterion, restricts subtropical gyres to the oligotrophic regimes of the gyres.

Hereafter, we define the range of the subtropical gyres based on an annual average Chl-*a* concentration ≤0.1 mg m^{-3} (Figure 2b) unless otherwise specified to focus our review on biogeochemistry. We did not adopt the other commonly used Chl-*a* threshold of 0.07 mg m^{-3} because the surface area based on this criterion was inconsistently too small compared to the dynamics-based estimation (Table 1). We must note that the spatial range of the subtropical gyres based on the Chl-*a* criterion changes seasonally (see Section 3) and interannually (see Section 6) with light availability and nutrient supplies.

2.2. General Oligotrophic Conditions of the Gyres and Inter-Gyre Comparison

2.2.1. Macronutrients

There are large differences in nutrient concentrations between the waters inside and outside the subtropical gyres. Concentrations of nitrate + nitrite (denoted NO_x hereafter) vary by approximately three orders of magnitude, while phosphate and silicate concentrations are less variable (Figures 3a, 3c, and 3e, Table 2). In contrast, in dimly lit waters (e.g., 200 m), except for phosphate in the NASG and silicate in the NASG and SPSG, nutrients are generally replenished inside the gyres, and their concentrations are similar to those outside the gyres (Figures 3b, 3d, and 3f). In the upper 200 m of subtropical gyres, the average concentrations of NO_x, phosphate, and silicate are approximately 19%, 33%, and 23%, respectively, of their global averages and account for 5.3%, 9.3%, and 6.5%, respectively, of the upper 200 m inventory of the global ocean (Table 2).

The budgets of macronutrients in the oligotrophic ocean have been an area of active research for several decades. Traditionally, diapycnal mixing was considered a major supply of new nutrients from deep waters to the EZ, which was presumed to roughly balance particulate nutrient export (Lewis et al., 1986). Later studies suggested that nutrient budgets are typically unbalanced based on one-dimensional vertical exchange processes (e.g., Jenkins & Doney, 2003; Reynolds et al., 2014; Torres-Valdés et al., 2009; Williams & Follows, 1998). Mesoscale

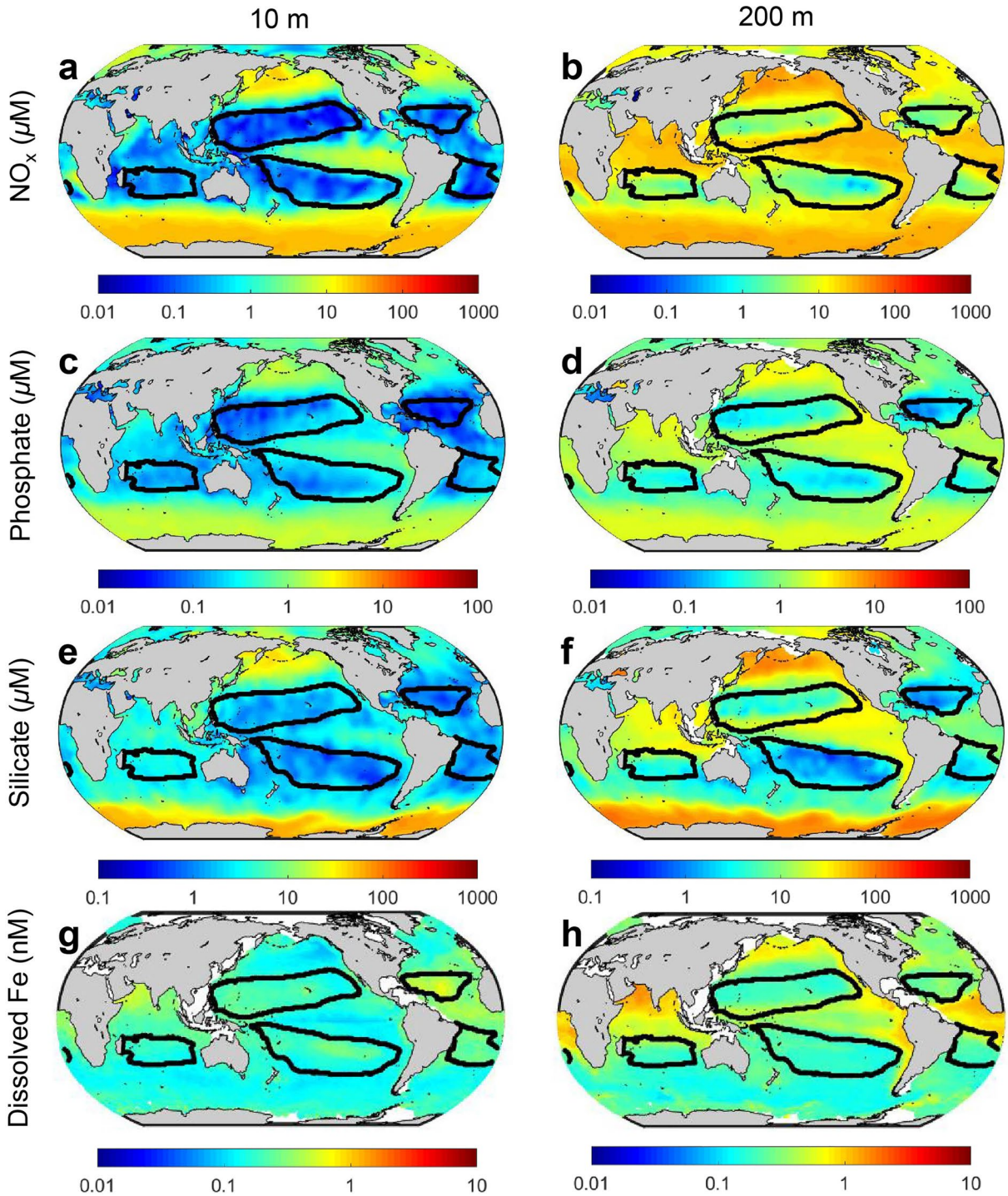

Figure 3. Climatological (a, b) NO_x, (c, d) phosphate, (e, f) silicate, and (g, h) dissolved iron (Fe) concentrations (μM) at 10 and 200 m. NO_x, phosphate, and silicate data are from World Ocean Atlas 2018 (WOA version 2018, https://www.ncei.noaa.gov/products/world-ocean-atlas) (Garcia et al., 2019). Dissolved Fe data are from a machine-learning product based on field measurements (https://zenodo.org/record/6385044#.Yn2AdBPMJhF) (Huang et al., 2022). The solid black lines represent the boundaries of the subtropical gyres using the criterion of Chl-*a* concentration ≤0.1 mg m^{-3}.

eddies also play an important role in nutrient budgets (Doddridge & Marshall, 2018; Martin & Pondaven, 2003; McGillicuddy et al., 1998; Siegel et al., 1999). However, estimating eddy contributions to the nutrient budget in subtropical gyres has proven to be extremely challenging given its dynamic nature (Barone, Church, et al., 2022; McGillicuddy et al., 1998). Additionally, Doddridge and Marshall (2018) described that the effect of mesoscale

Table 2
Total Inventories and Concentrations of Nutrients in Upper Subtropical Gyres

	Total inventory (Tg)		Concentration (μM: NO_x, phosphate, and silicate; nM: Dissolved iron)	
	0–100 m	0–200 m	0–100 m	0–200 m
NO_x (*nitrate + nitrite*)				
NPSG	13.0	192.9	0.30 ± 0.30	2.31 ± 2.22
SPSG	20.6	109.5	0.49 ± 0.81	1.36 ± 1.42
NASG	3.7	24.4	0.31 ± 0.23	1.06 ± 0.92
SASG	5.5	57.7	0.39 ± 0.49	2.13 ± 2.24
IOSG	8.5	61.9	0.51 ± 0.50	1.93 ± 1.62
Subtropical gyres	51.3	446.4	0.40 ± 0.57	1.81 ± 1.86
Global ocean	3,131.9	8,406.8	6.66 ± 9.19	9.41 ± 9.32
Phosphate				
NPSG	15.0	54.5	0.16 ± 0.09	0.30 ± 0.21
SPSG	20.1	49.7	0.22 ± 0.10	0.28 ± 0.13
NASG	1.6	5.0	0.06 ± 0.02	0.10 ± 0.06
SASG	6.0	18.7	0.19 ± 0.05	0.31 ± 0.13
IOSG	6.5	19.4	0.17 ± 0.05	0.27 ± 0.11
Subtropical gyres	49.2	147.4	0.17 ± 0.09	0.27 ± 0.17
Global ocean	651.6	1,584.0	0.63 ± 0.60	0.80 ± 0.62
Silicate				
NPSG	185.7	622.3	2.1 ± 0.8	3.7 ± 2.0
SPSG	112.9	231.6	1.3 ± 0.5	1.4 ± 0.6
NASG	24.0	52.6	1.0 ± 0.3	1.1 ± 0.4
SASG	41.7	106.4	1.5 ± 0.5	2.0 ± 0.8
IOSG	112.9	280.7	3.4 ± 0.8	4.4 ± 1.9
Subtropical gyres	477.3	1,293.5	1.9 ± 1.0	2.6 ± 1.9
Global ocean	7,996.2	19,920.5	8.5 ± 17.1	11.1 ± 19.4
Dissolved iron				
NPSG	0.02	0.04	0.18 ± 0.03	0.18 ± 0.04
SPSG	0.01	0.03	0.17 ± 0.04	0.17 ± 0.03
NASG	0.01	0.02	0.35 ± 0.09	0.31 ± 0.06
SASG	0.01	0.01	0.23 ± 0.04	0.22 ± 0.04
IOSG	0.01	0.01	0.16 ± 0.02	0.17 ± 0.03
Subtropical gyres	0.05	0.11	0.19 ± 0.07	0.19 ± 0.06
Global ocean	0.16	0.39	0.18 ± 0.07	0.21 ± 0.11

Note. The concentrations are shown as the mean ± standard deviation. NO_x (nitrate + nitrite), phosphate, and silicate data are from the World Ocean Atlas 2018 (Garcia et al., 2019), and dissolved iron data are from a machine-learning product based on field measurements (Huang et al., 2022).

eddies could partly offset Eulerian-mean Ekman nutrient pumping. Even after counting the eddy contributions, local diapycnal and isopycnal fluxes of nutrients are insufficient to support new production (McGillicuddy et al., 1998). A larger suite of processes is now recognized in supplying new nutrients to the EZ, including lateral transport, atmospheric deposition, and N_2 fixation (see Section 4) (Gupta et al., 2022; Lipschultz et al., 2002).

Lateral transport by advection and turbulent diffusion has now been recognized as an important source of nutrients (Palter et al., 2013). In the North Atlantic, the cross-frontal exchange of inorganic nutrients at the gyre margins helps replenish surface nutrients lost via sinking and downwelling (Dave et al., 2015; Palter et al., 2005;

Williams & Follows, 2011). A recent study further demonstrated that lateral transport of nutrients substantially replenishes subsurface nutrients along density surfaces on scales of 10–100 km in the NPSG interior (Gupta et al., 2022), resulting in elevated nutrient (particularly NO_x) concentrations in the southern part of the NPSG (Figure 3). In the northwestern NPSG, the lateral transport of dissolved inorganic N and P from continental shelves of the Yellow Sea and East China Sea was equivalent to 10%–20% of the vertical nutrient fluxes from the subsurface layer (Cho et al., 2019). Such lateral water exchanges are also a primary driver of variations in nutrient concentrations along the Kuroshio Current, particularly in the subsurface layers (Guo et al., 2012; Long et al., 2018). A modeling study revealed that lateral inputs exceed the vertical delivery of nutrients and supply by 24%–36% for N and 44%–67% for phosphorus (P) to close the nutrient budgets of subtropical gyres (Letscher et al., 2016). Their findings also indicate that nearly half of the annual lateral supply occurs during the summer-to-autumn period of stratification, which helps explain the enigmatic seasonal patterns of inorganic carbon drawdown and N_2 fixation at ALOHA and BATS. Dissolved organic N (DON) and P (DOP), when produced in the productive margins of subtropical gyres, can also be carried by lateral transport into the gyres. These organic nutrients are directly taken up by photoautotrophs or remineralized to inorganic phases before being consumed (Bronk, 2002; Bronk et al., 2007). This lateral transport of dissolved organic nutrients contributes significantly to nutrient budgets in the NASG, particularly for P (Letscher et al., 2016).

Atmospheric deposition of reactive N to the ocean was as low as 20 Tg N yr^{-1} during preindustrial times but has more than tripled (currently 67 Tg N yr^{-1}) due to anthropogenic emissions (Duce et al., 2008), accounting for 20%–30% of total N inputs to the ocean (B. B. Ward, 2008). In the NPSG, atmospheric deposition of inorganic N (NO_x + NH_4^+) was calculated to be 50–1,000 mg N m^{-2} yr^{-1} in 2000 based on a suite of 26 different global transport-chemistry models (Dentener et al., 2006). When DON was included, the estimate of total reactive N (NO_x + NH_4^+ + DON) deposition to the NPSG was 211–1,400 mg N m^{-2} yr^{-1} in 2000 (Duce et al., 2008). This reactive N deposition is predicted to increase by up to 30% from 2000 to 2030 (Duce et al., 2008). In addition to model simulations, observations of enhanced deposition of reactive N due to anthropogenic emissions from northeastern Asia have been made across the North Pacific (Kim et al., 2014). Limited cruise observations found that the total dry deposition of reactive N to the NPSG ranged from 5 to 1,100 μmol N m^{-2} d^{-1}, mostly on the order of 10–100 μmol N m^{-2} d^{-1}, and was highest in spring (Jung et al., 2011, 2019; L. Luo et al., 2016, 2018; Seok et al., 2021; Shi et al., 2021). Overall, atmospheric N deposition in the western NPSG shows strong seasonal and spatial variability, and some regions are influenced by episodic events. Monsoons and dust storms govern the depositional fluxes of various N species, which are influenced by a variety of anthropogenic activities on land and in the ocean over time.

The atmospheric deposition flux of P is significantly lower than that of N, with the N:P ratio of atmospheric deposition approximately one order of magnitude higher than the Redfield ratio (Qi et al., 2020). The atmospheric deposition flux of phosphate to the surface water of the western Pacific was estimated to be 0.04–0.08 μmol m^{-2} d^{-1} (Martino et al., 2014; Qi et al., 2020).

In addition to the sources discussed above, there are other external sources that could supply nutrients to the EZ. For instance, observations of phytoplankton isotopic anomalies (Fawcett et al., 2011) and studies on phytoplankton sinking and ascent (Wirtz et al., 2022) have shown connections between deep nutrient pools and surface productivity. Migrating diatom mats and other phytoplankton can form an upward transport of N to the EZ equivalent in magnitude to eddy injections of nitrate (Villareal et al., 2014).

Large uncertainties remain in estimating nutrient fluxes in the EZ of oligotrophic gyres (Doddridge & Marshall, 2018). Because of the complexity of the physical dynamics in these regions, some of the fluxes estimated with assumed physical parameters due to the lack of observations could introduce large uncertainties (Du et al., 2017). Spatiotemporal variations in nutrient fluxes are important to consider; for example, recent studies suggest a wide range of diapycnal nitrate fluxes (6.0×10^{-4}–2.0 mmol m^{-2} d^{-1}) in oligotrophic regimes (Du et al., 2017; Fernandez-Castro et al., 2015; Mouriño-Carballido et al., 2011; Painter et al., 2013). High-frequency observations over large spatial areas are needed to reduce the uncertainties of these estimates.

Although many common biogeochemical features exist across the surface waters of the subtropical gyres, there are also important differences among them that depend largely on the physical settings and nutrient supplies. For example, surface phosphate concentrations in subtropical gyres are generally lower in the Northern Hemisphere (NASG, NPSG) than in the Southern Hemisphere (Table 2). However, they can be locally more depleted in the western portions of the Southern Hemisphere subtropical gyres (SASG, SPSG) (Martiny et al., 2019). An

enhanced phosphate supply has been observed from the Eastern Boundary Upwelling Systems (EBUS) to the eastern regions of the NPSG, NASG, and SPSG and is related to the release of phosphate from sediments underlying oxygen minimum zones.

2.2.2. Iron

Dissolved iron (Fe) concentrations have been extensively measured (>30,000 observations) during cruises as part of the international GEOTRACES program (GEOTRACES Intermediate Data Product Group, 2021; Mawji et al., 2015; Tagliabue et al., 2012) and other studies. A machine-learning product based on these measurements (Huang et al., 2022) shows a pattern of dissolved Fe concentrations that is different from that of other macronutrients (Figure 3). Dissolved Fe concentrations are typically elevated in the NASG, where concentrations can be twice as high as the global ocean average, with elevated concentrations also observed in the SASG (Table 2). The dissolved Fe concentrations in the other subtropical gyres are near the global average (Table 2).

To date, various sources of Fe have been shown to contribute to the oceanic Fe budget, including inputs from atmospheric deposition, suspended sediments, continental margins, and hydrothermal vents (Tagliabue et al., 2017). Because subtropical gyres are remote from continents, variations in dissolved Fe concentrations are regulated mainly by background dust fluxes, which vary in magnitude both spatially and temporally (Brown et al., 2005). Fe supply to the surface ocean is highest in the North Atlantic, and because of the atmospheric circulation pattern, the Fe supply is greatest to the southern portion of the NASG (C. M. Moore et al., 2009; Wu et al., 2000). The supply of aerosol Fe to the NPSG is lower in magnitude than in the NASG and predominantly sourced from the Asian continent; it affects the northern portion of the gyre to a greater extent (Buck et al., 2013; Pinedo-González et al., 2020). However, observational data on aerosol Fe deposition are scarce in the NPSG. Recently, Kurisu et al. (2021) found higher deposition of soluble Fe in the northwestern Pacific Ocean (4.3 nmol m^{-2} d^{-1}) than in the central and eastern Pacific (0.2 nmol m^{-2} d^{-1}) and the northern Pacific Oceans (0.4 m^{-2} d^{-1}). These fluxes likely result in surface Fe concentrations of >1 nM in certain locations in the NPSG (Boyle et al., 2005) compared to those of <0.1 nM in the SASG (Noble et al., 2012).

Short-lived dust deposition episodes can result in daily to decadal variability in surface Fe concentrations by more than an order of magnitude. Such variability has been reported at HOT and BATS (Boyle et al., 2005; Fitzsimmons et al., 2015; Sedwick et al., 2005). Because of increasing anthropogenic activities and production of more soluble Fe by combustion processes, we expect the atmospheric deposition of bioavailable Fe to play a more significant role in the NPSG in the future. In the northwestern Pacific Ocean, one-third of soluble Fe deposition is contributed by combustion sources, as revealed by Fe isotope ratios (δ^{56}Fe) of approximately −4‰ (Kurisu et al., 2021). A recent model effort incorporating both seawater and aerosol Fe isotope ratios in the PISCES biogeochemical ocean model successfully disentangled the aerosol Fe sources from dust, fires, and anthropogenic activities, and it examined the impacts of anthropogenic aerosols on the Fe cycles and primary production across the different biogeochemical regimes in the North Pacific Ocean (König et al., 2022). While dust-derived soluble Fe shows the highest deposition during spring and early summer, combustion aerosols contribute more soluble Fe deposition during winter and spring than other seasons, and wildfires cause elevated soluble Fe deposition in spring (König et al., 2022). Nevertheless, more observational and model investigations are needed to precisely decipher the contribution and impacts of anthropogenic aerosol Fe in addition to dust on the biogeochemistry and ecological responses of the North Pacific Ocean under the ongoing variability of anthropogenic activities and climate.

Fe transport from the boundaries to the centers of gyres has also been reported. For example, the Fe-rich water mass associated with the formation of the North Pacific Intermediate Water is transported from the subarctic to the subtropical region (Nishioka, Nakatsuka, et al., 2013). The western boundary current system, including the NEC, Kuroshio Current, and Kuroshio Extension, may serve as an important conveyor by relaying Fe advected from the surrounding islands and marginal shelf sediments to the central and eastern parts of the gyre (Nishioka et al., 2020).

Other sources contributing to the fluxes of Fe into subtropical gyres include resuspension of island sediments and benthic pore water exchanges (e.g., Blain et al., 2008), volcanic inputs (Hawco et al., 2020) and mesoscale ocean circulation (Hawco et al., 2021). In the deep ocean, hydrothermal vents are an external source of Fe below many subtropical gyres (Boyle et al., 2005; Fitzsimmons et al., 2014). Fe supply to subsurface waters of the South Pacific has been reported to be elevated in the west from shallow subsurface hydrothermal activity (Guieu

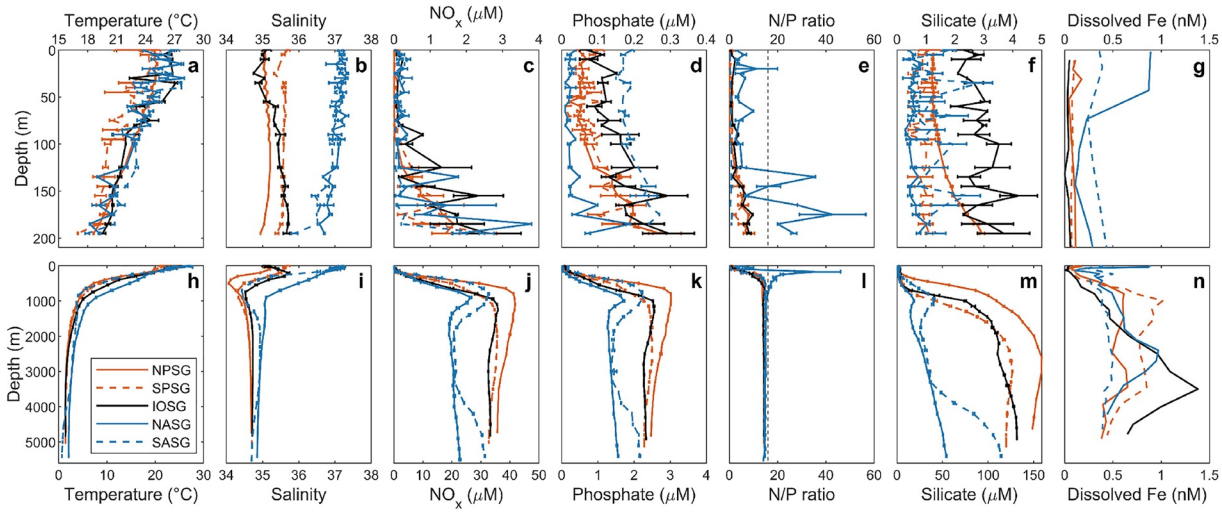

Figure 4. Depth profiles of (a, h) temperature, (b, i) salinity, (c, j) concentrations of NO_x, (d, k) phosphate, (f, m) silicate, and (g, n) dissolved iron (Fe), and (e, l) NO_x-to-phosphate (N/P) ratios in subtropical gyres. Except for dissolved Fe, measurements at Station ALOHA (https://hahana.soest.hawaii.edu/hot/hot-dogs/) are used for the plots of the North Pacific Subtropical Gyre (NPSG); data from Global Ocean Data Analysis Project version 2.2022 (https://www.glodap.info/index.php/merged-and-adjusted-data-product-v2-2022/), which is a merged and adjusted data product (Lauvset et al., 2022), are used for the other subtropical gyres. For dissolved Fe, NPSG and South Pacific Subtropical Gyres refer to Station 8 of the GPc06 cruise and Station GR18 of the GP19 cruise, respectively (GEOTRACES Intermediate Data Product Group, 2021); Indian Ocean Subtropical Gyre refers to Station ER11 in Nishioka, Obata, and Tsumune (2013); North Atlantic Subtropical Gyres refers to Station 14 in T. M. Conway and John (2014), and South Atlantic Subtropical Gyres refers to a station at 24.5°S, 36°W in Bergquist et al. (2007). The lines and error bars represent the mean and one standard error in each subtropical gyre. The dashed lines in panels (e, f) represent the Redfield ratio.

et al., 2018). Nevertheless, the extent to which hydrothermal-derived Fe can be entrained into the EZ and support biological productivity is still largely unknown.

2.2.3. Comparison of Vertical Nutrient Profiles

We compare the profiles of temperature, salinity, and nutrient concentrations in the subtropical gyres both in the upper 200 m of the water column and below (Figure 4). The annual average sea surface temperature (SST) is similar among the five gyres. All temperature profiles show a similar decreasing pattern with depth. Salinity in the Atlantic subtropical gyres is notably higher than in other gyres (Figure 4b), and unlike temperature, salinity exhibits less variation with depth (Figure 4b). The vertical distributions of the concentrations of each macronutrient display similar patterns in the upper 200 m of all the subtropical gyres (Figures 4c, 4d, and 4f). The NO_x concentrations are deficient in the upper 100 m and then increase abruptly with depth (Figure 4c). Phosphate concentrations also increase with depth in the upper 200 m, but the gradient is lower than that of NO_x (Figure 4d). Silicate concentrations, however, are generally uniform in the upper 200 m, except for a small increase below 100 m in the NPSG (Figure 4f). The relatively weaker vertical changes in silicate concentrations compared to those of nitrate and phosphate may be attributed to the faster dissolution of silica in warmer upper oceans. The molar ratio of NO_x to phosphate (N:P) in the upper 200 m is substantially lower than the Redfield ratio of 16:1 in all the subtropical gyres (Figure 4e), suggesting that they are overall N-limited. The highest N:P ratio is observed in the NASG due to the lower phosphate concentrations in the NASG (Figure 4d). The low phosphate concentrations in the NASG are consistent with results reported at BATS, where phosphate concentrations (0.2–1 nM) are more than one order of magnitude lower than those of 10–100 nM at Station ALOHA (Wu et al., 2000). In addition, the N:P ratios at BATS are lower than the Redfield ratio during periods of stratification, with the ratios exceeding the Redfield ratio following deep winter mixing (Cavender-Bares et al., 2001).

Below a depth of 200 m, the NO_x and phosphate concentrations continue to increase to maxima at depths near 1,000 m, mainly because of the remineralization of organic matter and its redistribution with the movement of different water masses (Figures 4j and 4k). The fact that the silicate concentration maximum occurs at a greater depth than the maxima of the NO_x and phosphate concentrations (Figure 4m) may reflect more rapid rates of remineralization for N and P relative to the dissolution of silicate from silica-containing particles, such as biogenic silica (P. J. Tréguer & Rocha, 2013). Overall, the relatively high nutrient concentrations in the deep waters of the

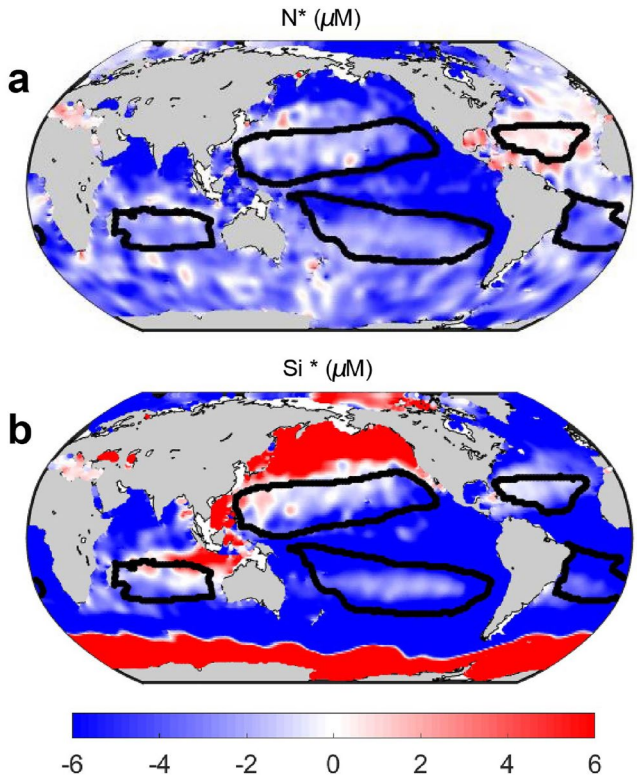

Figure 5. Climatological excess (a) NO_x (N* = [NO_x] − 16 × [phosphate]) and (b) silicate (Si* = [silicate] − 16 × [phosphate]) relative to phosphate concentration at a depth of 200 m using data from the World Ocean Atlas 2018 (https://www.ncei.noaa.gov/products/world-ocean-atlas). The solid black lines represent the boundaries of the subtropical gyres using the criterion of Chl-*a* concentration ≤0.1 mg m^{-3}.

NPSG compared to the NASG reflect the accumulation of nutrients as waters age along the path of deep ocean thermohaline circulation.

The potential limiting nutrients, such as N, P, and silicon (Si), and their relative strength of limitation in the EZ can also be evaluated by comparing the relative abundance between different nutrients to their Redfield stoichiometry, such as N* = [NO_x] − 16 × [phosphate] (Gruber & Sarmiento, 1997) and Si* = [silicate] − [NO_x] (Sarmiento et al., 2004). These geochemical proxies are sometimes more useful than ratios of nutrient concentrations that may be subject to artifacts associated with extremely low concentrations of the nutrient in the denominator of the ratio. Here, we modify the Si* indicated above using the Redfield ratio of 16 for [NO_x]:[phosphate], that is, Si* = [silicate] − 16 × [phosphate]. The N* and Si* at the depth of 200 m (Figure 5) can, to a certain degree, represent the relative limitation of nutrients supplied to the EZ (Figure 4). The positive N* at 200 m in the NASG likely reflects N_2 fixation and P limitation. In contrast, the most negative or near-zero values of N* at the depth of 200 m in other subtropical gyres demonstrate that they are N deficient relative to P (Figure 5a). Note that even in the NASG, N* typically returns to negative values at the surface as illustrated in Figure 4e, suggesting persistent N limitation. In the NPSG, the westward increase in N* suggests increasing P limitation toward the west (Figure 5a). It is worth noting that the NO_x and phosphate concentrations used here come from the World Ocean Atlas (WOA) and may be substantially overestimated, particularly in the western NPSG (Du et al., 2021; Martiny et al., 2019). Moreover, organic nutrients can also support plankton growth (see below) and hence modify the N- and P-limitation patterns derived based on inorganic nutrient concentrations. Most of the Si* values at 200 m are close to zero in the NPSG and NASG and are negative in the SPSG and SASG, suggesting that Si may be more limiting than P to those phytoplankton needing Si (e.g., diatoms) in subtropical gyres of the Southern Hemisphere (Figure 5b).

The vertical distribution of dissolved Fe concentrations in the upper subtropical gyres (Figures 4g and 4n) differs from that of other macronutrients, indicating a decoupling in processes supplying micro- and macro-nutrients. Dust deposition can generate a maximum of dissolved Fe in the near-surface ocean, while biological uptake and scavenging appear to promote a persistent subsurface Fe minimum often associated with the deep chlorophyll maximum (DCM) (e.g., Bergquist & Boyle, 2006; Bruland et al., 1994). This pattern is apparent across several stations sampled in the subtropical gyres. The vertical structure of the subsurface Fe minimum allows Fe to be supplied from both the upper mixed layer and lower ferricline. The subsurface dissolved Fe concentration minima show little spatial variability, especially in the interior of the subtropical gyre. The implication is that the subsurface distribution of dissolved Fe concentrations is controlled by processes such as aggregation at the DCM and remineralization (Fitzsimmons et al., 2015). Notably, dissolved Fe concentrations in the deeper waters also vary among subtropical gyres in terms of depth structure and magnitude of their maxima (Figures 4g and 4n). These differences may be attributable to atmospheric deposition, scavenging, and hydrothermal inputs at the bottom of the ocean (Bergquist et al., 2007; T. M. Conway & John, 2014; Fitzsimmons et al., 2014; Nishioka, Obata, & Tsumune, 2013; Tagliabue et al., 2017).

Fe is generally not considered a key limiting nutrient to primary production in subtropical gyres, and there is usually excess Fe when major nutrients become exhausted (J. K. Moore et al., 2013). However, Fe and P can limit or co-limit N_2 fixers in the subtropical gyres (Zehr & Capone, 2020). Furthermore, a recent study suggested that Fe may limit the abundance and growth of eukaryotic phytoplankton, especially diatoms, at the DCM, where dissolved Fe concentrations fall below 0.1 nM (Hogle et al., 2018). Although the status of Fe limitation at the DCM is unclear, several studies have indicated that there is sufficient Fe to support N acquisition by microorganisms in the DCM of the NPSG (Hawco et al., 2021, 2022).

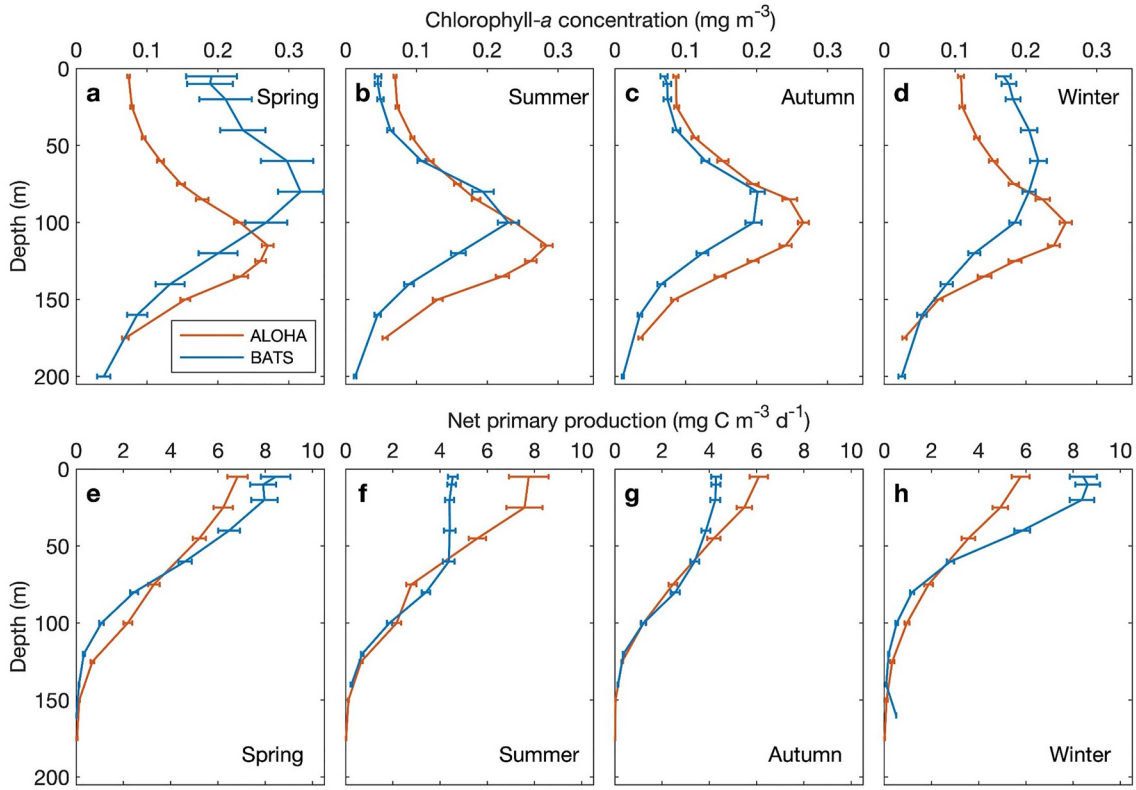

Figure 6. Profiles of (a–d) chlorophyll-*a* concentrations and (e–h) net primary production at Stations ALOHA and Bermuda Atlantic Time-series Study (BATS). The data were collected during 1988–2020 at Station ALOHA (https://hahana.soest.hawaii.edu/hot/hot-dogs/) and from 1988 to 2016 at BATS (http://bats.bios.edu/data/). Chlorophyll-*a* concentrations were measured by high-performance liquid chromatography. Original data in each profile were first interpolated to standard depth intervals and then averaged over spring (March–May), summer (June–August), autumn (September–November), and winter (December–February). The error bars represent one standard error.

2.2.4. Biomass and Productivity

The concentration of Chl-*a*, the primary light-harvesting pigment for photosynthesis, has long been used as an indicator of phytoplankton biomass, and its global distribution has been extensively studied since the launch of the first ocean color satellite, the coastal zone color scanner (Clarke et al., 1970). Based on satellite ocean color products, uniformly low Chl-*a* concentrations are found in all of the subtropical gyres (Figure 2b). The areas of low Chl-*a* concentrations largely correspond to the regions with low surface nutrient (particularly NO_x) concentrations (Figure 3). Chl-*a* concentrations are generally lowest at the centers of subtropical gyres and increase more strongly poleward than equatorward (Figure 2b).

In addition to low surface Chl-*a* concentrations, the subtropical gyres are also characterized by DCMs modulated primarily by light and nutrient availability, which significantly alter cellar pigment contents. However, other factors, such as phytoplankton buoyancy and/or motility, can also play a role (Cullen, 2015). The DCMs in subtropical gyres are typically located at depths below 100 m throughout the year (Cornec et al., 2021). In comparison, the DCM in high-latitude regions only exists during seasons with stratification, and its depth is generally shallower than 75 m (Cornec et al., 2021). Chl-*a* concentrations in the DCM of subtropical gyres are typically <0.5 mg m^{-3}, but can be 10-fold greater than those in near-surface waters. Field measurements at Station ALOHA also show a DCM layer at a depth of approximately 100 m with an average Chl-*a* concentration of approximately 0.2–0.3 mg m^{-3} in most seasons (Figures 6a–6d). It has been noted that seasonal light intensity and nutrient conditions can modify this layer (Guidi et al., 2012; Letelier et al., 2004). At Station ALOHA, the DCM is deeper in spring and summer when the irradiance is higher compared to autumn and winter (Figures 6a–6d) (Letelier et al., 2004). At BATS, a DCM forms in summer and autumn at depths and Chl-*a* concentrations similar to those at Station ALOHA (Figures 6b and 6c) (Steinberg et al., 2001). However, during other seasons, especially

winter, the mixed layer depth (MLD) at BATS can reach 150 m or deeper, resulting in relatively high surface Chl-*a* concentrations in the upper EZ and a weakened or nonexistent DCM (Figures 6a and 6d).

As a proxy of phytoplankton biomass, however, chlorophyll is also influenced by phytoplankton physiology, for example, variations in intracellular pigments due to changes in light (i.e., photoacclimation) and other factors (e.g., nutrients and temperature). The DCM in subtropical gyres is often not associated with elevated biomass and production. For example, the DCM is apparent during most seasons at Stations ALOHA and BATS; however, NPP almost always decreases with depth (Figure 6). The concentration of suspended particulate carbon (PC) and abundances of the dominant phytoplankton (e.g., *Prochlorococcus* and *Synechococcus*) also decrease with depth without a subsurface maximum, although there is often a subsurface maximum of non-dominant picoeukaryotes. Recently, Sato et al. (2022) found that abundance peaks of *Prochlorococcus* and *Synechococcus* are shallower than the DCM (88% and 74% of DCM depth, respectively) and the abundance peak for picoeukaryotes coincides with the depths of the DCM and in the Pacific and Indian Oceans. The DCM can result from acclimation-driven increases in the chlorophyll-to-carbon ratios of phytoplankton cells under low-light conditions (Cullen, 1982). In the water column, the chlorophyll-to-carbon ratio of phytoplankton cells varies considerably as a function of environmental conditions and growth rates (Laws et al., 1983, 2016). Consequently, chlorophyll concentrations may be good metrics of phytoplankton biomass in surface waters under light-sufficient conditions, but may not be as useful for biomass estimates in low-light regimes.

Because in situ measurements of net primary production (NPP) are very limited, studies of its spatial and temporal variations largely rely on satellite data. However, NPP estimates based on remote sensing are highly dependent on bio-optical models, where there are generally a factor of 2 uncertainties (Carr et al., 2006; Saba et al., 2011). The areal, depth-integrated annual NPP rates estimated from SeaWiFS products by a chlorophyll-based, vertically generalized production model (VGPM) (Behrenfeld & Falkowski, 1997) are much lower in the subtropical gyres compared to those estimated by a carbon-based production model (CbPM) (Behrenfeld et al., 2005) (Figures 7a and 7b), whereas the latter areal estimates of NPP in subtropical gyres are similar to the global oceanic average (Table 3). The subtropical gyres contribute 11% or 20% of the global oceanic NPP based on the VGPM or CbPM estimates, respectively (Table 3). Among the five subtropical gyres, the average areal, depth-integrated annual NPP estimates from the VGPM are similar, whereas there are large differences in the areal NPPs estimated by the CbPM. The NPP based on CbPM is approximately 40% higher, for example, in the NPSG than in the NASG (Table 3). Because of the limitations of both the VGPM and CbPM (Z. Lee & Marra, 2022; Z. Lee et al., 2015; J. Marra et al., 2003), an absorption-based production model has been developed based on the absorption coefficient of phytoplankton (a_{ph}) (Z. Lee et al., 2011). More efforts should be devoted to improving the estimation of NPP based on satellite measurements, along with extensive in situ measurements to validate the various remote sensing algorithms.

Although there is uncertainty associated with NPP measurements, evidence of uncoupled dynamics between biomass and productivity may reflect rapid phytoplankton growth and biomass turnover in these systems. Despite rapid growth of phytoplankton, macronutrient concentrations are extremely low, suggesting that NPP is largely supported by recycled nutrients. However, episodic events that supply nutrients to the upper ocean may not be adequately captured by the overall low temporal and spatial resolution sampling.

Vertically, the NPP values measured in situ at Station ALOHA generally peak in the well-lit upper layer and then decrease with depth (Figures 6e–6h). This pattern differs from the subsurface maxima observed in Chl-*a* concentrations. The vertical structure of NPP is similar over all seasons at Station ALOHA, although the slightly higher NPP in summer suggests seasonal changes in light and/or temperature are important controlls. At BATS, the vertical profiles of NPP are similar to those at Station ALOHA. However, in the upper 50 m, NPP is substantially lower in the summer and higher in winter at BATS than at Station ALOHA (Figures 6e–6h). This pattern is consistent with relatively large seasonal variations in nutrient supplies at the BATS.

The phytoplankton community has historically been classified based on size, including the picoplankton (0.2–2 μm), nanoplankton (2.0–20 μm), and microplankton (20–200 μm). Differences in phytoplankton community size structure have been used to understand ecosystem functions in the ocean. Picophytoplankton are generally the dominant contributors to phytoplankton biomass in subtropical gyres (e.g., Marañón et al., 2001). The significant contribution of picoplankton to biomass and primary production is likely related to the high efficiency in acquiring nutrients and capturing light. At Station ALOHA, a diverse assemblage of picoplankton, including photosynthetic picoeukaryotes and cyanobacteria (e.g., *Prochlorococcus* and *Synechococcus*), dominates (>60%)

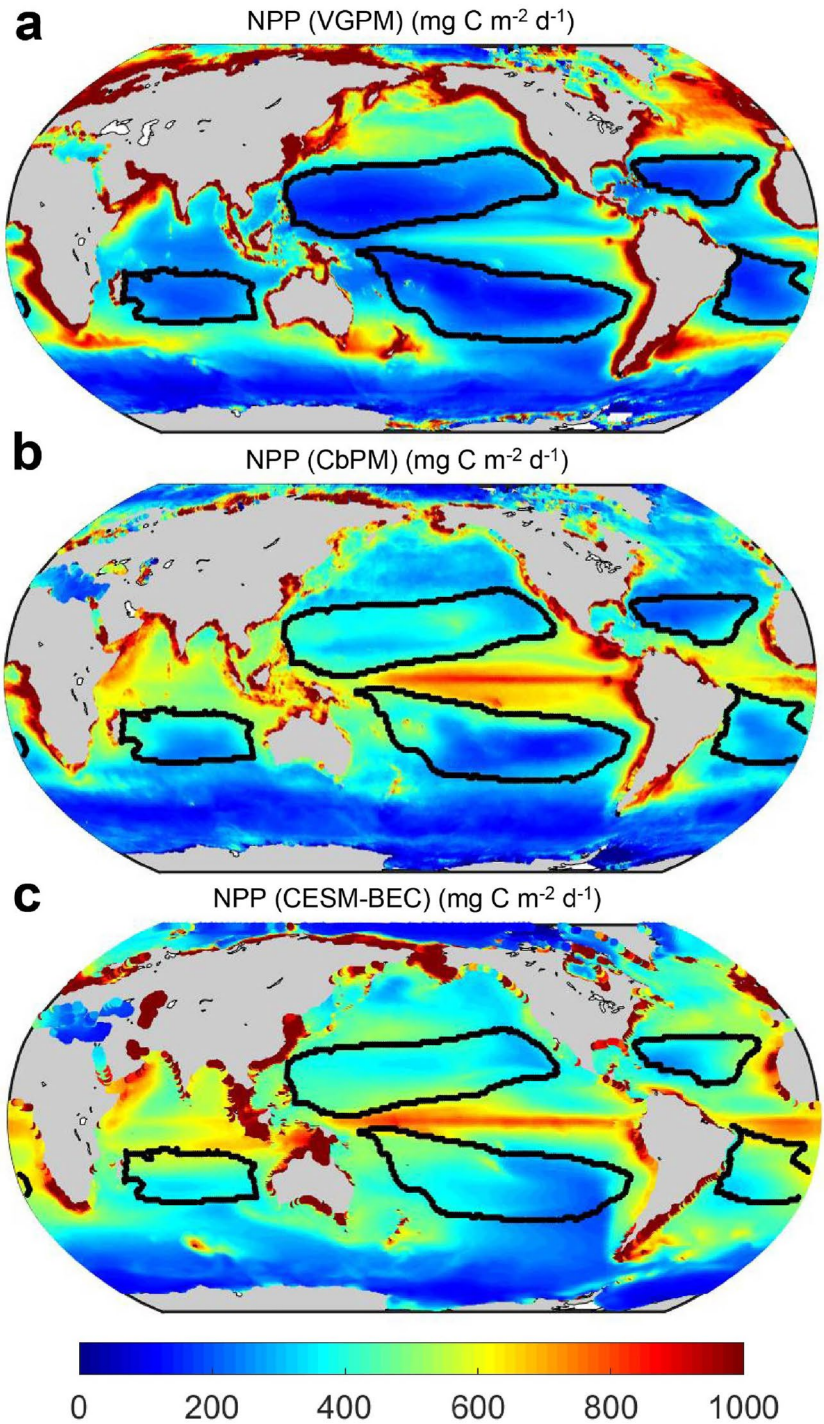

Figure 7. Net primary productivity (NPP) from 1988 estimated via two remote sensing algorithms (a) vertically generalized production model (Behrenfeld & Falkowski, 1997) and (b) carbon-based production model (Behrenfeld et al., 2005) (http://sites.science.oregonstate.edu/ocean.productivity/index.php), and (c) an Earth system model (CESM-BEC)-based results (J. K. Moore et al., 2013) (http://www.earthsystemgrid.org). The solid black lines represent the boundaries of the subtropical gyres based on the criterion of Chl-*a* concentration $\leq$0.1 mg m^{-3}.

the phytoplankton biomass and NPP integrated in the EZ (Campbell & Vaulot, 1993; B. Li et al., 2013; Rii et al., 2016), and *Prochlorococcus* contributes approximately 39% of total Chl-*a* (Chl-*a* plus divinyl Chl-*a*) concentrations in the DCM (Letelier et al., 1993). In the western NPSG, *Prochlorococcus* is similarly dominant in

Table 3
Net Primary Production Estimated Using Different Satellite Models

	Chlorophyll-based VGPM			Carbon-based CbPM		
	Daily areal rate (mg C m^{-2} d^{-1})	Annual rate (Gt C yr^{-1})	Fraction of global total	Daily areal rate (mg C m^{-2} d^{-1})	Annual rate (Gt C yr^{-1})	Fraction of global total
NPSG	212 ± 63	2.4	3.7%	376 ± 49	4.4	7.5%
SPSG	206 ± 64	2.3	3.5%	322 ± 122	3.7	6.3%
NASG	233 ± 54	0.7	1.1%	272 ± 64	0.9	1.5%
SASG	235 ± 54	0.9	1.3%	336 ± 73	1.3	2.2%
IOSG	248 ± 36	1.1	1.7%	351 ± 77	1.6	2.7%
Subtropical gyres	219 ± 61	7.5	11.4%	341 ± 92	11.8	20.3%
Global	505 ± 663	65.5		395 ± 269	58.1	

the EZ in the Philippine Sea, where it accounts for nearly half of the total Chl-*a* concentration (Yun et al., 2020). In the NASG, picoplankton are estimated to account for >60% of the total Chl-*a* concentration at the surface, and that contribution increases with depth (Perez et al., 2006). Picoplankton contributes approximately 50% of carbon fixation in the NASG (Marañón et al., 2003). Outside the subtropical gyres at high latitudes (>30°N), EBUS, and equatorial regions where nutrients are generally replete, there is a clear transition of phytoplankton carbon from picoplankton to nanoplankton as the dominant size category (Dutkiewicz et al., 2020; Mojica et al., 2015). A recent study also suggests that the contribution of picoplankton to NPP decreases from >60% in subtropical gyres to <30% in high-latitude regions (Juranek et al., 2020).

2.2.5. Biological Carbon Pump

The subtropical gyres are important sinks for atmospheric CO_2, accounting for 23% of the total oceanic CO_2 sink (Table 4) (Iida et al., 2021). The average areal sea-air CO_2 flux in the IOSG is similar to that in the global ocean, while the rates in the NPSG, SPSG, and NASG are also substantial, although lower than the global average. The SASG, however, appears to be a weak source of CO_2. Among the subtropical gyres, the SPSG, NPSG, and IOSG are the three gyres that contribute most to the CO_2 sink, while the contribution from the NASG is small due to its smaller area and lower areal sea-air CO_2 flux rate. There are also substantial seasonal variations in the sea-air CO_2 flux in the subtropical gyres, with an intensified CO_2 sink in winter and spring, while the CO_2 sink is greatly weakened or even switches to a CO_2 source in summer and autumn.

Table 4
Average Sea-Air CO_2 flux (mol m^{-2} yr^{-1}) in 1990–2020 in Subtropical Gyres and the Global Ocean (Mean ± Standard Deviation)

	Sea-air CO_2 flux rate (mol m^{-2} yr^{-1})					
	Spring	Summer	Autumn	Winter	Annual	Total flux (Pg yr^{-1}) Annual
NPSG	−0.84 ± 0.66	0.30 ± 0.21	0.06 ± 0.24	−1.30 ± 0.89	−0.45 ± 0.43	−0.16
SPSG	−0.88 ± 0.71	−0.04 ± 0.34	−0.35 ± 0.48	−1.23 ± 0.92	−0.62 ± 0.59	−0.22
NASG	−0.92 ± 0.43	0.46 ± 0.16	0.28 ± 0.22	−1.24 ± 0.51	−0.36 ± 0.32	−0.04
SASG	−0.22 ± 0.76	0.55 ± 0.29	0.42 ± 0.58	−0.32 ± 1.00	0.11 ± 0.64	0.02
IOSG	−1.04 ± 0.45	−0.04 ± 0.40	−0.53 ± 0.35	−1.80 ± 0.47	−0.85 ± 0.36	−0.12
Subtropical gyres	−0.82 ± 0.68	0.18 ± 0.37	−0.09 ± 0.50	−1.23 ± 0.92	−0.49 ± 0.56	−0.53
Global ocean	−0.87 ± 1.57	−0.59 ± 1.50	−0.69 ± 1.61	−0.87 ± 1.85	−0.83 ± 1.51	−2.31

Note. Data are from the Japan Meteorological Agency (https://www.data.jma.go.jp/gmd/kaiyou/english/oceanic_carbon_cycle_index.html) (Iida et al., 2021). Positive values represent that the ocean is a CO_2 source, and negative values represent that the ocean is a CO_2 sink.

Particulate organic carbon (POC) export from the EZ was found to be low in subtropical gyres. At Station ALOHA, sediment trap measurements of POC export at 150 m ranged from 0.33 to 1.86 mol C m^{-2} yr^{-1} between 1993 and 2019 with an average of 0.73 mol C m^{-2} yr^{-1}. ^{234}Th-based POC export in the NPSG was estimated at 0.15–1.50 mol C m^{-2} yr^{-1} (Umhau et al., 2019). In the NASG, POC export (^{234}Th-based) varied over space and time and was calculated to be up to 1.46 mol C m^{-2} d^{-1} (Owens et al., 2015). Furthermore, Zhou et al. (2021) concluded that the ratio of export to primary production (e-ratio) was typically <10% at Station ALOHA compared to >30% in high-latitude oceans.en

Annual NCP, which should be equivalent to the total carbon export over an annual cycle, displays large spatial variations when integrated from the surface to the base of the winter MLD (Quay et al., 2020; B. Yang et al., 2019). Using O_2 and DI^{13}C as tracers, Quay et al. (2020) estimated a threefold variation in NCP (1–3 mol C m^{-2} yr^{-1}) across the Pacific and North Atlantic Oceans. The annual NCP may be higher in the NPSG than in the SPSG (Quay et al., 2020; B. Yang et al., 2019). Additionally, the annual NCP in subtropical gyres appears to be less variable in the Northern Hemisphere than in the Southern Hemisphere (B. Yang et al., 2019). The comparison between POC flux and annual NCP reveals that other export mechanisms, such as dissolved organic carbon export and zooplankton migration, could be substantial in subtropical gyres (Roshan & DeVries, 2017). Spatial and temporal variabilities are other potential reasons for the difference in NCP and POC export; NCP is often integrated over large spatial areas over an annual cycle, while POC flux based on sediment traps and ^{234}Th are temporally integrated values over shorter time scales, for example, days to weeks.

The annual NCP in the NASG is found to be even higher than that in the subpolar region despite the larger spring blooms occurring in the subpolar waters (Quay et al., 2020). Explanations for the disproportionally high annual NCP compared to NPP in subtropical gyres include the following possible mechanisms. (a) The N:P and C:P ratios in biomass are higher in subtropical gyres than in nutrient-replete upwelling regions (e.g., Teng et al., 2014). (b) Subtropical gyres are hotspots of biological N_2 fixation which supplies fixed N to other phytoplankton and can support up to 50% of export production (Bonnet, Baklouti, et al., 2016; W. L. Wang et al., 2019). (c) The shallow MLD in subtropical gyres reduces the remineralization of organic matter and allows more organic matter to be exported. The MLD-mediated balance between remineralization and export also explains why the annual NCP is higher in the NASG than in subpolar regions (Quay et al., 2020). (d) DOP can serve as a source of N (Hashihama et al., 2021; Letscher et al., 2022; Yuan et al., 2023). Using an inverse biogeochemical model, Letscher et al. (2022) suggest that on a global scale, DOP supports 14% of the annual NCP, but regionally in subtropical gyres its contribution can be as high as 80%. It is difficult to determine the relative importance of the above four mechanisms, and their contributions may vary between regions. The higher-than-expected annual NCP with their vast surface area suggests that subtropical gyres are key contributors to mitigating climate change on Earth.

3. Spatial and Seasonal Variations in the NPSG

The perception of subtropical gyres as homogenous, temporally invariant ecosystems has changed as a result of the HOT and BATS programs and the development of highly sensitive nutrient analysis methods. New analytical methods, such as the magnesium-induced co-precipitation method (Karl & Tien, 1992) and long-path liquid-waveguide capillary cell spectrophotometry (Q. P. Li & Hansell, 2008), have lowered detection limits to 0.5–2 nM for phosphate and NO_x, which are 2 orders of magnitude lower than those of conventional colorimetric methods (50–100 nM). Subsequent studies using these sensitive techniques revealed that ecosystems in subtropical gyres have pronounced variations in biogeochemical properties. For example, phosphate concentrations in subtropical gyres range from <2 nM in the western NPSG and NASG to >100 nM in the eastern SPSG (Martiny et al., 2019). Phytoplankton blooms are also sporadic features of the gyres whose occurrence appears linked to dust inputs, tropical cyclones, and mesoscale eddies (Benitez-Nelson et al., 2007; Dore et al., 2008). Subtropical gyres are not static and homogeneous regions but are dynamic systems with variations in nutrient concentrations of three orders of magnitude as well as substantial variations in plankton biomass. In this section, we review spatial and seasonal variations in biogeochemical properties in the NPSG.

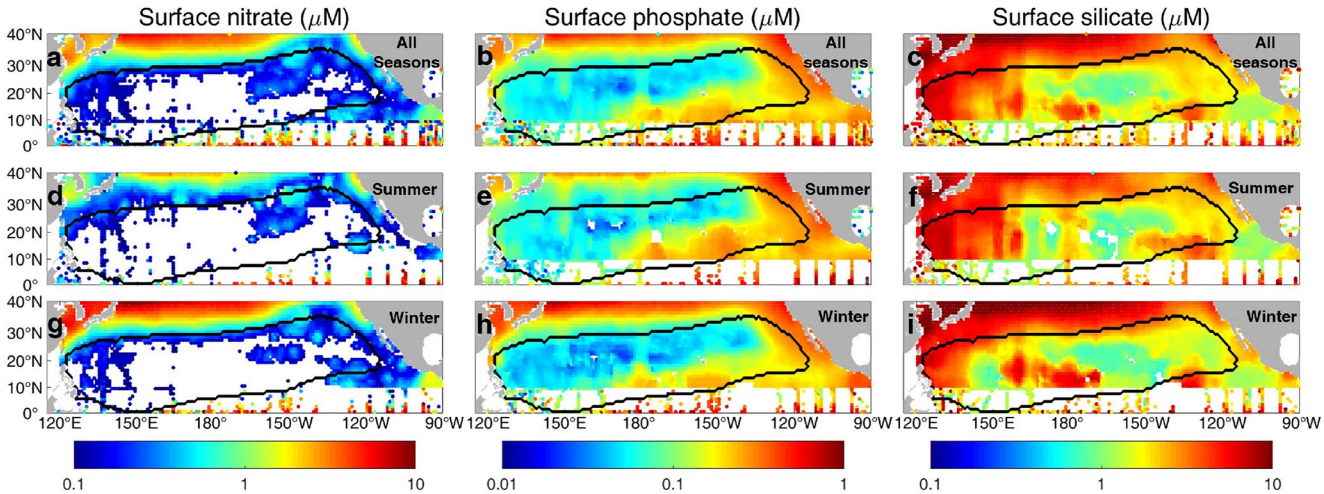

Figure 8. In situ measurements of (a, d, and g) surface NO_x, (b, e, and h) phosphate, and (c, f, and i) silicate concentrations in the oligotrophic North Pacific Ocean. The results are averaged in panels (a–c) all seasons, (d–f) summer (June–August), and (g–i) winter (December–February). The solid black lines represent the boundaries of the North Pacific Subtropical Gyre using the criterion of Chl-*a* concentration ≤0.1 mg m^{-3}. Nutrient measurements were extracted from the World Ocean Database 2018 (https://www.nodc.noaa.gov/OC5/WOD/pr_wod.html), a gridded nutrient data set in the North Pacific version 2 (https://www.jamstec.go.jp/rigc/ress/yasunaka/nutrient/v2/) (Yasunaka et al., 2021) and the Global Ocean Data Analysis Project v2.2022 (Lauvset et al., 2022) (https://www.glodap.info/index.php/merged-and-adjusted-data-product-v2-2022/). Data below the detection limits (0.1 μM for NO_x, 0.02 for PO_4^{3-}, and 0.6 μM for silicate) are not shown.

3.1. Spatial Variations in Nutrient Concentrations and Their Supplies

3.1.1. Macronutrients: NO_x, Phosphate, and Silicate

The NO_x concentrations in the surface waters of the NPSG tend to be <30 nM throughout the region (Hashihama et al., 2020; Karl, Björkman, et al., 2001) (Figures 8a, 8d, and 8g). In contrast, phosphate varies spatially with a large concentration gradient from the southeast (high) to the northwest (low) across the NPSG (Figures 8b, 8e, and 8h). The surface waters of the western NPSG are depleted in phosphate (<10 nM) but increase to >50 nM in the central and eastern NPSG (Hashihama et al., 2020). This phosphate depletion in the western NPSG is potentially caused by high rates of Fe supply relative to macronutrients from the subsurface layer, which potentially eases Fe limitation of photosynthesis and N_2 fixation (Karl, Björkman, et al., 2001; Martiny et al., 2019; Nishioka et al., 2020; Wen et al., 2022; also see Section 4). Although less pronounced, an observable north-south difference in phosphate concentrations also exists, with higher concentrations at the northern and southern boundaries of the NPSG, whereas its interior is relatively depleted (e.g., Yuan et al., 2023).

The concentration of silicate in the surface waters of the NPSG is much higher than that of NO_x and phosphate (Figure 8). A study using highly sensitive methods revealed that near-surface silicate concentrations were 0.5–1.0 μM in the NPSG (Hashihama et al., 2014). This elevated concentration has been attributed to the high half-saturation constant for silicate uptake by diatoms (mostly ranging between 1 and 100 μM) (Martin-Jézéquel et al., 2000) and the presence of an uptake threshold of 0.2–1.8 μM (H. L. Conway & Harrison, 1977; Paasche, 1973). In addition, diatoms can sometimes be outcompeted by non-silicious phytoplankton that use other essential nutrients (Egge & Aksnes, 1992), leaving residual silicate. Depletion of silicate concentrations to <20 nM has been sporadically observed and appears to be coupled with diatom blooms induced by nutrient additions from cyclonic eddies in the western NPSG (Hashihama et al., 2014).

3.1.2. Iron

In the NPSG, the surface dissolved Fe concentration based on a machine-learning product is moderate to high in the western and central regions (0.2–0.3 nM) (Huang et al., 2022), most likely because of the Fe supply from the Asian continent (Tanita et al., 2021), and low in the eastern region (near 0.1 nM) (Figure 3g).

However, the spatial coverage of dissolved Fe measurements is still very limited, particularly in the western NPSG (Figure 9), which can limit the reliability of the machine learning-based estimates. Interestingly, both field measurements and machine-learning models suggest that dissolved Fe levels are high around the Hawaiian Islands, and a recent cruise covering a meridional section in the NPSG has also revealed that dissolved Fe concentrations are

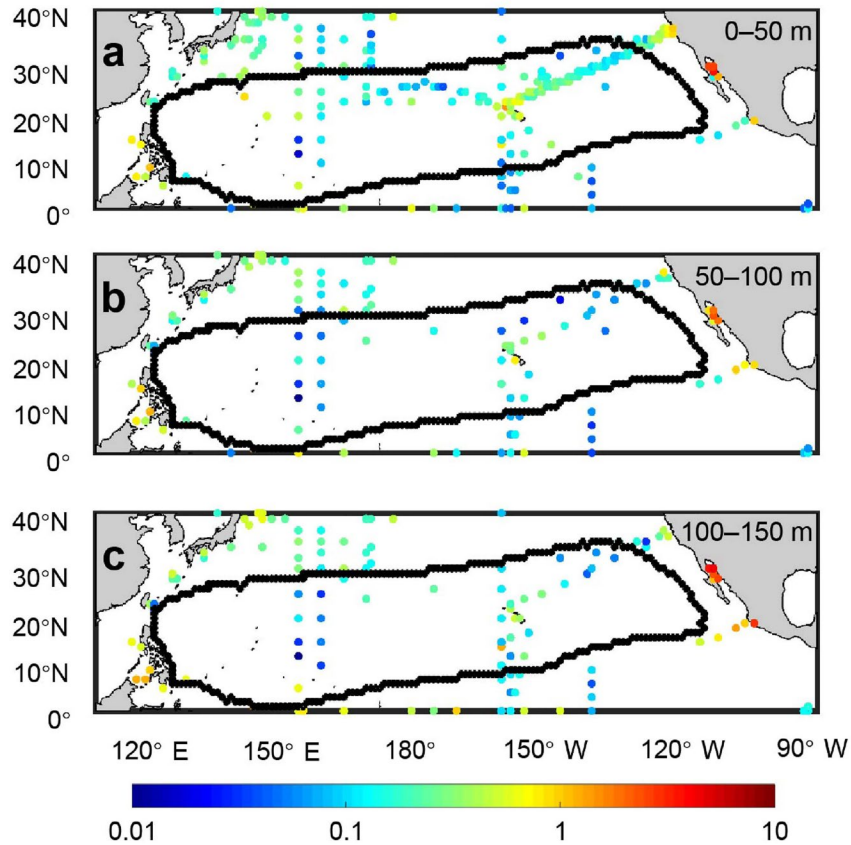

Figure 9. In situ measured dissolved Fe concentrations (nM) at (a) 0–50, (b) 50–100, and (b) 100–150 m. Data are merged products from Tagliabue et al. (2016), Nishioka et al. (2020), GEOTRACES Intermediate Data Product Group (2021), and Tanita et al. (2021) and are binned on 1° × 1° grids using averages over all seasons. The solid black lines represent the boundaries of the North Pacific Subtropical Gyre using the criterion of Chl-*a* concentration ≤0.1 mg m^{-3}.

elevated throughout the water column near Hawaii (GEOTRACES Intermediate Data Product Group, 2021). The high dissolved Fe concentrations observed at Station ALOHA have been attributed to processes such as instantaneous dust depositions (Boyle et al., 2005; Fitzsimmons et al., 2015) and mesoscale eddies (Hawco et al., 2021). However, it must be noted that dissolved Fe concentrations in surface waters exhibit large spatiotemporal variations in part owing to short residence times, ranging from days to a few months, and combined effects of biological uptake, passive adsorption, precipitation, and/or colloidal aggregation (Fitzsimmons et al., 2015). Therefore, the apparently high concentrations of dissolved Fe at Station ALOHA may result from higher resolution sampling in this region compared to more sparse observations elsewhere in the NPSG. Nevertheless, more observations are needed to better constrain dissolved Fe concentrations in the NPSG. Accurate measurements are now possible because advanced techniques and high-resolution sampling methods are becoming increasingly feasible for trace metals (Cutter & Bruland, 2012).

3.2. Spatial Variations in Biomass and Primary Production

Chl-*a* concentrations generally decrease from the east to the west in the NPSG, as revealed in both satellite-based observations (Figure 2b) and numerical model-based estimates (C. M. Moore et al., 2013). This spatial trend is consistent with the physical convergence induced by the strong west boundary current Kuroshio.

In 1961, a conference was held on the theme of "Pacific Ocean productivity" (Doty, 1962). At that time, and for the next two decades, NPP in the NPSG was considered to be largely invariant, ranging from 100 to 200 mg C m^{-2} d^{-1}, with negligible seasonal and interannual variability (Karl et al., 2002). With improvements to methods for measuring primary production, it has become evident that the NPP in the NPSG is much higher

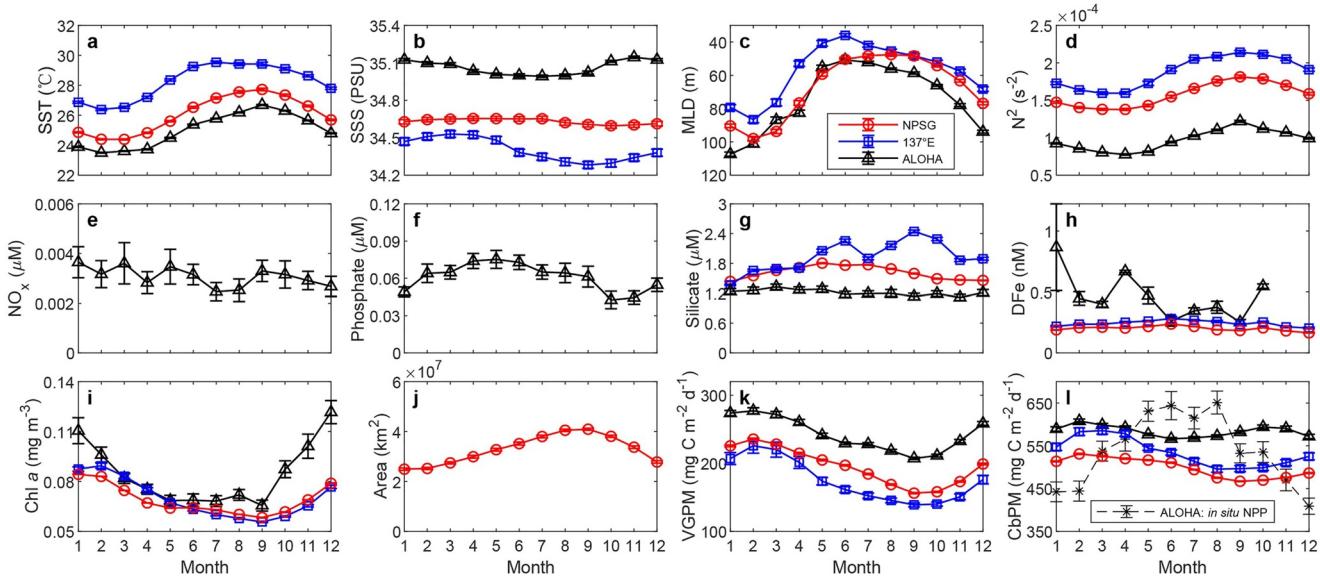

Figure 10. Monthly mean climatology of biogeochemical properties in the surface North Pacific Subtropical Gyre (NPSG). The values include the averages of the entire NPSG (red circles), along 137°E (blue squares) and at Station ALOHA (black triangles) (if available). The error bars represent one standard error. (a–d) Physical properties including sea surface temperature and sea surface salinity, mixed layer depth (MLD) and thermocline stratification defined by bin-averaging (150 m below the MLD) the squared buoyancy frequency (N^2). Global ocean Argo gridded data (H. Li et al., 2017; S. Lu et al., 2020) (http://www.argo.org.cn/) were used for the NPSG and 137°E averages. Note that lack of data along 137°E prevented deriving the monthly mean climatology for these physical properties. (e–i) Concentrations of NO_x, phosphate, silicate, dissolved iron (dFe), and chlorophyll *a* (Chl-*a*) at the sea surface (at a depth of 5 m at Station ALOHA). At Station ALOHA NO_x, and phosphate concentrations were analyzed using highly sensitive methods, and Chl-*a* concentrations were measured by high-performance liquid chromatography (https://hahana.soest.hawaii.edu/hot/hot-dogs/). Silicate concentrations in the NPSG and along 137°E were measured using conventional analyses and the same data sources as Figure 8. Simulations of dissolved Fe concentrations from a machine-learning model (Huang et al., 2022) and satellite-derived Chl-*a* concentrations (https://www.oceancolour.org) were used to calculate their climatology for the entire NPSG and along 137°E, whereas in situ measurements of dissolved Fe (Fitzsimmons et al., 2015; GEOTRACES Intermediate Data Product Group, 2021; Tagliabue et al., 2016) and Chl-*a* concentrations were used for Station ALOHA. (j) Area of the NPSG based on a threshold of Chl-*a* concentrations ≤0.1 mg m^{-3} using satellite-derived Chl-*a* concentrations. (k, l) Calculated net primary productivity (NPP) climatology in the entire NPSG, along 137°E and at Station ALOHA from satellite-based NPP using vertically generalized production model and carbon-based production model (CbPM) models (http://sites.science.oregonstate.edu/ocean.productivity/index.php). The monthly climatology of the in situ measured NPP at Station ALOHA (black dashed line and stars) is compared to the CbPM-NPP.

(by a factor of 2–3) than previously estimated and undergoes significant seasonal variations (Karl et al., 2002; Laws et al., 1987).

The VGPM-estimated NPP generally shows latitudinal variation across the NPSG, similar to surface Chl-*a* concentrations (Figures 2b and 7a). The spatial pattern of the CbPM-NPP differs greatly from that of satellite Chl-*a* concentrations, but interestingly, it more closely resembles the NPP simulated in an Earth system model CESM-BEC (C. M. Moore et al., 2013) (Figures 2b, 7b, and 7c). The Chl-*a* concentrations and VGPM-NPP are lowest in the western region of the NPSG, where the CbPM-NPP predicts elevated values (Figure 7). Along the 137°E meridian in the western NPSG, the mean daily VGPM-NPP increases from 130 mg C m^{-2} d^{-1} in the center (12°N) to 300 mg C m^{-2} d^{-1} at the northern boundary (26°N) of the gyre, and the CbPM-NPP varies slightly between 460 and 520 mg m^{-2} d^{-1} in the same region. In the eastern NPSG along 158°W, the VGPM-NPP increases from 180 in the center (15°N) to 330 mg C m^{-2} d^{-1} at the boundary (32°N) of the gyre, while the CbPM-NPP increases from 470 at 15°N to 640 mg C m^{-2} d^{-1} at 22°N (near Hawaii) and then decreases to 440 mg C m^{-2} d^{-1} at 32°N. The higher rates of NPP estimated from the CbPM are more comparable to the long-term mean of in situ NPP measured at Station ALOHA (577 mg C m^{-2} d^{-1}) (Karl & Church, 2017). These spatial patterns and comparisons further highlight the uncertainties in NPP estimated from satellite data using either VGPM or CbPM (Z. Lee & Marra, 2022; Song et al., 2023).

3.3. Seasonal Variations in Biogeochemistry

The SSTs averaged over the entire NPSG, along 137°E and at Station ALOHA show consistent seasonality, with the lowest SST in February and March and the highest SST in September (Figure 10a). Seasonal variability in

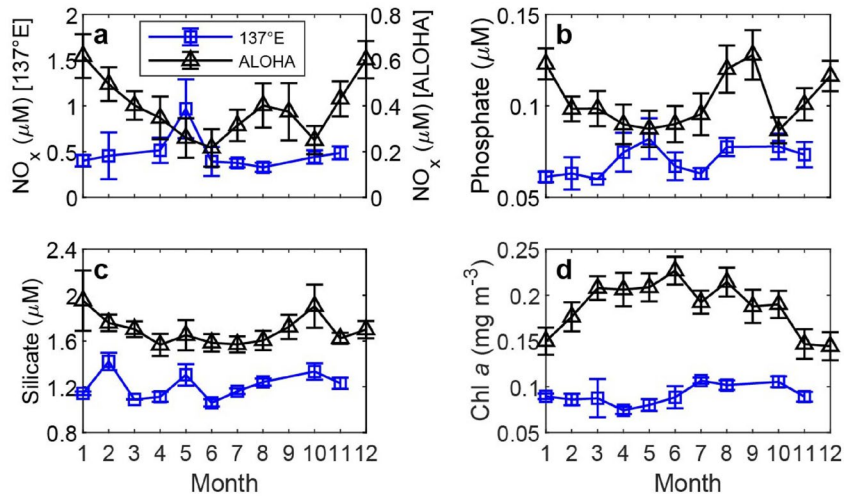

Figure 11. Subsurface isopycnal monthly mean climatology of biogeochemical properties along 137°E and at Station ALOHA in the North Pacific Subtropical Gyre (NPSG), including concentrations of (a) NO_x, (b) phosphate, (c) silicate, and (d) Chl *a*. Isopycnal layers with potential densities (σ_θ) of 23.0 and 24.5 kg m^{-3} were selected for 137°E and Station ALOHA, respectively, to represent the deep chlorophyll maximum layer. The data at 137°E are from the Global Ocean Data Analysis Project v2.2022 product (Lauvset et al., 2022) (https://www.glodap.info/index.php/merged-and-adjusted-data-product-v2-2022/) in the NPSG center (10°–20°N). The data at Station ALOHA are from Hawaii Ocean Times-series (https://hahana.soest.hawaii.edu/hot/hot-dogs/), in which the low-level concentrations of NO_x and phosphate measured by highly sensitive methods are used. Note that the concentrations of NO_x along 137°E and at Station ALOHA are plotted using different scales. Chl-*a* concentrations at Station ALOHA were measured by high-performance liquid chromatography.

surface salinity is not evident (Figure 10b). The seasonality of thermocline stratification is mainly attributed to temperature variations, resulting in the deepest MLD in January and February and shoaled MLD from May to October (Figures 10c and 10d).

At Station ALOHA near-surface NO_x and silicate concentrations do not show a clear seasonal pattern throughout the year (Figures 10e and 10g), whereas near-surface phosphate concentrations are elevated in spring (Figure 10e). The fact that the monthly climatology of near-surface NO_x concentrations at Station ALOHA is <4 nM demonstrates persistent depletion of NO_x in surface waters. Note that among the surface nutrient concentration data measured by conventional methods in the NPSG, 98% of NO_x and 64% of phosphate concentrations are below the detection limits (see Section 6), which prevents analysis of their seasonality.

In a subsurface isopycnal layer near the DCM (σ_θ = 23.0 kg m^{-3}) along 137°E, the absence of clear seasonal patterns of the macronutrient concentrations might result from insufficient data for climatology calculations and/or mesoscale activities (Figures 11a–11c). In an isopycnal layer near the DCM (σ_θ = 24.5 kg m^{-3}) at Station ALOHA, the concentrations of macronutrients, particularly NO_x, are generally higher in winter than in summer (Figures 11a–11c).

The machine-learning results indicate that the surface dissolved Fe concentrations are very low and that their seasonal variability is small when averaged over the entire NPSG and along 137°E in the western NPSG (Figure 10h). The dissolved Fe concentrations are slightly higher in early summer than in winter and may covary with the seasonal cycle of Asian continental dust deposition (Prospero, 1990). Dissolved Fe concentrations at Station ALOHA vary considerably among seasons without a clear pattern (Figure 10h), which could be largely due to the insufficient observations or episodic Fe sources.

Near-surface Chl-*a* concentrations in the NPSG are low in summer and slightly higher in winter, which likely results from variations in daily insolation (Figure 10i) (Maritorena et al., 2002; Signorini & McClain, 2012; Signorini et al., 2015). This seasonality applies to both the western (137°E) and eastern NPSG (Station ALOHA) (Figure 10i). Consequently, the size of the surface of the NPSG is largest in summer and shrinks by approximately 40% in winter (Figure 10j). In contrast, summer phytoplankton blooms in the surface layer have been regularly observed by satellite remote sensing (Chow et al., 2017; Dore et al., 2008; Fong et al., 2008; Lin, 2012) and ship-based observations (Guidi et al., 2012; Jiang et al., 2021; Karl & Church, 2017). These summer blooms are

often dominated by diatoms and *Trichodesmium*, although *Prochlorococcus*-dominated bloom events have also been observed (Jiang et al., 2021; Villareal et al., 2012).

In the lower EZ of the NPSG, particularly at Station ALOHA, Chl-*a* concentrations generally decrease from summer to winter (Figure 11d), reflecting a decrease in phytoplankton biomass and NCP caused by concurrent changes in light intensity and nutrients (Karl, Bidigare, & Letelier, 2001; Letelier et al., 2004; Venrick et al., 1987; Winn et al., 1995).

The satellite-based NPP estimated via either the VGPM or CbPM model is highest in winter (February) and lowest in summer (September) over the entire NPSG as well as along 137°E (Figures 10k and 10l) and is consistent with the satellite-derived Chl-*a* concentrations (Figure 10i). Although the VGPM-NPP at Station ALOHA follows a seasonal pattern similar to other NPSG regions, the CbPM-NPP is lowest in early summer (June) with two peaks in autumn (October) and winter (Figures 10k and 10l). However, neither satellite model captures the seasonal variations in NPP revealed by in situ measurements at Station ALOHA, where the NPP is maximal in summer and minimal in winter (Figure 10l), out of phase with that of Chl-*a* concentrations. This result is partly explained by the seasonal changes in light intensity and day length (Karl et al., 2007).

The general seasonal patterns of NPP in the NPSG are still unclear, not only because of the limitations of remote sensing models discussed above but also because of the complexity of the circulation characteristics in the NPSG (Longhurst et al., 1995). The mean results of 24 satellite Chl-*a*-based NPP models show subdued seasonal fluctuations in NPP (300–400 mg C m^{-2} d^{-1}) in the NPSG zone (10°–40°N) compared to other regions of the North Pacific (Carr et al., 2006). In these models, spring appears to be the most productive season. However, Polovina et al. (2011) reported much larger seasonal variations in NPP for a smaller subregion (27°–29°N) based on Chl-*a* concentrations estimated from a biogeochemical model, ranging from ∼300 in winter to ∼700 mg C m^{-2} d^{-1} in spring. These reports indicate that in the NPSG seasonal variations in NPP may differ depending on the region.

Biogeochemical models have also been useful tools for quantifying phytoplankton variability and for examining the potential controls across the gyre. In the northwestern NPSG, models have revealed significant seasonal variations in Chl-*a* concentrations and NPP that peak in early spring at Station S1 (30°N, 145°E), associated with the strong winter mixing that supplies nutrients from depth (Sasai et al., 2016). In contrast, another modeling study has demonstrated that the NPP peak at Station S1 is contributed by atmospheric deposition of Fe in winter (Xiu & Chai, 2021). In the eastern NPSG, a high-resolution modeling study has shown that variations in NPP could be driven by seasonal cycles of light, N_2 fixation, stochastic eddies, sporadic wind- and current-driven upwelling, and/or frontal dynamics (Friedrich et al., 2021).

4. N_2 Fixation in the NPSG

N_2 can be fixed by diazotrophs, which in the ocean include cyanobacteria such as filamentous *Trichodesmium*, heterocyst-forming cyanobacteria-diatom associations (diatom-diazotroph associations, DDAs), and unicellular cyanobacteria (UCYN) (Zehr & Capone, 2020), and non-cyanobacterial diazotrophs (NCDs) that are presumably heterotrophic or photoheterotrophic (Bombar et al., 2016). Three major UCYN groups were recognized, including uncultivated UCYN-A, free living *Crocosphaera* (UCYN-B) and uncultivated UCYN-C, while later studies have revealed that both UCYN-A and UCYN-C are putatively obligate symbionts with specific haptophyte and diatom alages, respectively (Schvarcz et al., 2022; Zehr, 2015; Zehr & Capone, 2020). Since marine N_2 fixation was discovered in the 1960s (see review by Benavides & Voss, 2015), its contribution to support new production in the world's oceans has been increasingly recognized (e.g., Benavides & Voss, 2015; Zehr & Capone, 2020). Moreover, the discovery of novel diazotrophs in diverse habitats, including dark oceans, eutrophic coastal zones, sediments, and high-latitude (sub)polar oceans, has greatly refined our knowledge of the geographical distribution of diazotrophs (Zehr & Capone, 2020). Recent data compilations and model-driven studies further suggest that high N_2 fixation rates are particularly pronounced in oligotrophic subtropical gyres where other biologically accessible sources of N are depleted (e.g., Tang et al., 2019; W. L. Wang et al., 2019; Zehr & Capone, 2020).

4.1. Horizontal Distribution

Longitudinal transects across the main ocean basins have shown that N_2 fixation is consistently higher in the center of subtropical gyres and decreases with distance from the gyre center in the North Atlantic (Marconi

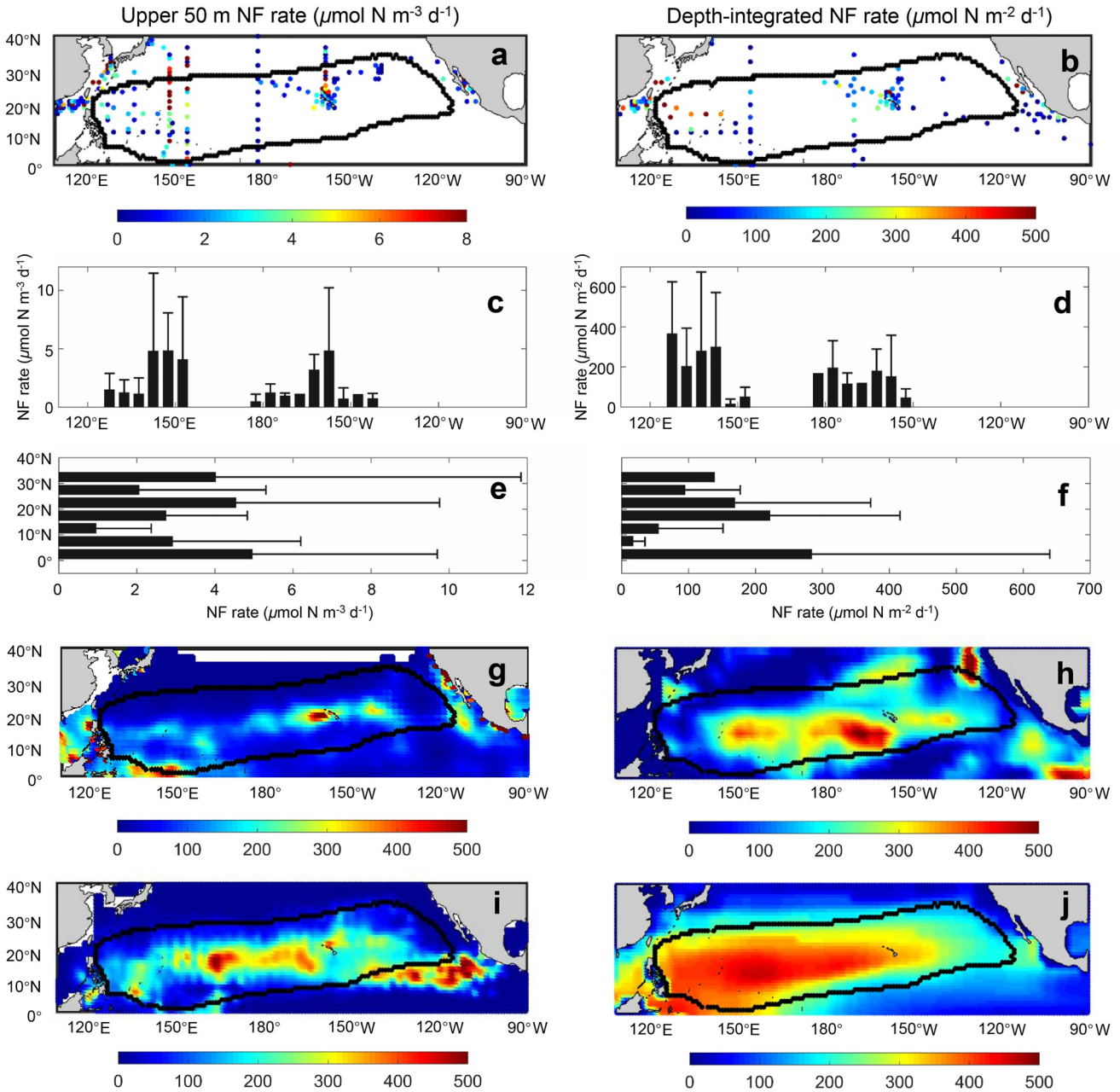

Figure 12. N_2 fixation rates in the North Pacific Subtropical Gyre (NPSG). (a) In situ N_2 fixation measurements (gridded on 1° × 1°) in the upper 50 m (μmol m^{-3} d^{-1}) and (b) integrated through the water column (μmol m^{-2} d^{-1}) (Shao et al., 2023). (c–f) Latitudinal and meridional averages of measured N_2 fixation in the NPSG for (a, b) using the samples inside a climatological surface chlorophyll-*a* concentration of 0.1 mg m^{-3} (marked by the black contours). Indirect estimates of depth-integrated N_2 fixation rates (μmol N m^{-2} d^{-1}) by (g) observation-based regression (Y.-W. Luo et al., 2014), (h) P* convergence (Deutsch et al., 2007), (i) an inverse model (W. L. Wang et al., 2019), and (j) a mechanistic model (CESM-BEC) (J. K. Moore et al., 2013).

et al., 2017), South Atlantic (Marshall et al., 2022), North Pacific (Gradoville et al., 2020; Kitajima et al., 2009; Shiozaki et al., 2010, 2017), and South Pacific (Shiozaki et al., 2018). In the NPSG, in situ measurements of N_2 fixation rates are on the order of ∼10 to 1,000 μmol N m^{-2} day^{-1} and appear moderate to high compared to other oceanic regions (Y.-W. Luo, Doney, et al., 2012; Tang et al., 2019; Wen et al., 2022) (Figures 12a and 12b). The highest surface N_2 fixation rates occur from 140°–150°E and from 155° to 165°W (Figures 12a and 12c). Interestingly, the depth-integrated N_2 fixation in the westernmost portion of the NPSG (120°–140°E) is highest, even though the surface N_2 fixation is low (Figures 12a–12d). In contrast, high surface N_2 fixation but low depth-integrated rates are observed near ∼150°E (Figures 12c and 12d). This inconsistency between the surface

Table 5
Depth-Integrated Areal N_2 Fixation (NF) Rates and Total N_2 Fixation in the North Pacific Subtropical Gyre by Four Different Methods, Including Observation-Based Regression (Y.-W. Luo et al., 2014), P Convergence (Deutsch et al., 2007), an Inverse Model (W. L. Wang et al., 2019), and a Mechanistic Model (CESM-BEC) (J. K. Moore et al., 2013)*

	Observational regression	P* convergence	Inverse model	Mechanistic model
Areal NF rate (μmol m^{-2} d^{-1})	81 ± 76	185 ± 109	155 ± 98	310 ± 88
99% areal NF range (μmol m^{-2} d^{-1})	2–438	0–485	3–435	115–456
NPSG total (Tg N yr^{-1})	13.4	30.3	25.5	50.8
Fraction of global NF	15.2%	18.8%	26.2%	21.4%

and depth-integrated N_2 fixation appears to reflect the paucity of observations in this region. Near 150°E, for example, most measurements of N_2 fixation rates were conducted in surface waters and captured relatively high rates in certain seasons, while the low depth-integrated N_2 fixation rates were mainly measured during a single cruise in March 2007 (Shiozaki et al., 2010). Meridional differences in N_2 fixation rates are less pronounced in the NPSG, primarily because the meridional differences are masked by large zonal variations that lead to large uncertainties when N_2 fixation rates are compared between latitudes (Figures 12e and 12f). Overall, our analyses of the relatively limited available data show that N_2 fixation in the NPSG is higher in the west than in the east, except occasional high rates of N_2 fixation measured around the Hawaiian Islands. The prominent hot spot of N_2 fixation in this region could merely reflect the higher frequency sampling of this region and relatively sparse sampling in the surrounding waters.

Gridded estimates of N_2 fixation rates in the global ocean have been determined by different methods. For example, in situ N_2 fixation measurements were extrapolated to the global ocean (Y.-W. Luo, Doney, et al., 2012; Tang et al., 2019). Rates were also produced by establishing a relationship between N_2 fixation and environmental factors through multiple linear regression (Y.-W. Luo et al., 2014) (Figure 12g) or machine-learning methods (Tang et al., 2019). The transport convergence of P* = [phosphate] − [NO_x]/16 was also used to generate gridded global ocean N_2 fixation rates (Deutsch et al., 2007) (Figure 12h). Additionally, rates were estimated by diagnosing the NO_x and phosphate concentrations in the EZ and N:P ratios in the exported organic matter (W. L. Wang et al., 2019) (Figure 12i) or by simulations using mechanistic biogeochemical models such as CESM-BEC (J. K. Moore et al., 2013) (Figure 12j). The resulting estimates of N_2 fixation rates differ greatly. The estimated average areal rate in the NPSG by these models ranges from 81 to 310 μmol N m^{-2} day^{-1}, and the estimated basin-scale N_2 fixation in the NPSG ranges from 13 to 51 Tg N yr^{-1}, accounting for 15%–26% of the global level (Table 5).

These methods also produce different spatial patterns of N_2 fixation in the NPSG (Figures 12g–12j), with rates relatively uniform from west to east (Deutsch et al., 2007; J. K. Moore et al., 2013; W. L. Wang et al., 2019) (Figures 12h–12j). These inconsistencies may likely reflect uncertainties associated with the methods employed. For example, the P* convergence method (Deutsch et al., 2007) assumes close spatial coupling between N_2 fixation and denitrification; however, this assumption is not supported by later observations (Bonnet et al., 2017; Knapp et al., 2016; Y.-W. Luo et al., 2014). The CESM-BEC mechanistic model is limited by our understanding of the environmental controls of N_2 fixation. Indeed, most Earth system models fail to reproduce observed N_2 fixation rates (Riche & Christian, 2018). This failure is likely attributable to our limited understanding of the environmental controls on N_2 fixation (see Section 4.4).

Inconsistencies in the spatial patterns of the estimated rates of N_2 fixation could also be due to the different methods used for the measurements. Traditional N_2 fixation measurements used $^{15}N_2$ gas bubble methods, which appear to underestimate rates because of slow and incomplete dissolution of the added $^{15}N_2$ gas into seawater (Großkopf et al., 2012; Mohr et al., 2010). These measurements using the $^{15}N_2$ gas bubble methods have shown that N_2 fixation rates are low in the western NPSG but substantially higher in the eastern NPSG around the Hawaiian Islands (Tang et al., 2019). Indeed, most of the high depth-integrated N_2 fixation rates in the western NPSG (125°–145°E) identified in this review (Figures 12b and 12d) are associated with recent $^{15}N_2$-enriched water-based measurements (320–573 μmol N m^{-2} day^{-1}) (Wen et al., 2022). Those rates are approximately twice the 9-year average at Station ALOHA (230 ± 136 μmol N m^{-2} day^{-1}), where both the bubble and enriched water-based methods have been used (Böttjer et al., 2016). Additionally, the high N_2 fixation rates in surface

waters in the western NPSG along ~150°E were measured using acetylene reduction assays (Kitajima et al., 2009) (Figures 12a and 12c).

The diazotrophic communities in the NPSG demonstrate prominent spatial variations. At the gyre's western boundary, that is, the Kuroshio Current, *Trichodesmium*, UCYN-A and *Crocosphaera* are the major diazotrophs (Shiozaki et al., 2014). To the east at 155°E, UCYNs, especially *Crocosphaera*, dominate the diazotrophic community (Konno et al., 2010; Wen et al., 2022). In the eastern NPSG near 160°W, UCYNs, especially UCYN-A, are the most abundant diazotrophic phylotype during most of the year (Church et al., 2008, 2009; Gradoville et al., 2020). At the east near the boundary of the NPSG (i.e., the Southern California Current), UCYN-A dominates the diazotrophic community, while members of proteobacteria are also abundant (Turk-Kubo et al., 2021). Latitudinally, the abundances of UCYN-A and *Crocosphaera* appear dome-shaped, with the highest values observed between 20° and 30°N. In contrast, *Trichodesmium* is typically most abundant at low latitudes and decreases northward. No clear latitudinal patterns have been observed for NCD phylotypes (Cheung et al., 2020, 2021; Church et al., 2008; Shao & Luo, 2022; Shiozaki et al., 2017). Notably, however, the distribution of the diazotrophic community shows seasonal variations (see Section 4.3), and because the field surveys were conducted in different seasons, it is likely that the spatial patterns of the diazotrophic community shown here are confounded by seasonal variability (Turk-Kubo et al., 2023).

4.2. Vertical Distributions

The vertical distributions of diazotrophs and N_2 fixation rates are less constrained than their horizontal distributions in the gyres. *Trichodesmium* and DDAs tend to be most abundant in near-surface waters, decreasing sharply with depth. High abundances of *Trichodesmium* have occasionally been observed at Station ALOHA, although *Crocosphaera* appears more homogeneously distributed in the upper EZ (above ~75 m), and UCYN-A can be found throughout the upper ocean (50–100 m) (Church et al., 2005; Shiozaki et al., 2017; Wen et al., 2022). Although the capability of NCDs to fix N_2 remains unclear, their widespread presence across various habitats extending from the surface layer to sediments has been identified in recent years (Zehr & Capone, 2020), leaving uncertain the mechanisms controlling the distributions and magnitude of N_2 fixation in the global ocean.

Inconsistent with the variability in the vertical distributions of diazotrophs, measurements of N_2 fixation rates in the water column show a broadly decreasing trend from the surface toward greater depths (Böttjer et al., 2016; Shiozaki et al., 2017; Wen et al., 2022). However, a closer look reveals a unimodal vertical pattern of N_2 fixation in tropical and subtropical waters, with the highest rates frequently being detected at a lower depth in the mixed layer (Y. Lu et al., 2019; Shiozaki et al., 2017; Wen et al., 2022). Both laboratory and field studies have found a decrease in N_2 fixation activity under oversaturated light conditions (Bell & Fu, 2005; Y. Lu et al., 2018), implying a potential inhibition of N_2 fixation by light in the near-surface layer. These results indicate the need to use a sampling strategy with higher vertical resolution and/or consider light intensity as a criterion to better capture the vertical distribution of N_2 fixation in the EZ.

4.3. Seasonality

To date, our understanding of the seasonality of N_2 fixation and the diazotroph community is largely hindered by a dearth of observations covering full seasonal cycles across the global ocean. Perhaps the best set of observations covering intra- and interannual variability is from Station ALOHA (Appendix B) (Böttjer et al., 2016; Church et al., 2009; Karl & Church, 2014). At this site, UCYN-A and NCDs are present throughout most of the year, although blooms of these organisms have rarely been recorded. In contrast, periodic blooms of *Trichodesmium* are observed, while the *Crocosphaera* and DDA abundances are elevated in late summer and early autumn. N_2 fixation at the site increases in early summer and starts to decrease at the end of autumn (Böttjer et al., 2016; Church et al., 2009), which matches the increased contribution of N_2 fixation to export production during summer (Dore et al., 2002). One of the prominent but still poorly understood phenomena at Station ALOHA is the pulse of sinking POM in late summer, for which transient DDA blooms are hypothesized to be the primary cause (Follett et al., 2018; Karl & Church, 2014; Karl et al., 2012). At present, however, it is unclear whether this export pulse is ubiquitous in the NPSG or restricted to Station ALOHA. In light of the recent identification of widespread DDAs in the global ocean (Schvarcz et al., 2022), DDA-triggered export pulses might be more ubiquitous than previously recognized; more field efforts are needed to capture such transient but biogeochemically critical events.

A few studies at other sites of the NPSG have also revealed strong seasonal variations in the diazotroph communities and N_2 fixation rates despite the temporal resolution and duration being much lower than those at Station ALOHA (Appendix B). In the western boundary of the NPSG (Kuroshio Current), N_2 fixation rates are higher in warm seasons than in winter (Y. L. L. Chen et al., 2014). The higher rates in warm seasons are mostly due to large diazotrophs (>10 μm), which are replaced by smaller diazotrophs in winter (Y. L. L. Chen et al., 2014). Interestingly, the seasonal variation in N_2 fixation along 155°E is the opposite, with the winter rate twice as high as in the summer (Kitajima et al., 2009). The seasonal pattern of major diazotrophs also varies among phylotypes. Similar to Station ALOHA, the abundance of *Trichodesmium* and *Crocosphaera* in the Kuroshio Current is generally consistent with the N_2 fixation rate, that is, high in warm seasons and low in winter (Shiozaki et al., 2014). A recent investigation of diazotrophs at the basin scale in the NPSG shows that UCYN-A1 (a prominent oceanic sub-type of UCYN-A), *Trichodesmium*, and NCDs are abundant during spring-autumn, summer-autumn and spring, respectively, indicating a seasonal transition of dominant diazotrophs in the NPSG (Cheung et al., 2020). Although the mechanisms underpinning the seasonality of the diazotrophic community and N_2 fixation are still under debate, they are presumably attributed to the physiological differences between various diazotrophs and seasonal changes in nutrients, light, and temperature (Zehr & Capone, 2020). Given the distinct roles that different diazotrophs play in the food web, carbon export and N recycling in the ocean, understanding the causes and ecological consequences of their seasonal variability is an area of research that is crucial to resolving the marine biogeochemistry observed in a changing ocean.

4.4. Controlling Factors

N_2 fixation by phototrophic diazotrophs requires high levels of solar radiation to satisfy their high-energy demands, elevated temperatures to maintain nitrogenase activity (enzyme for N_2 fixation), and sufficient nutrient supplies, particularly P and Fe (Y.-W. Luo et al., 2014; Yuan et al., 2023). High concentrations of O_2 inhibit nitrogenase, but marine diazotrophs have developed a series of strategies to avoid this inhibition (W. Luo et al., 2022; Zehr & Capone, 2020) and are prosperous in the oxygenated EZ. Interactions with other organisms, such as competition with non-N_2-fixing phytoplankton under low nitrate to Fe or phosphate supply ratios (Karl & Letelier, 2008; B. A. Ward et al., 2013) or grazing by zooplankton (Landolfi et al., 2021; H. Wang & Luo, 2022), can also impact the distribution of diazotrophs. At the global scale, research has shown that light and subsurface deoxygenation are most correlated with N_2 fixation rates (Y.-W. Luo et al., 2014). Regionally, Fe rather than P has been proposed to be the most important factor regulating N_2 fixation biogeography along a north–south transect in the Atlantic Ocean (C. M. Moore et al., 2009). In the Pacific Ocean, Fe has also been posited to be the main nutrient controlling N_2 fixation based on observational data of dust inputs, nutrient concentrations and limited experimental evidence (Sohm et al., 2011). However, dust transport and Fe deposition from the Asian continent show some inconsistencies when compared to the gradient of measured N_2 fixation rates across the NPSG (Figures 3g and 12a–12d).

The ability of diazotrophs to outcompete non-diazotrophs in an environment depends on ecological tradeoffs between their ability to fix their own N with enhanced Fe requirements and their slower growth rates (Dutkiewicz et al., 2014). Accordingly, resource competition theory predicts that the external supply rate of fixed N, not phosphate, relative to that of Fe is the primary determinant of where diazotrophs occur (Dutkiewicz et al., 2014). Diazotrophs may therefore be more successful in outcompeting non-diazotrophs when Fe:N supply rates are elevated (B. A. Ward et al., 2013). This theory is supported by recent studies in the western NPSG, where deepened nitraclines and enhanced aerosol Fe deposition increased the Fe:N supply ratios, stimulated N_2 fixation and consequently lowered phosphate to a limiting level (Browning et al., 2022; Wen et al., 2022; Yuan et al., 2023; Figure 13). The combination of these processes is also evident for the entire NASG as well as the western SPSG (Bonnet et al., 2018; C. M. Moore et al., 2009; Wu et al., 2000). In contrast, further to the east and southeast NPSG, shoaling of the nitracline around the NEC enhances the turbulent nitrate supply from below, which, alongside reduced aerosol Fe supply, lowers Fe:N supply ratios. As a result, N_2 fixation becomes Fe limited (Wen et al., 2022; Figure 13). In the South China Sea and the northern boundary of the NPSG, the inconsistency between relatively low N_2 fixation (Gradoville et al., 2020; Shiozaki et al., 2017) and high Fe inputs from aerosols and shelf sediments (Jickells et al., 2005) can be explained by the elevated nitrate supply, which lowers the Fe:N supply ratio (Wen et al., 2022). N_2 fixation in these regions has been observed to be co-limited by both Fe and P (Figure 13).

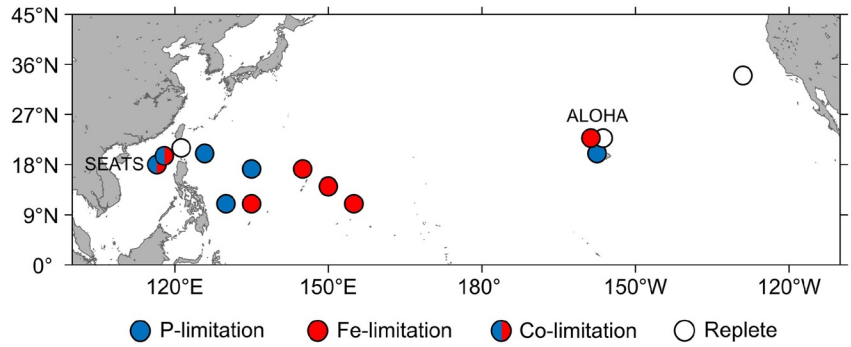

Figure 13. Nutrient (Fe and/or P) limitation patterns of N_2 fixation across subtropical North Pacific. These results are from previously reported nutrient amendment bioassay experiments (Grabowski et al., 2008; Needoba et al., 2007; Tanita et al., 2021; Wen et al., 2022). Red, Fe limitation; blue, P limitation; split red/blue, Fe-P colimitation; and white, Fe and P replete.

Seasonal variability of the limiting factors on N_2 fixation in the NPSG is not well known. In the western NPSG, dust-derived Fe deposition is high during spring and early summer (König et al., 2022), while wintertime cooling may lead to the overturning of the nutrient-depleted surface layer and thus increase the nutrient supply from deeper waters (Karl et al., 2021). These processes can lead to higher Fe:N supply ratios in spring and early summer than in winter, consistent with the same seasonal pattern of N_2 fixation found in the Kuroshio Current (Y. L. L. Chen et al., 2008; Shiozaki et al., 2014). Elevated N_2 fixation in spring and early summer depletes surface phosphate and leads to P limitation of diazotrophs, while Fe is the nutrient more likely to limit N_2 fixation in winter. However, this mechanism seems unable to explain the higher winter N_2 fixation rates along 155°E (Kitajima et al., 2009). Seasonal shifts in the limiting nutrients for diazotrophs are apparent in the eastern NPSG around Station ALOHA, from P limitation in autumn to Fe limitation in spring, as shown by shipboard nutrient amendment experiments (Grabowski et al., 2008). It should be noted, however, N_2 fixation can also be modulated by the mesoscale eddies (e.g., Church et al., 2009; Dugenne et al., 2023) and dust deposition events (e.g., Benavides et al., 2013), further complicating environmental control of the seasonality of N_2 fixation in the NPSG.

There is also a lack of knowledge about what controls the spatial and temporal variations in the diazotroph community across the NPSG. Nutrient utilization strategies can vary greatly among diazotrophic phylotypes. For example, *Trichodesmium* appears able to use particulate Fe (Rubin et al., 2011) to meet its elevated Fe demands (Sohm et al., 2011). This capability may partly explain the elevated contribution of this species in regions with enhanced Fe supply (e.g., the South China Sea, tropical North Atlantic, and western South Pacific) (Bonnet et al., 2018; Stenegren et al., 2018; Wen et al., 2022). *Trichodesmium* also employs a number of mechanisms to alleviate P limitation, including increased phosphate and DOP uptake, as well as reduced requirements for cellular P (Sohm et al., 2011). Conversely, UCYNs may be more competitive than *Trichodesmium* in regions with lower Fe supply. This and several potential explanations have been proposed for why UCYNs dominate the diazotrophic community across the NPSG (Church et al., 2009; Gradoville et al., 2020; Moisander et al., 2010; Turk-Kubo et al., 2021). In addition to having a higher surface-to-volume ratio that favors Fe uptake (Hudson & Morel, 1990), *Crocosphaera* may employ a repertoire of Fe conservation strategies, for example, daily synthesis and breakdown of metalloproteins to recycle Fe between the photosynthetic and N_2 fixation metalloenzymes and increased expression of flavodoxin at night (Saito et al., 2011).

Other environmental factors, such as temperature and light intensity, may also affect diazotroph distribution. Field observations have demonstrated that the optimal temperatures for both *Trichodesmium* and *Crocosphaera* are approximately 27–30°C (Church et al., 2009; Moisander et al., 2010), while UCYN-A has a lower optimal temperature of ~24°C (Church et al., 2009; Moisander et al., 2010; Shiozaki et al., 2014), making it more competitive with other diazotrophs in cooler seasons or regions of the NPSG (Church et al., 2009; Gradoville et al., 2020; Shiozaki et al., 2014). At Station ALOHA, high light intensity together with abundant P and Fe supply in the early summer may stimulate DDA blooms (Follett et al., 2018). Studies have also suggested that top-down controls on different groups of marine diazotrophs are potentially important. For example, at the global scale, *Trichodesmium* may be under a weak but stable degree of top-down control, while the degree of top-down control on UCYNs varies substantially over space and time (H. Wang & Luo, 2022). Finally, NCDs, which are frequently found in

the NPSG, appear to occupy different environmental niches from those of phototrophic cyanobacteria (Cheung et al., 2021; Shao & Luo, 2022), further hindering explanations of the observed distribution of N_2 fixation.

4.5. Fate of Diazotroph-Derived Nitrogen

The fate of diazotrophs and their newly fixed N (termed diazotroph-derived N, diazotroph-derived nitrogen [DDN]) remain mostly unknown (Bonnet, Baklouti, et al., 2016; Mulholland, 2007). Multiple mechanisms potentially involved in DDN release include direct release from diazotrophs (Mulholland & Capone, 2001), viral-induced cell lysis (Hewson et al., 2004), grazing (Dugenne et al., 2020; O'Neil et al., 1996), and programmed cell death or apoptosis (Berman-Frank et al., 2004). The total fraction of DDN release is highly variable, ranging from 0% to 97% (Mulholland, 2007). The relative contribution of each mechanism exhibits large spatiotemporal variability and differs among individual species or groups, and this remains difficult to quantify. Even less is known about the dynamics and factors that regulate DDN release. Nevertheless, the fraction of DDN released appears to be higher in the field than in laboratory cultures (Bonnet, Berthlot, Turk-Kubo, et al., 2016) and might be tightly linked to the physiological state of diazotrophs and enhanced environmental stressors such as nutrient or light limitation (Y. Lu et al., 2018).

The transfer of DDN from diazotrophs to non-diazotrophic plankton and/or other diazotrophic counterparts is even more difficult to track due to the instantaneous uptake of the released DDN by diverse plankton. Earlier lines of evidence on the transfer of DDN mainly come from the depleted δ^{15}N-PON in collected zooplankton or sediment trap materials (Capone et al., 1997; Karl et al., 2002; Landrum et al., 2011), a significant positive correlation between the N_2 fixation rate and bacterial productivity (Tseng et al., 2005), and the succession from *Trichodesmium* blooms to diatom and dinoflagellate blooms (Walsh & Steidinger, 2001), suggesting transfer of DDN to zooplankton, heterotrophic bacteria, and non-diazotrophic phytoplankton. However, such results are unable to disentangle the potential multiple short-term transfer processes and distribution of DDN to different plankton in the field. Moreover, studies on DDN transfer have largely focused on *Trichodesmium*, while those on other diazotrophs are more limited. Emerging evidence has further shown that the prominent unicellular diazotroph *Crocosphaera* has advantages in competing with other phytoplankton for bioavailable N, indicating a potential pathway of DDN transfer from other diazotrophs to *Crocosphaera* (Masuda et al., 2022).

A breakthrough in disentangling the complex process of DDN transfer has come from the combined use of flow cytometric sorting and isotopic analysis of different planktonic groups at the single-cell level, which provide robust estimates of the complex transfer and partitioning of DDN to multiple non-diazotrophic compartments (Bonnet, Baklouti, et al., 2016). Subsequent use of this new approach in the subtropical South Pacific reveals that the release and transfer of DDN to non-diazotrophic picophytoplankton is negligible in DDAs (Bonnet, Berthelot, et al., 2016) but is rapid and highly efficient in *Crocosphaera*-dominated systems (Bonnet, Berthlot, Turk-Kubo, et al., 2016; Caffin et al., 2018). A substantial part of DDN has also been found to be transferred to zooplankton through grazing on unicellular diazotrophs (Hunt et al., 2016) or transferred to bacteria (Caffin et al., 2018). Future application of this state-of-the-art technology in other subtropical gyres thus holds great promise for addressing the underlying mechanism of how N_2 fixation contributes to carbon sequestration via the biological pump.

A review of the above studies reveals large spatial and seasonal variations in N_2 fixation in the NPSG, which, due to infrequent and spatially sparse sampling, prevents a complete understanding of controlling factors (Letelier et al., 2019). Many studies of N_2 fixation in the NPSG focus on Station ALOHA, while studies in other regions, particularly in the western NPSG, remain rare. Nevertheless, our analyses show that N_2 fixation rates, controlling factors, seasonal patterns, and associated biogeochemical characteristics in the western NPSG can differ from those at Station ALOHA.

5. Metabolic Structure of the Euphotic Zone in Subtropical Gyres

5.1. Conceptualization of a Two-Layered Vertical Structure

The EZ in subtropical gyres shows a complex structure in terms of its physics, chemistry and biology. As early as 1967, Dugdale (1967) separated the EZ into a nutrient-limited and a light-limited layer. The two-layered framework has since been gradually recognized as a more appropriate paradigm than a single layer to investigate

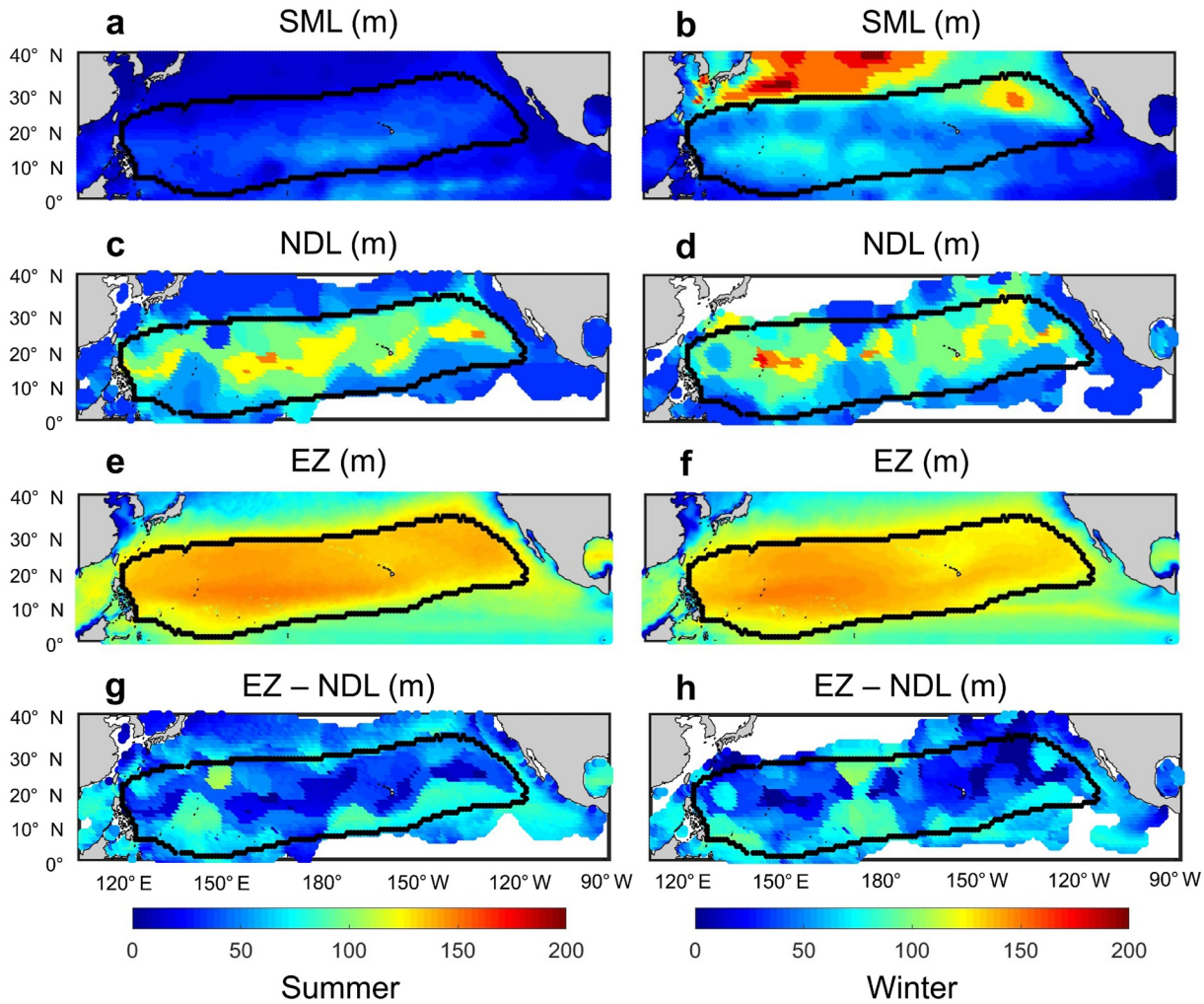

Figure 14. Spatial and seasonal (summer, left panels; winter, right panels) distributions of critical vertical depths in the North Pacific Subtropical Gyre (NPSG): the bottom depths (m) of the (a, b) surface mixed layer (SML), (c, d) nutrient-depleted layer (NDL), (e, f) euphotic zone (EZ), and (g, h) comparison of the NDL and EZ (bottom depth of EZ minus bottom depth of NDL). The bottom of the SML is defined as the depth where the potential density differs from that at 10 m by 0.125 kg m^{-3}. The bottom of the NDL is defined at the depth where the vertical gradient of NO_x concentration exceeds 8 nmol L^{-1} m^{-1} (the white area denotes NO_x concentrations higher than 1 μmol L^{-1} throughout the whole water column). The depth of EZ is defined as where usable solar radiation is 1% of the surface (data from Wu et al. (2021)). Density and NO_x data are calculated or obtained from the World Ocean Atlas (WOA2018; https://www.nodc.noaa.gov/OC5/woa18/).The solid black lines represent the boundaries of the NPSG using the criterion of Chl-*a* concentration ≤0.1 mg m^{-3}. See Box 1 for the definition of the NDL and EZ depths.

the vertical structure of biogeochemical features of the EZ, particularly in oligotrophic oceans (see Section 1). Compared to its lower part, the upper EZ is characterized by the following features (see Section 2): higher temperature, sufficient light availability (Dave & Lozier, 2010; Dugdale & Goering, 1967), lower macronutrient concentrations (Cavender-Bares et al., 2001; Karl & Lukas, 1996; Karl, Björkman, et al., 2001; Painter et al., 2013), and generally higher concentrations of organic matter (Hashihama et al., 2020; Reynolds et al., 2014). The upper EZ also features negligible diffusive and diapycnal nutrient fluxes due to minimal nutrient gradients (Du et al., 2017; Karl & Lukas, 1996; Villareal et al., 2014) but higher rates of primary production (Letelier et al., 1996; Siegel et al., 2001) and lower POC scavenging revealed by longer dissolved ^{234}Th residence times (Coale & Bruland, 1987). Moreover, the upper EZ is typically the dominant zone of N_2 fixation (see Section 4) with variable phytoplankton community structure (Venrick, 1993) and very active microbial activities (Karl, 2002a).

Without a clear conceptual basis, many studies have distinguished the two layers in the EZ by the base of the SML (e.g., Dave & Lozier, 2010; Hashihama et al., 2020). Within subtropical gyres such as the NPSG, the SML is often shallow due to strong stratification and is found above the top of the nutricline (Figures 14a–14d). At Station ALOHA, the top of the nutricline is typically located ~70 m below the SML (Dore et al., 2008; Karl &

Box 1. Definition of the nutrient-depleted and nutrient-replete layers

The precise constraint of the NDL and NRL in oligotrophic oceans depends on the depths of the EZ and the top of the nutricline. The EZ is a layer of water where light is sufficient to support positive net primary production (Falkowski, 1994). In other words, the base depth of the EZ (Z_{eu}) is the compensation depth (Z_c), where the rate of photosynthesis equals the rate of respiration (Sverdrup, 1953). Conventionally, for easier determination, Z_{eu} is defined, or assumed to be the depth of 1% surface photosynthetically active radiation (PAR, 400–700 nm) (Ryther, 1956), a definition widely used over the past five decades. However, at the very beginning, Ryther (1956) warned that it "has no biological significance other than defining the water mass below which no appreciable photosynthesis can occur." Indeed, it has been the subject of debate that this conventional Z_{eu} of 1% surface PAR apparently did not match Z_c (Banse, 2004; J. F. Marra et al., 2014). Z. Lee et al. (2014) defined a new radiometric term named usable solar radiation (USR) to represent the spectrally integrated solar irradiance in the window of 400–560 nm, the domain where photons penetrate the most in oceanic waters and thus contribute to photosynthesis at deeper depths. A recent analysis using a large data set covering waters in the tropics, subtropics and temperate regions found that the depth of 1% surface PAR is too shallow (by ∼16%) compared to Z_c, suggesting that the depth of ∼1% surface USR could offer a promising alternative to determine EZ depth (Wu et al., 2021). We therefore adopt this new definition for the determination of EZ depth in the present paper (Figures 14e and 14f).

There are several proposed criteria to identify the top of the nutricline or bottom of the NDL. Studies have used a depth of fixed NO_x concentrations, such as 2.0 μmol L^{-1} (Wilson & Coles, 2005), 0.5 μmol L^{-1} (Cianca et al., 2007), 0.1 μmol L^{-1} (Painter et al., 2013; Winn et al., 1995), and 0.05 μmol L^{-1} (Bouruet-Aubertot et al., 2018), while others used the depth of maximal nutrient gradient (Fernandez et al., 2005). Letelier et al. (2004) also used the shallowest depth at which the vertical gradient of NO_x concentration exceeds 2 nmol kg^{-1} m^{-1} as the top of the nutricline. These studies suggest that the optimal criteria for identifying the top of the nutricline vary across the studied regions and data sources. In our study, using the WOA2018 data, we discovered that a criterion of a vertical NO_x gradient higher than 8 nmol kg^{-1} m^{-1} best identified the top of the nutricline in the NPSG (Figures 14c and 14d). However, this determination may be subject to uncertainties stemming from noise in the NO_x profiles and the low sampling resolution of WOA2018 in the EZ.

Finally, the NRL is defined here as the region extending from the top of the nutricline to the base of the EZ.

Lukas, 1996). This feature significantly constrains diapycnal nutrient fluxes from the nutricline to the surface waters.

The traditional paradigm is that oligotrophic conditions in subtropical gyres result in low primary productivity and strong competition for nutrients such as N and P among autotrophs and heterotrophic bacteria (Duarte et al., 2013). Overall, the rapid recycling of nutrients and organic matter in the EZ of subtropical gyres yields low fluxes of particulate matter to depth and therefore low efficiency of the biological pump. Compared to productive waters where e-ratios can be up to ∼50%, they are <10% in oligotrophic regions (Karl et al., 2021) and often near 5% in subtropical oceans (Weber et al., 2016). At Stations ALOHA and BATS, the e-ratios at 150 m lie in the range of 2%–15% (Karl et al., 2012; Steinberg et al., 2001). Moreover, the upper EZ has been considered to have minimal supply of new nutrients and hence the productivity therein mainly depends on nutrient recycling, while the lower EZ has been considered predominantly responsible for new production (Coale & Bruland, 1987; Small et al., 1987).

However, this paradigm of low export from the upper euphotic layer has been challenged. Phytoplankton blooms above the nutricline in the northeastern NPSG are often observed in summer and associated with strong stratification (e.g., Dore et al., 2008); thus, sinking organic particles can originate from the surface in subtropical gyres (Dore et al., 2002; Scharek, Latasa, et al., 1999; Scharek, Tupas, & Karl, 1999). The ^{234}Th method also reveals

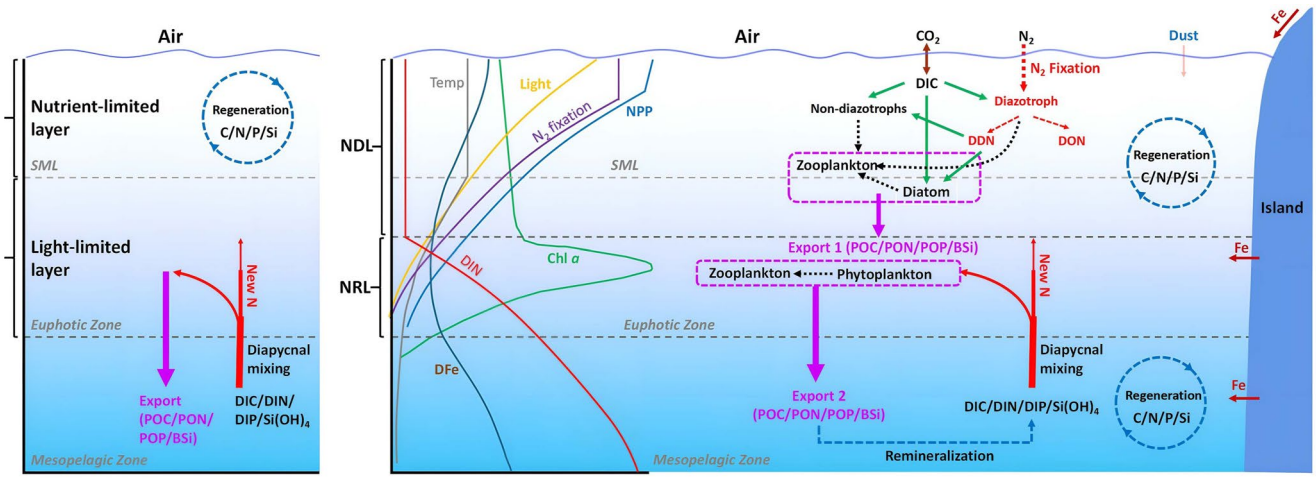

Figure 15. The traditional (left panel) and reframed (right panel) two-layered structure of upper ocean biogeochemistry in oligotrophic gyres. In the left panel, the surface mixed layer divides the euphotic zone (EZ) into the upper nutrient-limited layer and the lower light-limited layer. In the right panel, the top of the nutricline divides the EZ into the upper nutrient-depleted layer and the lower nutrient-replete layer. Vertical profiles of temperature (Temp), light intensity, concentrations of dissolved inorganic nitrogen (DIN), dissolved iron (DFe) and chlorophyll-*a* (Chl-*a*) concentrations, and rates of N_2 fixation and net primary production are schematically shown, as well as major processes and elemental cycles considered in this paper. DIC, DIN, and DIP: dissolved inorganic carbon (C), nitrogen (N), and phosphorus (P); $Si(OH)_4$: dissolved silicate; POC, PON, and POP: particulate organic C, N, and P; BSi: biogenic silica (Si); DON: dissolved organic N; and DDN: diazotroph-derived nitrogen.

significant export from a depth of 50 m at Station ALOHA (Benitez-Nelson et al., 2001), with N_2 fixation mostly occurring above this depth (Böttjer et al., 2016). Diazotrophs can thus directly or indirectly contribute to particle export and drive summer export pulses at Station ALOHA (see Section 4). These results imply that the previously used two-layered structure based on SML depth is incapable of describing nutrient sources, primary production, and subsequent carbon export processes, thereby calling for an improved conceptual model to better elucidate the distinct physical, chemical, and biological properties of the EZ in oligotrophic subtropical gyres.

To develop an improved conceptual model of upper ocean biogeochemistry and, in particular, to strengthen the link between nutrient sources and carbon export in oligotrophic oceans, we propose an alternative two-layered framework in which the EZ is vertically categorized into two regimes based on the nutricline, with the upper EZ above the nutricline as the NDL and the lower EZ as the NRL between the top of the nutricline and the base of the EZ (Du et al., 2017) (Figure 15). This framework highlights distinctions between the NDL and NRL in terms of physical settings, nutrient sources and stoichiometry, ecosystem compositions, and primary production.

Phytoplankton photosynthesis depends on the interaction between ambient solar radiation and phytoplankton absorption spectra. While the former varies, the latter is primarily centered at a spectral band in the blue domain at approximately 440 nm with a bandwidth of ~40 nm. Thus, for the same light intensity, blue light has significantly higher contributions to photosynthesis, indicating that light quality is also important for phytoplankton productivity (Sathyendranath & Platt, 1989). While light intensity is significantly greater in the NDL due to the exponential reduction in solar radiation with depth, light quality also shifts from "white" at the surface to light blue in the upper 30 m and deep blue at the bottom of the NRL in the NPSG (Z. Lee et al., 2022), which is then more favorable for photosynthesis.

The NDL often features high levels, and sometimes even the majority, of primary productivity in the EZ (see Section 2), along with considerable net community productivity and/or export production. This could partly be the result of new N being introduced into the NDL, such as biological N_2 fixation, atmospheric deposition, and lateral transport. As low Fe and/or P supply can limit N_2 fixation (see Section 4), their source strengths may determine the amount of carbon exported from the NDL. In the NRL, however, carbon export can be driven by the nutrients supplied from greater depths and is commonly observed to be tightly coupled with the DCM (Ma et al., 2023).

Owing to their efficient nutrient acquisition and light capture, picophytoplankton are the main contributors to phytoplankton biomass and primary productivity in the oligotrophic ocean (see Section 2). Much of the primary

productivity by picophytoplankton can be maintained by rapid nutrient recycling via microbial food webs (Karl, 2002b). Due to differences in the organismal traits of phytoplankton, community structure differs markedly throughout the water column. Even for the same species, different ecotypes show distinctive vertical distributions (Z. I. Johnson et al., 2006). *Prochlorococcus* is present from the surface to a depth of ~150 m between 40°N and 40°S (Flombaum et al., 2013) and is absent at temperatures below 15°C (Z. I. Johnson et al., 2006); thus, it is distributed throughout the EZ in subtropical gyres. In contrast, *Synechococcus* resides primarily in the NDL under high temperature and light conditions (Partensky et al., 1999). Due to the larger cell sizes of photosynthetic eukaryotes, their contribution is much more significant to carbon biomass than to total cell abundance (C. Li et al., 2022; Worden et al., 2004). Diatoms, having overall low-standing stocks in the NDL, have been recognized as significant players in POC export when they are associated with diazotrophs (Kemp & Villareal, 2013; Scharek, Latasa, et al., 1999). In addition, diatoms and other picoeukaryotes could be rapidly exported not only because they are larger and have higher densities but also because they are usually abundant at the bottom of the NRL with relatively abundant nutrients (Delhez & Deleersnijder, 2010).

Such nutrient-dependent phytoplankton composition not only regulates the efficiency of the biological pump but also exerts profound control on N regeneration processes. Phytoplankton are more competitive than nitrifiers in accessing ammonium in the NDL (Wan et al., 2018). However, this relationship is reversed in the NRL, where the affinity of phytoplankton toward ammonium decreases under elevated ambient nitrate concentrations, and phytoplankton can assimilate nitrate as the primary N source, creating a niche for ammonia oxidizers to access trace amounts of ammonium (Wan et al., 2018; Zakem et al., 2018). Likewise, more recent observations on the competition of phytoplankton and nitrite oxidizers for nitrite reveal a similar nutrient-dependent mechanism in controlling the cycling of nitrite in the EZ (Wan et al., 2021). Such findings provide support for our reframed two-layered structure in articulating the distinct cycling and distribution of key nutrients in the NDL and NRL.

5.2. Spatial and Seasonal Variations in the NDL and NRL in the NPSG

The bottom depth of the SML in the NPSG exhibits marked seasonal variations, being mostly shallower than 50 m in summer, increasing to as deep as 150 m in winter (Figure 14). The NDL in the NPSG is mostly located in the upper 120 m and its thickness varies both spatially and seasonally (Figures 14c and 14d). During winter, a significant expanse outside the NPSG experiences nutrient replenishment, leading to the disappearance of NDL (Figures 14c and 14d). The SML is mostly shallower than the NDL, particularly in the central NPSG (Figures 14a–14d) with the exception of the northeastern NPSG in winter when strong mixing deepens the SML to 150 m. The depths of the EZ range from 100 to 150 m, most often deepest in the central NPSG, and are relatively stable seasonally (Figures 14e and 14f). The two-layered framework is present in most regions of the NPSG (Figures 14c–14f). In certain regions in the central NPSG, physically driven water convergence can deepen the nutricline to close to the bottom of the EZ (Figures 14c–14f) and the thickness of NRL can become very thin (Figures 14g and 14h). It is noteworthy that this two-layered structure has also been observed in the EZ of the NASG (Painter et al., 2013).

At Station ALOHA, the monthly mean bottom depth of the SML ranges between 36 in May and 90 m in January. That of the NDL, ranging between 97 and 114 m, is notably deeper than that of the SML, particularly in summer. In the NDL, NO_x and phosphate concentrations are consistently low throughout the year (Figures 10e, 10f, and 16). The bottom of the EZ is on average 155 and 126 m deep in summer and winter, respectively, and it is deeper than the NDL, particularly in summer. The DCM is generally located immediately below the NDL (i.e., at the top of the NRL) throughout the year.

5.3. Partitioning of New Nutrient Sources in the NDL and NRL

5.3.1. Nutrient Sources to the NDL

N_2 fixation has been established as a significant source of new N to the vast subtropical gyres (see Section 4). At Station ALOHA in the eastern NPSG, N_2 fixation (estimated to average 41 mmol N m^{-2} yr^{-1}) contributes 14% of the N requirement for NCP (K. S. Johnson et al., 2010). In the western NPSG, the N_2 fixation rate (81 mmol N m^{-2} yr^{-1}) is an order of magnitude higher than the diffusive supply (3.9 mmol N m^{-2} yr^{-1}) into the top 100 m of the water column (Hashihama et al., 2021).

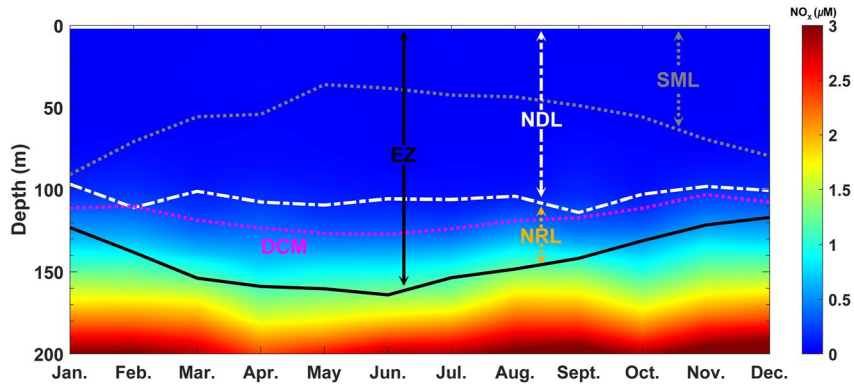

Figure 16. Depth of the surface mixed layer, nutrient-depleted layer (NDL), deep chlorophyll maximum, nutrient-replete layer, and euphotic zone (EZ) at Station ALOHA. The depth of the NDL is defined as where the NO_x concentration equals 0.1 μmol L^{-1} and the depth of the EZ is calculated using 1% of the surface usable solar radiation (USR; see Box 1). The background shows the monthly climatology of NO_x concentrations. Density, chlorophyll-*a* and nutrient data are from https://hahana.soest.hawaii.edu/hot/hot-dogs/. USR data are from Wu et al. (2021).

The second obvious new nutrient source is the atmospheric deposition of N and P (see Section 2). Currently, studies on the atmospheric deposition of N and P to the NPSG and its impact on marine ecosystems are still restricted to their fluxes to the surface water (i.e., the NDL) and the resultant magnitude of carbon export; however, the fate of the atmospheric nutrients in the water column remains largely underexplored. The magnitude and mechanism for their transport and release to the NRL have yet to be assessed.

Other sources of nutrient inputs to the NDL include lateral transport of DON and DOP (see Section 2), which are enriched by orders of magnitude in the NDL of subtropical gyres (Letscher et al., 2016; Reynolds et al., 2014). However, quantitative estimation of these fluxes and their contributions to NCP remain debated (Hashihama et al., 2021; Letscher et al., 2016).

5.3.2. Nutrient Sources to the NRL

The diapycnal flux of nutrients across the base of the EZ is expected to be the most important supplier to the NRL (see Section 2), but few of these nutrients reach the NDL due to its strong stratification and low nutrient gradients. Nutrient supply from convective mixing should be small in the NPSG because the SML is rarely found to reach the nutricline (Figure 14, Dave & Lozier, 2010). The salt fingering effect can also be important and has been found to account for ∼20% of nitrate diffusive fluxes in some regions of oligotrophic oceans (Fernandez-Castro et al., 2015).

The N:P molar ratio of the dissolved inorganic nutrient pools is near 14:1 in the NRL of the NPSG and is largely controlled by the near-Redfield stoichiometry of nutrient fluxes (N:P = ∼14) to the NRL from the subsurface layer (Hashihama et al., 2021; K. S. Johnson et al., 2010; Karl, Björkman, et al., 2001). In contrast to inorganic nutrients, dissolved organic nutrients contribute to downward material fluxes through turbulent mixing. DON in the NDL can be transported to the NRL, where it is degraded to inorganic N that may support production for export (Letscher et al., 2013). Additionally, the sinking of POM from the NDL and its subsequent remineralization in the NRL have rarely been investigated and warrant further studies in the future.

Overall, the nutrient sources, fluxes, and stoichiometry involved in the NRL are distinct from those in the NDL.

5.4. Partitioning of Carbon Export in the NDL and NRL

In general, areal export production in subtropical gyres is low due to low primary production and low ratios of export to primary production. Quantification of export partitioning between NDL and NRL has been rare (Ma et al., 2023). Taking advantage of the higher number of observations at Station ALOHA, a handful of studies have found that export fluxes can sometimes be enhanced in the NDL, as indicated by large deficits in ^{234}Th relative to ^{238}U (Figure 17, Benitez-Nelson et al., 2001; Umhau et al., 2019). Such high export events may be induced by high N_2 fixation rates, particularly mediated by DDAs (see Section 4). In addition, the ^{15}N signal in sinking

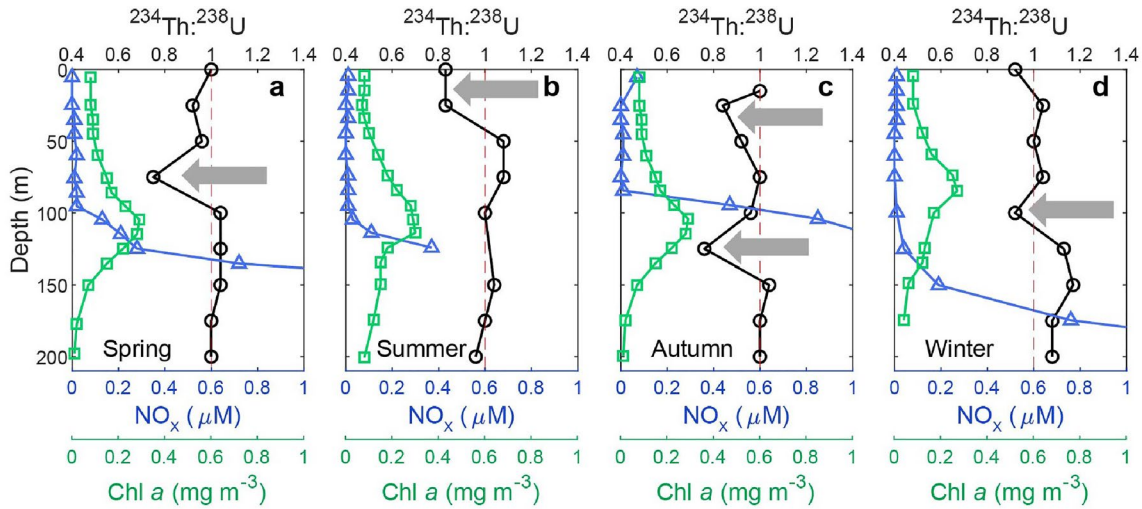

Figure 17. Vertical profiles of the total ^{234}Th: ^{238}U ratio at Station ALOHA in (a) spring, (b) summer, (c) autumn, and (d) winter. Profiles of the concentrations of nitrate + nitrite (NO_x) and fluorescence-based chlorophyll *a* (Chl *a*) are also shown (spring: May 1999; summer: July 1999; autumn: September 2014; and winter: February 2000). The arrows represent export hotspots in the euphotic zone. The ^{234}Th data were reprocessed based on Benitez-Nelson et al. (2001) and Umhau et al. (2019). The Chl-*a* and NO_x data were downloaded from Hawaii Ocean Times-series (https://hahana.soest.hawaii.edu/hot/hot-dogs/).

particles collected at the bottom of the EZ has shown that 26%–47% of the export flux could be supported by N_2 fixation (Böttjer et al., 2016), suggesting that the bulk of sinking particles might be derived from the NDL.

The export from the NDL is further supported by large-scale modeling studies. In the NPSG and NASG, organic P in the surface waters can sustain 30%–80% of total organic carbon export (Letscher et al., 2016; Torres-Valdés et al., 2009), with elevated ratios in the western part of each basin. Annually, N_2 fixation in the NDL can sustain ~30% of the total carbon export averaged over all the subtropical gyres, and this contribution can exceed 50% in the NPSG and NASG (W. L. Wang et al., 2019).

During periods of low N_2 fixation rates, however, high export could occur in the NRL near DCM fed by nutrient inputs from below (Figure 17c, Letelier et al., 2004). We thus conclude that the relative contributions from N_2 fixation, lateral nutrient transport, and subsurface nutrient supply determine the vertical structure of the export fluxes in the NPSG, as discussed further below.

Although surface nutrient concentrations in the NPSG are uniformly low, limited field observations have revealed that export fluxes are spatially variable (Umhau et al., 2019). Along a transect of 155°W in the eastern NPSG, export flux gradually increased from the center of the NPSG to the equator (Figure 18), similar to that observed in the NASG (Thomalla et al., 2006). Note that the export at Station ALOHA, particularly in summer (>30 mg C m^{-2} d^{-1}), appears higher than that reported at other stations along 155°W in the NPSG (<10 mg C m^{-2} d^{-1}) (Figure 18). This higher export at Station ALOHA could be partly caused by the summer DDA blooms (see Section 4), which have not been reported at other stations along 158°W. The comparable POC fluxes estimated at the bases of the NDL and EZ at Station ALOHA and other stations in the NPSG (Figure 18b) potentially suggest that a large fraction of export may originate from the NDL. Due to the considerable spatial and temporal variability, a comprehensive estimate of the export flux and high-resolution sampling are needed for the entire NPSG.

5.5. Processes Mediating Export in the Two-Layered Structure

Subtropical gyres are generally known for their low export efficiency and strong temporal (and likely also spatial) decoupling between primary and export production that is modulated by a suite of complex physical, chemical, and biological processes. These factors determine how the organic matter produced by phytoplankton ultimately forms sinking particles and DOM and what fraction escapes remineralization to be exported out of the EZ. The primary causes could be the predominance of small picophytoplankton (Campbell & Vaulot, 1993; Rii et al., 2016) that are grazed at approximately the same rate as they grow and a background phytoplankton

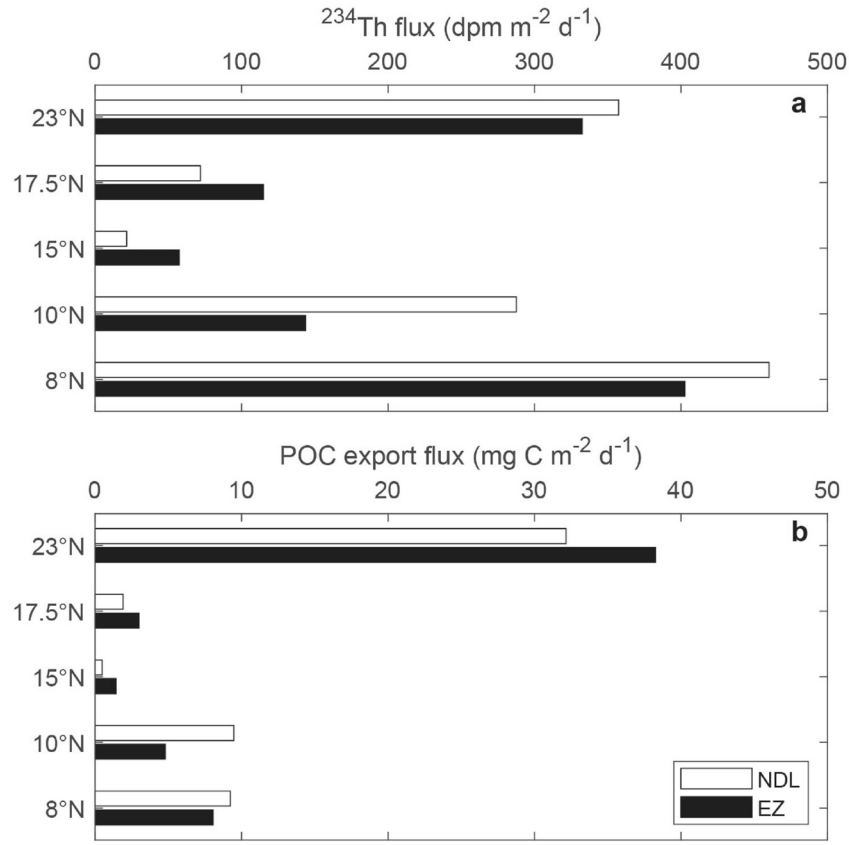

Figure 18. (a) One-dimensional steady-state ^{234}Th and (b) particulate organic carbon (POC) fluxes at the base of the nutrient-depleted layer and euphotic zone along 155°W in the North Pacific Subtropical Gyre (data reprocessed from Umhau et al. (2019)). Note that the data at 23°N are from Station ALOHA located at 158°W. POC fluxes are calculated by multiplying ^{234}Th flux with POC:^{234}Th ratios that are measured in trap-collected sinking particles at 150 m.

community composition that generally lacks ballasting by dense mineral shells (silica and calcium carbonate) (Letelier et al., 1993), although DDAs in the NDL or diatoms at the lower NRL can sometimes stimulate export production.

Multiple mechanisms—supported by observations—have been proposed to boost the carbon export potential of these low-efficiency systems. First, the dominant small phytoplankton can aggregate, enhancing their sinking (Lomas & Moran, 2011; Richardson & Jackson, 2007). Lomas and Moran (2011) estimated that ungrazed *Prochlorococcus* and *Synechococcus* contributed 1%–20% and 2%–13% of sinking POC fluxes at the BATS, respectively. Second, grazer consumption of small phytoplankton can produce larger, denser fecal particles that sink more readily (Goldthwait & Steinberg, 2008). In addition, diel migrant zooplankton graze during the night and migrate to deeper layers where they respire carbon and produce fecal pellets, contributing an active carbon pool for export (Al-Mutairi & Landry, 2001). Third, periodic nutrient entrainment can rapidly enhance the growth of larger, faster-growing phytoplankton in oligotrophic gyre systems, where their proliferation can significantly outpace grazing pressure (Browning et al., 2022), and these larger cells sink more efficiently (P. Tréguer et al., 2018). Similarly, nutrient injection from depth to DCM depths can enhance the background contribution of diatoms (Kemp & Villareal, 2013). This enhancement can be several orders of magnitude within cyclonic eddies that result in shoaling of nitraclines toward the surface (Benitez-Nelson et al., 2007). Fourth, conditions of low nitrate supply relative to an enhanced supply of Fe may allow for the establishment of diazotrophs, potentially forming intense blooms and contributing to export from the NDL (see Section 4). Recent research has shown that cyanobacterial and diverse NCDs are abundant in sinking particles at 150 m in the NPSG in the summer (Farnelid et al., 2019).

As described above, common processes operate throughout the entire EZ water column, whereas distinctions between NDL and NRL also exist. It remains largely unclear how N_2 fixation in the NDL fuels biological productivity in both the NDL and NRL and contributes to export production. Diazotrophs typically account for only a small fraction of plankton biomass (<10% in oligotrophic oceans) (Mills & Arrigo, 2010). Their direct contribution to export production is also limited (Walsby, 1992), except for some export pulses during the decay of diazotroph blooms (Bonnet, Baklouti, et al., 2016; Caffin et al., 2018) or sinking of DDAs (see Section 4). In parallel, nitrate isotopic analysis reveals a ubiquitous $\delta^{15}N$ minimum at the base of the EZ in subtropical gyres, which is interpreted as regenerated nitrate sourced from N_2 fixation (Knapp et al., 2005; J.-Y. T. Yang et al., 2022). These results indicate that a large fraction of DDN in the NDL must be released and recycled in both the NDL and NRL before its export.

Nevertheless, two fundamental differences associated with export pathways are nutrient levels and phytoplankton composition between the NDL and NRL (Figure 15). The picoplankton-dominated community in the NDL (see Section 2) contributes relatively little to the downward export flux, as indicated by ^{234}Th analysis (Benitez-Nelson et al., 2001). In the NRL, although its contribution to the total biomass and productivity may be less than that of prokaryotic groups, eukaryotic phytoplankton play an important role in elemental biogeochemical cycling. Generally, large diatoms are relatively more abundant at the DCM in the NRL, and they may elevate export owing to their fast-sinking speed. Indeed, diatom abundance was found to be disproportionately higher in sediment traps than in the water column (Scharek, Latasa, et al., 1999). Diatoms can be functionally classified into two groups: carbon-sinkers (Group 1) and Si-sinkers (Group 2) (P. Tréguer et al., 2018), and Endo et al. (2018) used molecular techniques to reveal a predominance of the pennate diatoms *Pseudo-nitzschia* and *Mastogloia* in the NPSG during summer, both of which are generally heavily silicified (i.e., Si-sinkers). B. Li et al. (2013) reported that prymnesiophytes (haptophytes) and pelagophytes appeared to capitalize on the relatively nutrient-enriched but low-light conditions characteristic of the NRL. The abundance and composition of these eukaryotic phytoplankton in subtropical gyres vary greatly in response to physical and chemical environmental changes (e.g., N supply; Rii et al., 2018, 2022).

The two-layered framework calls for high-resolution vertical samplings in the EZ and introduces challenges and opportunities in modeling regional and global oceanic biogeochemistry. Distinctions between the NDL and NRL of subtropical gyres pose additional challenges in the conceptualization and parametrization of already complex upper ocean processes. With the addition of N_2 fixation and variable plankton stoichiometry, we are not very far away from understanding many of the observed patterns. Differences in all aspects of the NDL and NRL, including the physical settings and chemical and biological conditions (including their feedbacks), would require different parameterizations with much higher vertical resolutions in the upper ocean than the present numerical models allow.

6. Long-Term Variability

The temperature of Earth's surface has risen by 1.09°C since preindustrial times and is projected to rise by 1.0–5.7°C by the end of this century depending on different scenarios of greenhouse gas emissions (IPCC, 2021). Warming of the ocean should lead to increased upper ocean stratification and shallower mixing, with corresponding decreases in the vertical supply of nutrients. Such changes, which specifically decrease nutrient delivery to the upper ocean, should result in declines in marine primary productivity and phytoplankton biomass (Behrenfeld et al., 2006; Boyce et al., 2010). Given the already low nutrient inventories, such warming-related dynamics are predicted to be most pronounced in subtropical gyres (e.g., Steinacher et al., 2010). As a result, the spatial extent of low chlorophyll waters characteristic of oligotrophic gyres appears to have already expanded (Polovina et al., 2008).

In this section, we quantify the long-term variability in physical and biogeochemical properties across the NPSG. The spatial extent of the NPSG varies over time (e.g., on a seasonal scale); as a result, we define the areal extent of the NPSG, as already discussed, based on the annual climatological Chl-*a* concentrations $\leq$0.1 mg m^{-3}. For most analyses, we remove seasonal signals by subtracting the climatological monthly mean values from the time-series data; the resulting anomalies provide insights into longer-term (e.g., interannual) variability.

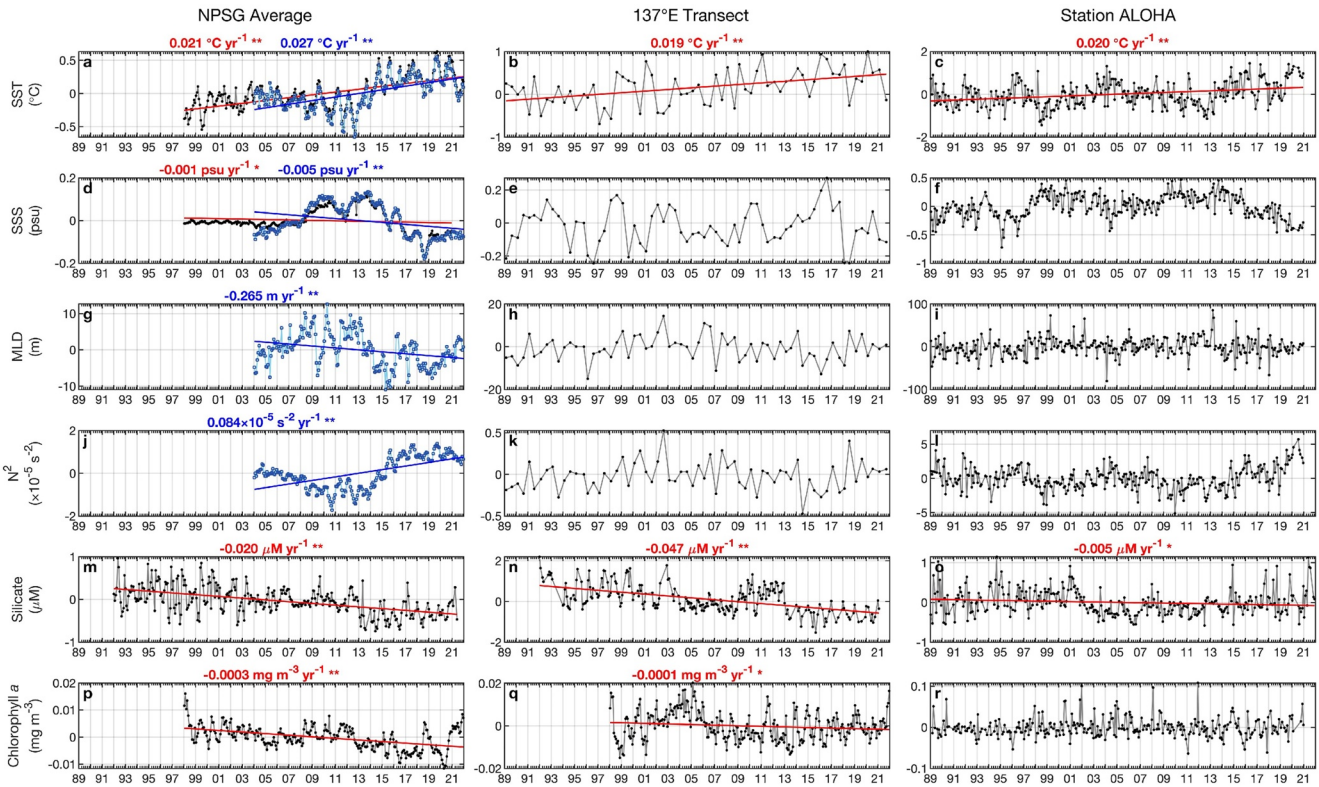

Figure 19. Long-term variability in (a–c) sea surface temperature, (d–f) sea surface salinity, (g–i) mixed layer depth (MLD), (j–l) thermocline stratification, (m–o) surface silicate concentrations, and (p–r) surface chlorophyll-*a* concentration in the North Pacific Subtropical Gyre (NPSG). Depicted are the anomalies (monthly mean value subtracted) of each property. The three columns of the panels, from left to right, are the results of the averages in the NPSG, of the averages along the 137°E transect, and at Station ALOHA. Only significant trendlines ($p < 0.05$) are plotted (solid red or blue lines), with the rates of the trends marked on top of each panel (*: $p < 0.05$; **: $p < 0.01$). All the data for Station ALOHA are from the Hawaii Ocean Times-series program (https://hahana.soest.hawaii.edu/hot/hot-dogs/). (a, d, g, and j) Black dots and their trends (red lines) are from satellite remote sensing data (https://www.oceancolour.org), and blue dots and their trends (blue lines) are from the Argo data (http://www.argo.org.cn/). (m, n) Silicate concentrations are from the same data sources as in Figure 8. (o) Silicate concentrations at Station ALOHA are near-surface (5 m) values. (j–l) Thermocline stratification is defined by bin-averaging (150 m below the MLD) squared buoyancy frequency (N^2). (r) Chlorophyll-*a* concentrations at Station ALOHA were measured by high-performance liquid chromatography.

6.1. Physical Properties

The SST in the NPSG was reported to increase at 0.012°C yr^{-1} between 1998 and 2013 (Signorini et al., 2015), and is higher (0.021°C yr^{-1}) when we extend the analysis period to 1998–2021 (Figure 19a). The rate is even higher (0.027°C yr^{-1}) if we focus on the later period (2004–2021) using Argo float measurements (Figure 19a). For the whole NPSG region, the sea surface salinity (SSS) has a negative trend based on either remote sensing data over 1998–2021 or Argo float data over 2004–2021 (Figure 19d). Using Argo float records, we find a shoaling trend of the MLD (−0.265 m yr^{-1}) accompanied by a trend of enhanced thermocline stratification (8.4×10^{-3} s^{-2} yr^{-1}) in the NPSG (Figures 19g and 19j). Our correlation analyses indicate that the shoaling of the MLD and increased thermocline stratification trends are likely determined by trends in both SST and SSS (Table 6). More detailed reviews of long-term variabilities in the physical properties of the NPSG can be found in Text S1 in Supporting Information S1.

To provide insights into the larger-scale dynamics associated with the trends described above, we examine the relationships between NPSG properties (i.e., SST, SSS, MLD, and buoyancy frequency) and various climate indices. This analysis reveals that low-frequency variations in the spatial area of the NPSG and its MLD appear partly driven by fluctuations in both the Pacific

Table 6
The Correlation Coefficients Between the Properties of the North Pacific Subtropical Gyre

	Area	SST	SSS	MLD	N^2
Area	1	0.52**	−0.31**	−0.55**	0.54**
SST		1	−0.41**	−0.65**	0.81**
SSS			1	0.42**	−0.82**
MLD				1	−0.47**
N^2					1

Note. The time series of the parameters are subtracted by the climatological monthly mean values before being analyzed (see text). Values of significant trends are marked by ** ($p < 0.01$). SST: sea surface temperature; SSS: sea surface salinity; MLD: mixed layer depth; and N^2: squared buoyancy frequency.

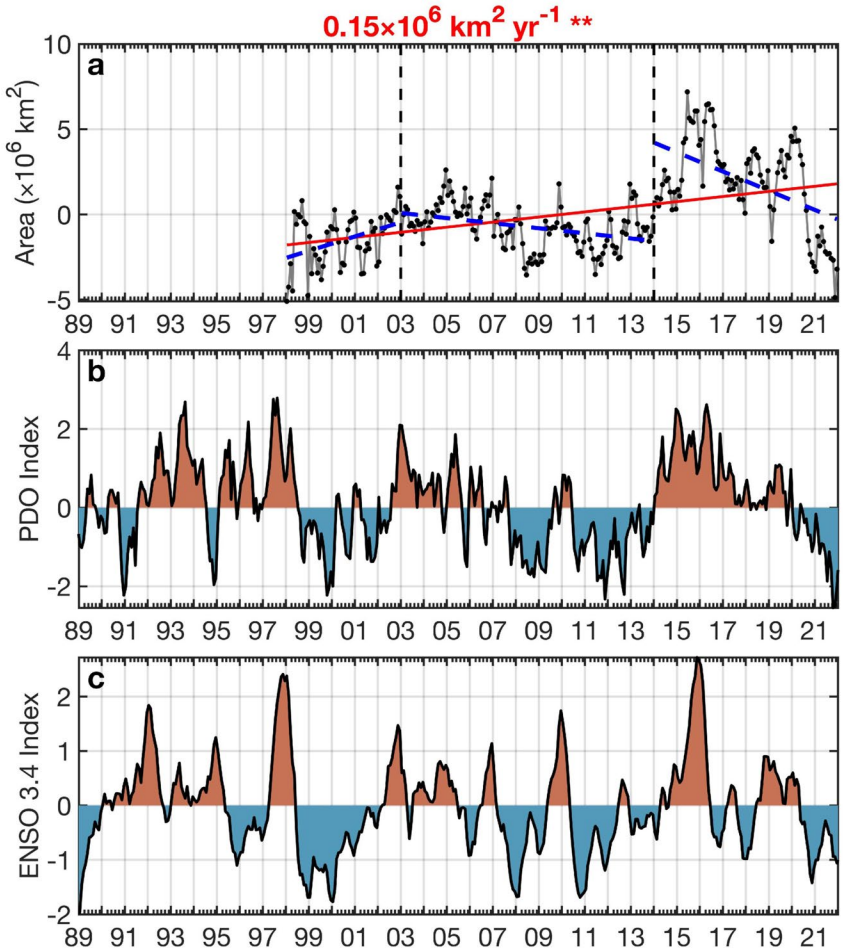

Figure 20. *Long-term changes in the estimated surface area of the North Pacific Subtropical Gyre (NPSG) and climate indices*. (a) The estimated area of NPSG is based on a threshold of satellite-derived Chl-*a* concentration of less than 0.1 mg m^{-3}. The trend over the whole period (solid red line, with the rate marked on top of the panel, $p < 0.01$) and during three subperiods (1998–2002, 2003–2013, and 2014–2020) (dashed blue lines) are overlaid. (b) Pacific Decadal Oscillation index and (c) Niño 3.4 index are from https://psl.noaa.gov/data/climateindices/list/.

Decadal Oscillation (PDO) and the El Niño-Southern Oscillation (ENSO) (Figures 20b and 20c and Table 7). Specifically, periods of shallower MLD, higher SST and intensified stratification (e.g., 2014–2019) appear to be associated with the positive phase of the PDO (Table 7, Figures 19 and 20b). Indeed, many of the significant long-term trends reported above seem to be driven by anomalous values associated with different PDO and/or ENSO phases. The relationship between these NPSG properties and climate indices serves as an important reminder that "long-term trends" depend on the period of observations, including those that may reflect variability in the sign of oscillations controlled by basin-scale processes.

Table 7
Correlation Coefficients Describing Relationships Between Various Properties of the North Pacific Subtropical Gyre and the Climate Indices

	Area	SST	SSS	MLD	N^2
PDO Index	0.55**	0.36**	−0.18**	−0.53**	0.37**
Niño 3.4 Index	0.45**	0.12*	−0.05	−0.44**	0.17*

Note. The time-series measurements of the parameters are subtracted by the climatological monthly mean values before being analyzed (see text). Values with significant trends are marked by * ($p < 0.05$) or ** ($p < 0.01$).

6.1.1. Station ALOHA and 137°E Transect

In addition to the gyre-averaged trends, we examined the long-term trends derived from the time-series measurements conducted at Station ALOHA and along a transect at 137°E. Somewhat unexpectedly, only SST demonstrates significant ($p < 0.01$) long-term trends, increasing by 0.020°C yr^{-1} at ALOHA and 0.019°C yr^{-1} along 137°E (Figure 19). This suggests spatial heterogeneity in terms of the long-term trends or oscillations for SSS, SML, and stratification in the NPSG. This spatial heterogeneity may also be caused by differences in the measurements: the parameters analyzed for the NPSG

average are derived from satellite remote sensing or drifting floats, while the measurements at Station ALOHA and along 137°E are ship-based, Eulerian time series.

6.2. Macronutrients

Long-term trends in upper ocean nutrient concentrations in subtropical gyres are poorly constrained owing to a scarcity of long-term records at multiple sites spread across such geographically expansive systems (Bindoff et al., 2019). Synthesis of data from observations made on research cruises transecting subtropical gyres as well as repeat observations at Station ALOHA and BATS show a mixture of intra-annual to sub-decadal scales of variability in surface water nutrient concentrations (Letelier et al., 2019; Macovei et al., 2019; Stramma et al., 2020; Yasunaka et al., 2016). Intra-annual variability depends in part on seasonality in mixing, with entrainment of elevated subsurface nutrients via mixing more pronounced at the poleward boundaries of the gyres (Macovei et al., 2019). The mechanisms underlying interannual variability are less clear and potentially related to broad-scale modes of atmospheric circulation that alter the intensity of stratification, the position of ocean fronts (e.g., PDO; North Atlantic Oscillation, NAO), the magnitude of aerosol nutrient deposition (Letelier et al., 2019; Macovei et al., 2019; Stramma et al., 2020), and N_2 fixation (Kitajima et al., 2009). Enhanced N deposition has been suggested to drive periods of decreasing phosphate concentrations at the northwestern edge of the NPSG (Kim et al., 2014). Periods of elevated Fe deposition have been suggested to result in phosphate decreases due to an increase in N_2 fixation in the eastern NPSG (Letelier et al., 2019). Projecting into the future, models suggest that warming-induced stratification will likely reduce the mixing-driven subsurface supply of nutrients, but confidence in these projections is limited due to the smaller number of historical data sets for model comparison and supporting measurements to account for the underlying mechanisms behind the changes (Bindoff et al., 2019). The aerosol supply of N to the ocean has increased greatly (see Section 2), with most of this being deposited into low-latitude subtropical gyre regions (Duce et al., 2008). Past and future changes in aerosol Fe are much more uncertain, with some evidence for increased fluxes over the past century and uncertainty over even the direction of change expected in the future (Mahowald et al., 2009, 2010).

Based on historical measurements, Yasunaka et al. (2016) have shown that average surface phosphate and silicate concentrations in the North Pacific decreased significantly at rates of -0.012 ± 0.005 (s.d.) and -0.38 ± 0.13 (s.d.) μmol L^{-1} $decade^{-1}$ from 1961 to 2012, respectively, whereas the same analysis for NO_x revealed a negligible trend. However, these trends were derived from measurements over the entire North Pacific and may not apply to the NPSG. We then examined historical macronutrient concentration data measured using conventional colorimetric methods in the NPSG (https://www.jamstec.go.jp/rigc/ress/yasunaka/nutrient/v2/index.html). Ninety-eight percent of the NO_x data and 64% of the phosphate data were removed because they were below the detection limits (0.1 for NO_x, 0.02 μM for phosphate; Yasunaka et al., 2021), while all the silicate data were above the detection limit of 0.6 μM (Yasunaka et al., 2021). The resulting intra-annual variability in NO_x concentrations in the NPSG generally appeared to be low (Figure S1a in Supporting Information S1). This conclusion, however, certainly needs further validation considering that most of the NO_x concentration data were below the detection limit and were removed in the analysis. The intra-annual variability of phosphate and silicate concentrations was high before 1986 and 1992, respectively (Figures S1b and S1c in Supporting Information S1). The more stable concentrations of phosphate and silicate thereafter (Figures S1b and S1c in Supporting Information S1) likely reflect improved data quality caused by the implementation of analytical methods associated with the Joint Global Ocean Flux Study program and, more recently, the Global Ocean Ship-Based Hydrographic Investigations Program, where standardized measurement protocols for nutrients and other parameters are now commonly applied (Becker et al., 2020; Knap et al., 1996).

Because the NO_x and phosphate concentrations measured using conventional methods were mostly below the detection limits in the NPSG, we did not analyze their long-term variability. At Station ALOHA, NO_x and phosphate concentrations measured using highly sensitive methods have been reported. These data reveal relatively small changes in near-surface NO_x and phosphate during 1989–2019 and 1989–2021, respectively (Figure 21). Nevertheless, the near-surface concentrations of both NO_x and phosphate at Station ALOHA appeared low from 1995 to 2005 and were higher during the rest of the period. This pattern is consistent with what has been reported (Karl & Letelier, 2008; Karl et al., 2021).

Given the presumably acceptable quality of silicate data after 1992, we analyzed the long-term variability in silicate concentrations in the NPSG. The data reveal that surface silicate concentrations have significantly decreased

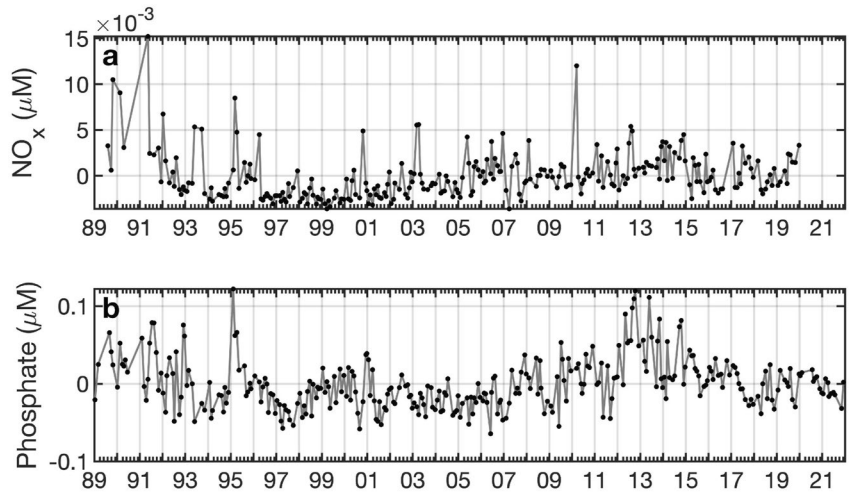

Figure 21. Long-term variability in (a) NO_x and (b) phosphate concentrations at a depth of ~5 m at Station ALOHA (measured using highly sensitive methods). Depicted are the anomalies (monthly mean value subtracted) of each property. Data are from Hawaii Ocean Times-series (https://hahana.soest.hawaii.edu/hot/hot-dogs/).

over the whole NPSG, along the 137°E transect, and at Station ALOHA (Figures 19m–19o). Low silicate concentrations in the NPSG and along the 137°E transect occurred mainly during 2013–2020 (Figures 19m and 19n). This pattern appears to be attributable to the low temperature, strong stratification and positive PDO during that period (Figures 19a, 19g, 19j, and 20b). At Station ALOHA, systematically low near-surface silicate concentrations occurred during 2001–2012 (Figure 19o), a period different from the times of low NO_x and phosphate concentrations.

6.3. Biomass and Production

6.3.1. Global Perspective

Ocean warming is predicted to lead to declines in phytoplankton biomass and primary production in the global ocean (Behrenfeld et al., 2006; Gregg & Rousseaux, 2019; Signorini et al., 2015). Using remote sensing data, Behrenfeld et al. (2006) determined that the Chl-*a* standing stock and NPP in surface waters of the global ocean showed a downward trend from 1997 to 2006 and linked this change with the increase in SST. Similarly, expansion of the area of low Chl-*a* waters has also been observed (Irwin & Oliver, 2009; Polovina et al., 2008). Polovina et al. (2011) predicted that the areas of temperate and equatorial upwelling biomes would decrease by 34% and 28%, respectively, by 2100. In addition, changes in dynamics such as wind mixing and horizontal convection may also strongly affect future ocean biomass and productivity (Dave & Lozier, 2013). Model predictions show a projected 50% decline in average Chl-*a* concentrations from 2000 to 2200 in response to these changes (Hofmann et al., 2011). However, establishing linkages among stratification, mixing, and Chl-*a* concentrations can be challenging. For example, the increase in the dynamic height and SST in the SPSG and SASG did not result in a decrease in Chl-*a* concentrations (McClain et al., 2004). In contrast, reduced Chl-*a* concentrations in surface layers should lead to increases in water transparency, increasing the flux of solar energy to depth and benefitting phytoplankton growth in the lower EZ, assuming nutrients are available.

Furthermore, increases in temperature also affect the metabolic rates of both phytoplankton and zooplankton, with subsequent impacts on phytoplankton standing stocks and primary productivity through top-down control (B. Z. Chen et al., 2012; Rose & Caron, 2007). Phytoplankton and zooplankton metabolic rates are projected to increase with rising temperatures, and heterotrophic processes appear to be more sensitive than autotrophic processes (O'Connor et al., 2009). For example, the temperature coefficient Q_{10} (the multiple of the increase in the metabolic rate when the temperature rises by 10°C) for the maximum growth rate of phytoplankton has been estimated to be 1.88 (Bissinger et al., 2008; Eppley, 1972), a value substantially lower than that of microzooplankton (3.75 and 2.97 for those grazing on phytoplankton and bacteria, respectively) (Rose & Caron, 2007). Warming thereby potentially lowers phytoplankton biomass via intensified top-down control (O'Connor et al., 2009; Sommer &

Lewandowska, 2011). At the same time, the biomass of zooplankton will also decline, even more significantly (Pulsifer & Laws, 2021), to maintain the steady state of the ecosystem. At present, these conjectures still need more field observation evidence in marine ecosystems.

6.3.2. North Pacific Subtropical Gyre

It is currently difficult to ascertain long-term trends in Chl-*a* concentrations and NPP in the NPSG, in part due to temporal variability at shorter time scales (e.g., decadal and sub-decadal) (Dave & Lozier, 2013). During the early period from 1968 to 1985, the average in situ Chl-*a* concentration in the North Pacific nearly doubled during summer (May–October) (Venrick et al., 1987). Based on satellite ocean color products, no significant trend in Chl-*a* concentrations in the NPSG was found between 1998 and 2002 (Behrenfeld et al., 2005), while a 7.7% non-significant increase in Chl-*a* concentrations was noted during the period 2003–2013 (O'Reilly, 2017). However, from 1998 to 2013, the entire period of the above two studies, Signorini et al. (2015) also used satellite products and reported a significant downward trend in mean Chl-*a* concentration (-0.0058 ± 0.0005 mg m^{-3} de $cade^{-1}$) in the NPSG. Over a longer timescale throughout the 20th century, ocean transparency and in situ chlorophyll measurements indicate that phytoplankton biomass in the NPSG declined (Boyce et al., 2010). However, field-based measurements from Station ALOHA indicate that concentrations of Chl-*a*, particulate carbon stocks, particulate N stocks, and NPP in the lower EZ (75–125 m) have all increased significantly since 1989 but show no significant trend in the upper EZ (Karl et al., 2021). These patterns are hypothesized to stem from increasing nutrient supply to the lower EZ (Karl et al., 2021).

Here, we also use OC-CCI (version 5.0) data sets to examine long-term trends in surface Chl-*a* concentrations in the NPSG over the period of 1998–2021, which is longer than the above historical analyses based on satellite products (Figures 19p and 19q). Across the entire NPSG, Chl-*a* concentrations decreased significantly at a rate of 0.3% yr^{-1}, mostly due to a sharp decrease of 18% in a single year (1998) and a sub-decadal decrease (1.2% yr^{-1}) from 2012 to 2017. However, concentrations remained relatively stable between 1999 and 2011 (Figure 19p). The sharp decrease in Chl-*a* concentrations in 1998 appeared to be related to a rapid positive-to-negative switch in PDO and ENSO indices, while the decrease in Chl-*a* concentrations from 2012 to 2017 coincided with an increase in PDO over this period (Figures 20b and 20c). We suggest that this reflects intensified stratification during these positive PDO/ENSO periods, which inhibited the nutrient supply from deep waters. It is noteworthy that most recently (2021), the Chl-*a* concentrations in the NPSG increased substantially and exceeded the long-term average of this analysis, a time from which a period of strong negative PDO/ENSO appears to start (Figures 19p, 20b, and 20c). Our analysis suggests that the average Chl-*a* concentration in the NPSG is negatively correlated with decadal climate indices, particularly the PDO, while a long-term trend in Chl-*a* concentrations cannot be confirmed.

In the western NPSG, along the 137°E transect, the decrease in Chl-*a* concentrations from 1998 to 2021 was significant but relatively weak (0.2% yr^{-1}) (Figure 19q). Although a sharp decrease in Chl-*a* concentrations (47% yr^{-1}) also occurred in 1998, there was a subdecadal marked Chl-*a* increase from 1999 to 2004 (3.3% yr^{-1}) and a subsequent strong decrease from 2005 to 2010 (3.3% yr^{-1}). No clear trends could be identified after 2010 along 137°E. At Station ALOHA, consistent with the findings in a previous study (Karl et al., 2021), in situ measurements of surface Chl-*a* concentrations showed no obvious trend or subdecadal variation from 1998 to 2020 (Figure 19r). These analyses suggest that spatial variation in Chl-*a* concentrations obscures gyre-wide long-term and sub-decadal variability.

Variations in Chl-*a* concentrations can lead to changes in the size of the oligotrophic NPSG. Based on a 7-year (November 1996–October 2003) ocean color data set, McClain et al. (2004) found an increase in the size of subtropical gyres (defined by Chl-*a* concentration <0.07 mg m^{-3}) in the Northern Hemisphere (NPSG and NASG) but undetectable changes in the Southern Hemisphere. Using the same definition but somewhat longer records (1998–2006) of remote sensing data, Polovina et al. (2008) suggested that subtropical gyres in both hemispheres are expanding, particularly in winter. We verify the significant expansion of the size of the NPSG based on a longer time series from 1998 to 2021 (Figure 20a). The increase in gyre area is not sensitive to the threshold chosen to define the oligotrophic area; the rate of gyre expansion is 1.56×10^5 km^2 yr^{-1} when it is defined by Chl-*a* concentrations <0.07 mg m^{-3} and 1.50×10^5 km^2 yr^{-1} if defined by Chl-*a* concentrations <0.1 mg m^{-3} (Figure 20a). As found for variations in Chl-*a* concentrations, the size of the NPSG is positively related to the PDO index, with a period of gyre expansion observed from 2014 to 2019, followed by decreasing areal extent during the strong negative-PDO period in 2020–2021 (Figures 20a and 20b). There is also evidence that the eastern

NPSG is expanding at a rate faster than that observed in the west (Figure S2 in Supporting Information S1). It is noteworthy that a recent paleoceanographic study also shows evidence of northward migration of the NPSG's northern boundary, indicative of its size expansion during warm interglacial periods (Taylor et al., 2022).

It is worth noting that due to the decoupling between phytoplankton carbon and Chl-*a*, using only the latter to examine interannual and long-term variations in marine ecosystems may also confound interpretation, as climate change can also affect phytoplankton physiological states (Xiu & Chai, 2012).

Systematic, long-term trends of NPP in subtropical gyres also remain unclear. Based on NPP estimates from satellite ocean color measurements in the NPSG, similar to those reported for Chl-*a* concentrations, NPP did not vary significantly between 1998 and 2002 (Behrenfeld et al., 2005). However, when NPP was estimated using the OPAL model (J. Marra et al., 2003), it showed a significant increase from 2003 to 2013 (O'Reilly, 2017), while a significant downward trend in NPP was reported using the CbPM model (-7.4 ± 0.4 mg C m^{-2} d^{-1} yr^{-1}) from 1998 through 2013 (Signorini et al., 2015). In particular, from 1999 to at least 2004, satellite-based estimates of NPP showed a prolonged but more moderate decrease in the NPSG (Behrenfeld et al., 2006), a phenomenon also observed in situ at Station ALOHA (Y.-W. Luo, Ducklow, et al., 2012). In contrast, by assimilating ocean color satellite data into a biogeochemical model, Gregg and Rousseaux (2019) reported an increasing trend for NPP during the 1998–2014 period in the subtropical North Pacific (15°–45°N). This increase is also reflected in the 30-year (1988–2018) long NPP time series at Station ALOHA, where NPP in the EZ is increasing at 4.1 mg C m^{-2} d^{-1} yr^{-1}, due in large part to increasing NPP in the lower EZ (Karl et al., 2021). However, no obvious trend was found when focusing on the 2000–2016 period (Krumhardt et al., 2017). These results indicate that the selection of time periods is obviously critical to ascertaining any systematic change in gyre NPP, suggesting its substantial sub-decadal or interannual variability. The contradictory results based on satellite models and field observations suggest that additional effort is required to improve the models.

6.4. Carbon Export

The oceanic CO_2 sink has been increasing globally since the 1990s, although there are zonal differences in the rate of change (Iida et al., 2021; Wanninkhof et al., 2013). At the global scale, the oceanic CO_2 sink increased at a rate of 0.3 ± 0.05 Pg C yr^{-1} $decade^{-1}$ during the period from 1993 to 2018 (Iida et al., 2021). The CO_2 sink specific to the Pacific Ocean has been increasing by 0.13–0.14 Pg C yr^{-1} $decade^{-1}$ from 1990 to 2012 (Iida et al., 2015), but the equatorial region of the Pacific acts as a CO_2 source, which increases at a rate of 0.04 Pg C yr^{-1} $decade^{-1}$ (Cosca, 2003). In the North Pacific subpolar gyre, however, the CO_2 sink decreased between 1993 and 2003, mainly due to the intense warming of the surface ocean (Corbière et al., 2007).

Measurements of POC concentrations in the upper ocean (Figure S3 in Supporting Information S1) and POC downward export fluxes have been conducted at very few locations in the NPSG. The temporal coverage of these measurements is even scarcer, and long-term variability in POC export is largely unknown. Station ALOHA is the only site where both particulate carbon concentrations and export fluxes at the bottom of the EZ have been monitored for decades (Karl et al., 2021). Particulate carbon concentrations at both the surface and 100 m depth near the DCM (Figures 22a and 22b) and particulate carbon export fluxes at 150 m (Figure 22c) do not show significant trends or clear relationships to climate indices at Station ALOHA (Figures 20b and 20c). The reason for the lack of systematic, long-term variability in particulate carbon export remains unclear. Considering the complex impacts of climate change on not only POC production but also its size spectra and sinking speeds (e.g., Henson et al., 2021; Q. Zhang & Luo, 2022), comprehensive studies of interacting ecosystem dynamics is required to reliably predict POC export in the future.

6.5. Long-Term Variability in Subsurface Waters

Similar to findings in the near-surface ocean, in the isopycnal layer near the DCM along 137°E in the NPSG there were no clear long-term patterns in concentrations of NO_x, phosphate, and Chl-*a* between 1994 and 2000, while a significant but weak decreasing trend was found in silicate concentrations (Figures 23a, 23c, 23e, and 23g). In an isopycnal layer ($\sigma_\theta = 24.5$ kg m^{-3}) near the DCM at Station ALOHA, significant increasing trends were found in the concentrations of NO_x, phosphate and silicate from 1989 to 2020 (Figures 23b, 23d, 23f, and 23h) but not in Chl-*a* concentrations. In comparison, there is a significant increasing trend in Chl-*a* concentrations at 75–125 m at Station ALOHA from 1989 to 2020 (Karl et al., 2021). The inconsistency could be because our analysis uses

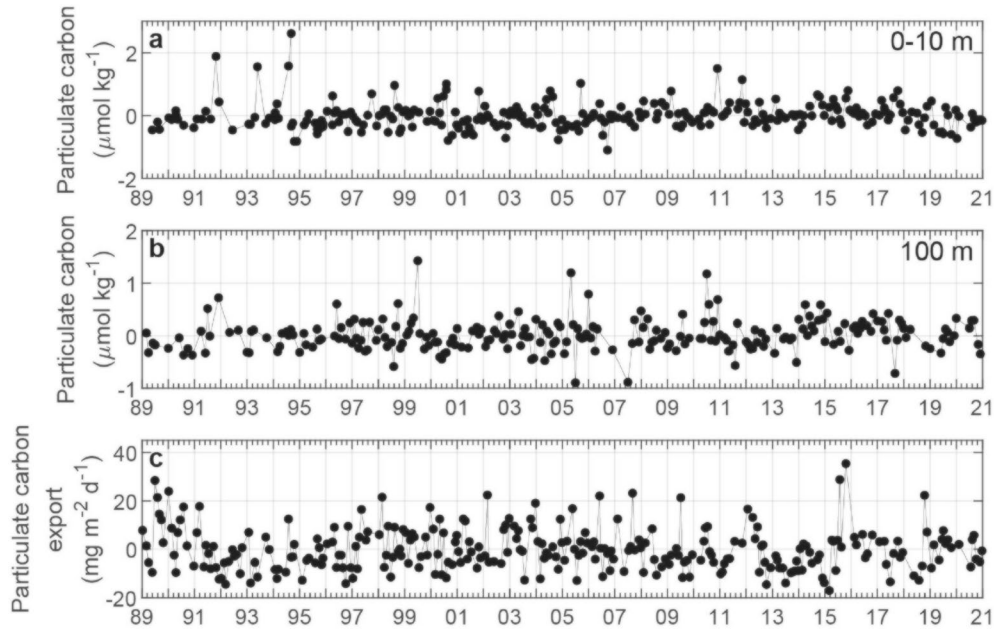

Figure 22. Interannual variations in concentrations and export fluxes of suspended particulate carbon (PC) at Station ALOHA. Depicted are the anomalies (monthly mean value subtracted) of each property. (a) Surface (0–10 m) suspended PC concentration, (b) subsurface (100 m, near the depth of the deep chlorophyll maximum) suspended PC concentration, and (c) PC flux at a depth of 150 m.

Chl-*a* concentrations along an isopycnal (σ_θ = 24.5 kg m^{-3}) instead of a fixed depth range, and the depth of the isopycnal deepens at 0.47 m yr^{-1} during this period (Figure S4 in Supporting Information S1). However, the identified trends were relatively weak when compared to the larger intra-annual variability.

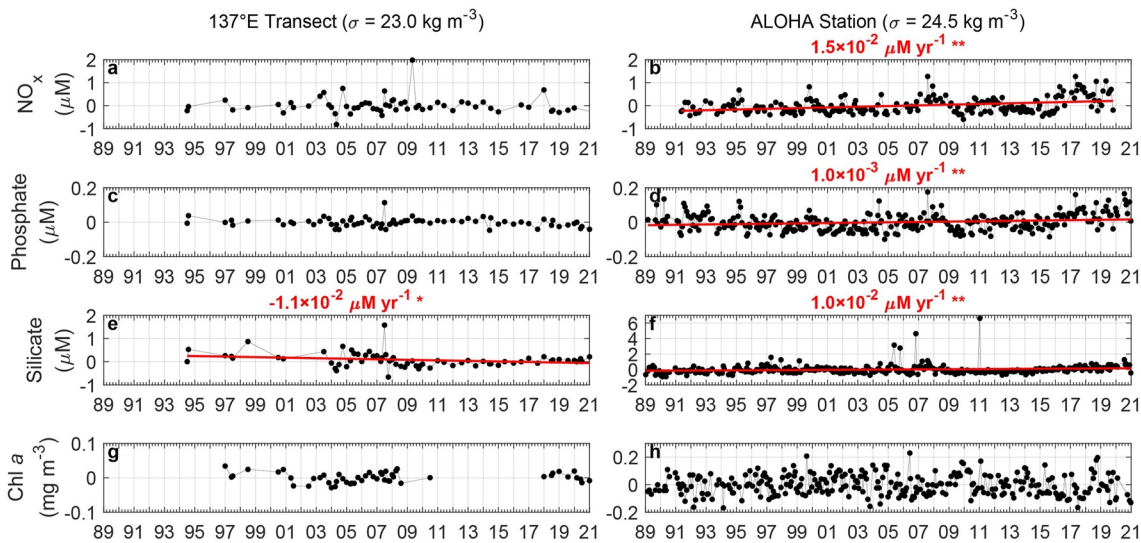

Figure 23. Subsurface isopycnal long-term variations in biogeochemical properties along 137°E in the North Pacific Subtropical Gyre (panels in the left column) and at Station ALOHA (panels in the right column), including concentrations of (a, b) NO_x, (c, d) phosphate, (e, f), silicate, and (g, h) Chl *a*. Isopycnal layers with potential densities (σ_θ) of 23.0 and 24.5 kg m^{-3} were selected for 137°E and Station ALOHA, respectively, to represent the deep chlorophyll maximum layer. Depicted are the anomalies (monthly mean value subtracted) of each property. Only significant trendlines ($p < 0.05$) are plotted (solid red or blue lines), with the rates of the trends marked on top of each panel (*: $p < 0.05$; **: $p < 0.01$). The data along 137°E are from the Global Ocean Data Analysis Project v2.2022 product (Lauvset et al., 2022) (https://www.glodap.info/index.php/merged-and-adjusted-data-product-v2-2022/) between 4° and 26°N. The data at Station ALOHA are from Hawaii Ocean Times-series (https://hahana.soest.hawaii.edu/hot/hot-dogs/), in which the low-level concentrations of NO_x and phosphate were measured using highly sensitive methods. Chl-*a* concentrations at Station ALOHA were measured by high-performance liquid chromatography.

Deciphering the long-term trends in physical and biogeochemical properties in the NPSG is complicated by multiple scale temporal changes, particularly at decadal scales. It is also difficult to deconvolve the long-term trends from spatial variations. Previous studies have attributed many of the interannual trends to decadal- or subdecadal-scale climate oscillations such as the PDO and ENSO (Karl et al., 1995; Y. Zhang et al., 2021). Such relationships with climate oscillations were also found in our analyses, supporting the need for sustained observations over relatively long periods, likely even longer than 40 years as previously proposed (Henson et al., 2010; Yoder et al., 2010), to conclusively disentangle long-term trends from interannual and decadal variability.

Analyses are also hindered by the paucity of spatial data coverage in this large expansive gyre, in which the transect along 137°E and Station ALOHA are probably the only two sites where substantial data have been accumulated. The interannual variations in physical and biogeochemical properties at these two sites are inconsistent, showing the heterogeneity within the NPSG where important unknown mechanisms exist and behave differently across the gyre. Our analyses rely heavily on satellite remote sensing products to achieve greater spatial coverage. However, some algorithms are immature, and some products from satellite remote sensing, particularly NPP and POC, are still not well constrained and reliable.

7. Summary, Challenges, and Future Directions

7.1. Summary

This review concludes that the subtropical gyres cover ~26% of the world's ocean surface area and 30% of its volume. These percentages are smaller than the previously reported coverage of up to 40% of the surface area; however, they support the notion that the subtropical gyres are the largest continuous ecosystems on the planet. These oligotrophic gyres share many common biogeochemical features, but we highlight important differences as a function of physical settings and nutrient supply.

Building on several milestone reviews of the biogeochemistry and ecology of subtropical gyres (e.g., Karl, 1999; Karl & Church, 2014, 2017), we have collectively shown that these systems experience much larger spatial and temporal changes in biogeochemistry and ecosystem metabolism than previously believed. The variability results from diverse nutrient sources, including N_2 fixation, the impacts of low nutrient supplies on limiting primary production and N_2 fixation rates, different microbial community structures and the mechanisms that control carbon export.

At interannual and decadal timescales, we see clear trends of increasing SST and stratification in the NPSG as a consequence of global warming. These patterns are presumably closely linked to large-scale ocean-atmosphere interactions reflected in the ENSO and/or PDO. However, our understanding of long-term biogeochemical variability is much more limited, owing to a lack of reliable long-term observations at adequate spatial scales and the potential for complex, interacting controls.

Additionally, building upon previous studies (e.g., Dore et al., 2008; Dugdale & Goering, 1967), our review advocates for a more definitive two-layered conceptual framework of the EZ based on nutrient profiles in subtropical gyres. We suggest adopting this framework to better understand the processes needed to model and predict the spatiotemporal variabilities of the upper oligotrophic ocean in these systems. Nutrient sources and the intensity and spectral composition of light can determine the different phytoplankton and zooplankton communities inhabiting the two layers. These are two distinct ecosystems of the EZ sustained by differently sourced nutrients. New N supply in the form of N_2 fixation and atmospheric deposition to the NDL can lead to a higher efficiency of carbon sequestration than if nitrate is supplied from the deeper ocean to the NRL, as the upward transfer of deeper waters also brings elevated concentrations of DIC. Because there is a diversity of nutrient-limitation scenarios, including limitation and co-limitation of primary production by N, P, and Fe, as well as those of N_2 fixation by Fe and P across oligotrophic gyres, P and Fe availability presents a central linkage between the classically defined food web and N_2 fixation pathways (Tyrrell, 1999).

7.2. Unresolved Issues, Challenges, and Future Issues

As remote and vast oceanic regimes, the oligotrophic gyres are particularly understudied in terms of their physical dynamics and biogeochemistry. Even less is known about the biological components of these ecosystems. Among the five major ocean subtropical gyres, the NASG and NPSG are the most studied in regard to their upper ocean

biogeochemistry; however, even for these two systems, our understanding is largely based on only two time-series studies, HOT, and BATS.

Specific to the NPSG, our advances in understanding NPSG biogeochemistry have largely been derived from the HOT program with its near-monthly sampling at Station ALOHA in the eastern NPSG. This location is not located in the gyre center, as shown by the convergence of currents and the Chl-*a* minimum (Figure 2). The analyses based on limited data (Section 3) have shown differences between the western NPSG and Station ALOHA, such as in the seasonal and interannual variations and/or magnitude of temperature, stratification, nutrient sources and concentrations, and biological activities. The upper-ocean concentration of Fe, which is the most important micronutrient in oligotrophic systems, appears elevated near Station ALOHA, although the phenomenon needs further confirmation from more measurements. The implications and underlying causes of such differences have yet to be elucidated.

While short-term variability in ocean gyres appears strongly linked to micro- and mesoscale physical processes, long-term trends in NPSG biogeochemistry can be attributed to larger scale ocean–atmosphere interactions, for example, via ENSO at interannual scales and PDO at decadal scales. How such long-term trends are modified by anthropogenically induced climate change remains largely unknown and will have to be explored by increasing the frequency and spatial extent of observations.

Tackling this presents a major challenge. Given the vast spatial coverage of gyre systems, traditional shipboard oceanographic surveys remain essential but generally insufficient for improving spatial and temporal sampling resolution. We thus offer the following suggestions to improve observation strategies in future studies to enhance the spatial coverage and fit-to-purpose observations efficiently.

Deployments of autonomous platforms with advanced biogeochemical sensors are becoming increasingly essential. Collaborative observational networks, including BGC-Argo floats, gliders, saildrones, and wavegliders among others, allow for significant advances in acquiring biogeochemical data. These autonomous tools could also be adaptively modified to meet specific requirements in spatial and temporal resolution (Claustre et al., 2020), for example, the need for measuring detailed features in the NDL and NRL at a highest possible vertical resolution. Observational networks that can adaptively capture these highly variable systems are also required (Graff et al., 2015). In addition, it is important to link biogeochemistry to large-scale satellite observations. For example, Barone et al. (2019) indicated that satellite measurements of sea surface height could be used to infer the ecological and biogeochemical state in the NPSG.

Measurements at the HOT (Station ALOHA) and BATS locations have accumulated much valuable information and knowledge and have laid the foundations of contemporary ocean biogeochemistry in ocean gyres. Large-scale programs such as these with designated designs are essential to rapidly further our understanding of global ocean processes.

We also urge continued development and implementation of methods capable of measuring nutrients at the exceedingly low concentrations found in subtropical gyres. The existing data on NO_x are mostly below detection limits and are unreliable for discerning any long-term trends or even seasonal variations. It is also a challenge to accurately measure phosphate concentrations in the large regions of subtropical gyres, particularly near their western boundaries (Martiny et al., 2019). Efforts focused on developing, improving, and implementing high sensitivity nutrient methodologies would be an important future contribution.

Biogeochemical models can further provide an important approach for understanding the current state and predicting the future state of the oceans via the assimilation of observational data sets. Although biogeochemical observations are still too sparse for comprehensive validation, initialization, and optimization of biogeochemical models at global scales, they provide a fundamental benchmark for optimizing the parameterization of biogeochemical models (Fennel et al., 2019). Optimizing the model parameterization will clarify which parameters are the most important to measure and what time and spatial scales are needed in future studies (Chai et al., 2020). The community is actively working on how to improve the technological readiness for assimilating observations from BGC-Argo, among other observational platforms, into biogeochemical models (Cossarini et al., 2019). Assimilation of multiple observations in the biogeochemical models can improve the delineation of physical and biogeochemical variables by disentangling their relationships (Yu et al., 2018). For example, modeling can enhance understanding of the dependence between NRL and NDL in the NPSG. New biogeochemical models that are capable of delineating complex biogeochemical processes, that is, Fe fertilization (H. R. Zhang

et al., 2021) and N_2 fixation with enhanced vertical resolution in the EZ (Xiu & Chai, 2021), are being developed for accurately simulating the marine ecosystem of the NPSG region. The use of new algorithms, that is, including neutral network, machine learning and artificial intelligence, can further improve the usage of four-dimensional data sets from floats and gliders among others (Chai et al., 2020), which is expected to be an important resource for increasing the capability and credibility of ocean models (X. Zhang et al., 2017).

Among many other key issues to be resolved, it would be particularly beneficial to better constrain the processes described in the two-layered framework put forward in this review to improve our mechanistic understanding of subtropical gyre biogeochemistry. However, details of this framework have yet to be established. A better formulation of the two-layer scheme requires better knowledge of how the physical settings interact with nutrient supplies and cycling and biological processes, for example, how physical forcing alongside external and regenerated nutrient supplies regulates the community structure of both primary producers and diazotrophs. Such ecosystem structures are likely a strong driver of export productivity. Ultimately, the identification and quantification of the full range of operating biogeochemical pathways, their processes, and their interactions present a major challenge but are required to gain a fuller understanding of the biogeochemistry of these systems.

As a rapidly regenerating system, internal nutrient recycling must predominate in sustaining the biological metabolism of oligotrophic ecosystems. However, quantifying the regeneration rates of different nutrient species is only in its infancy. This is particularly true for organic nutrients such as DOP and DON, which have orders of magnitude higher concentrations than their inorganic nutrient counterparts (Letscher et al., 2013, 2016). These organic forms of nutrients may also be directly assimilated by microbes and exported into the deep ocean.

Several outstanding questions remain to be addressed to improve our quantitative understanding of the contribution of marine N_2 fixation to carbon export. What is the contribution of diverse NCDs to marine N_2 fixation? What are the mechanisms and pathways by which marine N_2 fixation drives export? In other words, how is DDN released and transferred from various diazotrophs to sinking particles? Given that N_2 fixation mostly occurs in the NDL and export is measured at the NRL, putting DDN release and transfer into the two-layer framework holds promise to resolve the outstanding question of the mechanism of N_2 fixation in driving export.

Another key unknown is the fate of the sinking particles originating from the NDL when they enter the NRL: To what extent are they consumed by zooplankton and bacteria, and what are the subsequent impacts on the food web and community structures? What processes and pathways are responsible for particle remineralization, regenerating nutrients required to support primary production? How much of them continues to be exported out of the NRL?

We advocate for collaborative and interdisciplinary research that targets our mechanistic understanding of biogeochemistry in ocean gyres. One example of a process study with adequate spatial coverage is the Carbon-FE program funded by the National Natural Science of China, which examines Carbon Fixation and Export in ocean deserts. In addition to the general purpose of filling data gaps in the western NPSG, the project implements the proposed two-layer framework into its sampling strategy to (a) reveal the high-resolution vertical structure of biogeochemical properties; (b) elucidate the controlling mechanisms of carbon export; and (c) improve our understanding of the spatiotemporal variations in biogeochemistry in the NPSG.

Last, while this review focuses on the upper ocean, we must be aware that the deeper part of the ocean, including the twilight zone (200–1,000 m) and deeper dark ocean, is interactively linked with the upper euphotic ocean. Much is yet to be learned about the interconnected physical and biological processes between the surface and deep waters and how the ocean as a whole regulates Earth's climate. The downward fluxes of POM and DOM via the biological pump constitute the main mechanism that transports both materials and microbes from the EZ to the deep ocean, providing essential energy and nutrient sources to the starved deep ocean ecosystem and shaping microbial communities (E. Luo et al., 2022; Mestre et al., 2018). The subsequent remineralization and cycling of the sinking organic matter sustain vertical gradients in inorganic carbon and nutrient pools and consume oxygen, ultimately regulating ocean sequestration of CO_2 (Gruber et al., 2008; Karl & Letelier, 2008). Recent time-series studies have revealed a rapid response of the microbial community and activity in the deep ocean to seasonal variability in productivity and elevated carbon flux events from the surface ocean, indicating a tight connection between primary productivity and deep-sea ecosystem processes (Poff et al., 2021; Wenley et al., 2021). Given the predicted changes in primary productivity and export efficiency in the global ocean under warming (Garcia-Corral et al., 2017; Wohlers et al., 2009), although distinct trends, as discussed above, have

not been conclusively discerned, the deep-sea ecosystem might also be sensitive to climate change. Oligotrophic systems are also susceptible to external inputs and are thus subject to large-scale, transient Earth system processes such as submarine eruptions (Barone, Letelier, et al., 2022), and wildfires, which are intensifying under current climatic changes (Liu et al., 2022). While climatology is often a focus of our current oceanographic studies, these large-scale processes and how they would impact gyre biogeochemistry and ecosystems are very difficult to estimate and evaluate. They therefore warrant particular attention in future research.

Appendix A: This List Includes All the Acronyms Used in Present Article

List of Acronyms

ADT	Absolute dynamic topography
BATS	Bermuda Atlantic Time-series Study
Chl-*a*	Chlorophyll-*a*
CbPM	Carbon-based production model
DCM	Deep chlorophyll maximum
DDN	Diazotroph-derived nitrogen
DDA	Diatom-diazotroph association
DIC	Dissolved inorganic carbon
DOM	Dissolved organic matter
DOC	Dissolved organic carbon
DON	Dissolved organic nitrogen
DOP	Dissolved organic phosphorus
e-ratio	Ratio of export to primary production
EBC	Eastern Boundary Current
EBUS	Eastern Boundary Upwelling Systems
ENSO	El Niño-Southern Oscillation
EZ	Euphotic zone
Fe	Iron
HOT	Hawaii Ocean Times-series
IOSG	Indian Ocean Subtropical Gyre
N	Nitrogen
NASG	North Atlantic Subtropical Gyres
NAO	North Atlantic Oscillation
NCD	Non-cyanobacterial diazotroph
NCP	Net community production
NDL	Nutrient-depleted layer
NEC	North Equatorial Current
NO_x	Nitrate + nitrite
NPSG	North Pacific Subtropical Gyres
NPP	Net primary production
NRL	Nutrient-replete layer
P	Phosphorus
PAR	Photosynthetically active radiation
PDO	Pacific Decadal Oscillation
POC	Particulate organic carbon
POM	Particulate organic matter
Reactive N:	$NO_x + NH_4^+ + DON$
Si	Silicon
SPSG	South Pacific Subtropical Gyres
SASG	South Atlantic Subtropical Gyres
SEC	South Equatorial Current
SML	Surface mixed layer
SST	Sea surface temperature
STCC	Subtropical countercurrent

STMW	Subtropical Mode Water
UCYN	Unicellular cyanobacteria
VGPM	Vertically generalized production model
WBC	Western Boundary Current
WOA	World Ocean Atlas
σ_θ	Potential density

Appendix B: This Table Summarizes the Observed Seasonal Variability in the N_2 Fixation Rates and Dominant Diazotrophic Groups in the North Pacific Subtropical Gyre (NPSG) Reported in Previous Studies

Table B1

Reviews of Geophysics

10.1029/2022RG000800

Table B1
Summary of Seasonal Variability in the N_2 Fixation Rates and Dominant Diazotrophic Groups in the North Pacific Subtropical Gyre

	Spring	Summer	Autumn	Winter	Reference
N_2 fixation rate					
Eastern NPSG (Station ALOHA)	Medium-high	High	High	Low	Böttjer et al. (2016) and Church et al. (2009)
Western boundary (Kuroshio Current)	High	High	High	Low	Y. L. L. Chen et al. (2008, 2014)
Western NPSG (155°E)		Low		High	Kitajima et al. (2009)
Dominant diazotrophs					
Eastern NPSG (Station ALOHA)	UCYN-A	UCYN-A, Crocosphaera, Trichodesmium	UCYN-A, Crocosphaera	UCYN-A	Church et al. (2009)
Western boundary (Kuroshio Current)	*Crocosphaera*, *Trichodesmium*	*Crocosphaera*		UCYN-A, *Crocosphaera*	C. Chen et al. (2019), Shiozaki et al. (2014), and Wen et al. (2022)
Western NPSG (155°E)		DDA		DDA	Kitajima et al. (2009)

Data Availability Statement

The absolute dynamic topography data used in Figure 2 and to produce results in Table 1 can be downloaded from https://doi.org/10.24381/cds.4c328c78. The chlorophyll-*a* data used in Figure 2 and to produce results in Table 1 can be downloaded from https://www.oceancolour.org/. The NO_x, phosphate, and silicate data used in Figures 3 and 5 and to produce results in Table 2 can be downloaded from https://www.ncei.noaa.gov/products/world-ocean-atlas. The dissolved Fe data in Figure 3 and to produce the results in Table 2 can be downloaded from https://doi.org/10.5281/zenodo.6385044. In Figure 4, data used for NPSG (except for dissolved Fe) can be downloaded from https://www.glodap.info/index.php/merged-and-adjusted-data-product-v2-2022/ and all the other data are available at https://hahana.soest.hawaii.edu/hot/hot-dogs/. The chlorophyll-*a* and NPP data used in producing Figure 6 can be downloaded from https://hahana.soest.hawaii.edu/hot/hot-dogs/ (for Station ALOHA) and http://bats.bios.edu/data/ (for BATS). The satellite-based NPP in Figures 7a and 7b and used to produce results in Table 3 can be downloaded from http://sites.science.oregonstate.edu/ocean.productivity/index.php. The Earth system model-based NPP in Figure 7c can be downloaded from http://www.earthsystemgrid.org. The sea-air CO_2 flux data used to produce results in Table 4 can be downloaded from https://www.data.jma.go.jp/gmd/kaiyou/english/oceanic_carbon_cycle_index.html. The PDO and Niño 3.4 indices used in Figure 20 can be downloaded from https://psl.noaa.gov/data/climateindices/list/.

The data generated by reprocessing original data in this study are available in tables and/or figures and are deposited in the Science Data Bank (https://doi.org/10.57760/sciencedb.07646). These data include: ranges of subtropical gyres (shown in Figures 2, 3, 5, 7–9, 12, and 14 and used in producing results in Tables 1, 2, and 5), vertical profiles of biogeochemical properties (Figure 4), N* and Si* (used in Figure 5), the interpolated chlorophyll-*a* concentrations and NPP (Figure 6), the gridded NO_x, phosphate, and silicate concentrations (Figure 8), the gridded dissolved Fe measurements (Figure 9), the monthly climatology of biogeochemical properties (Figures 10 and 11), the N_2 fixation measurements, analyses, and simulated results (Figure 12), the nutrient limitation on N_2 fixation (Figure 13), the depth of SML, NDL, and EZ (Figures 14 and 16), vertical profiles of ^{234}Th:^{238}U, chlorophyll-*a*, and NO_x concentrations (Figure 17), ^{234}Th and POC flux data (Figure 18), and long-term time series of biogeochemical properties (Figures 19–23).

Acknowledgments

The authors would like to thank Yanping Xu, Yangchun Xu, and Yuhong Huang for their support and help in preparing the data and figures used in this contribution. The authors thank the scientists and staff of the HOT, BATS, WOCE, GEOTRACES, JAMSTEC, JMA, NOAA, and GLODAP for generating valuable hydrographic and biogeochemical data. The authors also thank three anonymous reviewers for their very constructive and thorough comments, which greatly improved the quality of this paper. The initiation of this review was associated with the Carbon-FE (Carbon Fixation and Export in ocean desert) program funded by the National Natural Science of China (NSFC) through Grant 41890800 (and its subprojects 41890801–5). Carbon-FE is an endorsed project by the Surface Ocean Lower Atmosphere Study (SOLAS). This project was also partly supported by NSFC Grants 41730533 (to MD), 42076153 (to YWL), 42188102 (to MD), and 92258302 (to ZC), the Simons Foundation (SCOPE 721221 to MJC), Southern Marine Science and Engineering Guangdong Laboratory (Guangzhou) Grant (SMSEGL20SC02 to BC), and Leverhulme Trust (RPG-2020-389 to BC).

References

Al-Mutairi, H., & Landry, M. R. (2001). Active export of carbon and nitrogen at Station ALOHA by diel migrant zooplankton. *Deep Sea Research Part II: Topical Studies in Oceanography*, *48*(8), 2083–2103. https://doi.org/10.1016/S0967-0645(00)00174-0

Azam, F., Fenchel, T., Field, J. G., Gray, J. S., Meyer-Reil, L. A., & Thingstad, F. (1983). The ecological role of water-column microbes in the sea. *Marine Ecology Progress Series*, *10*(3), 257–263. https://doi.org/10.3354/meps010257

Banse, K. (2004). Should we continue to use the 1% light depth convention for estimating the compensation depth of phytoplankton for another 70 years? *Limnology and Oceanography Bulletin*, *13*(3), 49–52. https://doi.org/10.1002/lob.200413349

Barone, B., Church, M. J., Dugenne, M., Hawco, N. J., Jahn, O., White, A. E., et al. (2022). Biogeochemical dynamics in adjacent mesoscale eddies of opposite polarity. *Global Biogeochemical Cycles*, *36*(2), e2021GB007115. https://doi.org/10.1029/2021GB007115

Barone, B., Coenen, A. R., Beckett, S. J., McGillicuddy, D. J., Weitz, J. S., & Karl, D. M. (2019). The ecological and biogeochemical state of the North Pacific Subtropical Gyre is linked to sea surface height. *Journal of Marine Research*, *77*(2), 215–245. https://doi.org/10.1357/002224019828474241

Barone, B., Letelier, R. M., Rubin, K. H., & Karl, D. M. (2022). Satellite detection of a massive phytoplankton bloom following the 2022 submarine eruption of the Hunga Tonga-Hunga Ha'apai Volcano. *Geophysical Research Letters*, *49*(17), e2022GL099293. https://doi.org/10.1029/2022GL099293

Becker, S., Aoyama, M., Woodward, E. M. S., Bakker, K., Coverly, S., Mahaffey, C., & Tanhua, T. (2020). GO-SHIP repeat hydrography nutrient manual: The precise and accurate determination of dissolved inorganic nutrients in seawater, using continuous flow analysis methods. *Frontiers in Marine Science*, *7*, 581790. https://doi.org/10.3389/fmars.2020.581790

Behrenfeld, M. J., Boss, E., Siegel, D. A., & Shea, D. M. (2005). Carbon-based ocean productivity and phytoplankton physiology from space. *Global Biogeochemical Cycles*, *19*(1), GB1006. https://doi.org/10.1029/2004gb002299

Behrenfeld, M. J., & Falkowski, P. G. (1997). Photosynthetic rates derived from satellite-based chlorophyll concentration. *Limnology and Oceanography*, *42*(1), 1–20. https://doi.org/10.4319/lo.1997.42.1.0001

Behrenfeld, M. J., O'Malley, R. T., Siegel, D. A., McClain, C. R., Sarmiento, J. L., Feldman, G. C., et al. (2006). Climate-driven trends in contemporary ocean productivity. *Nature*, *444*(7120), 752–755. https://doi.org/10.1038/nature05317

Bell, P. R. F., & Fu, F. X. (2005). Effect of light on growth, pigmentation and N_2 fixation of cultured *Trichodesmium* sp. from the Great Barrier Reef lagoon. *Hydrobiologia*, *543*(1), 25–35. https://doi.org/10.1007/s10750-004-5713-2

Benavides, M., Arístegui, J., Agawin, N. S. R., Cancio, J. L., & Hernàndez-León, S. (2013). Enhancement of nitrogen fixation rates by unicellular diazotrophs vs. *Trichodesmium* after a dust deposition event in the Canary Islands. *Limnology and Oceanography*, *58*(1), 267–275. https://doi.org/10.4319/lo.2013.58.1.0267

Benavides, M., & Voss, M. (2015). Five decades of N_2 fixation research in the North Atlantic Ocean. *Frontiers in Marine Science*, *2*, 40. https://doi.org/10.3389/fmars.2015.00040

Benitez-Nelson, C. R., Bidigare, R. R., Dickey, T. D., Landry, M. R., Leonard, C. L., Brown, S. L., et al. (2007). Mesoscale eddies drive increased silica export in the subtropical Pacific Ocean. *Science*, *316*(5827), 1017–1021. https://doi.org/10.1126/science.1136221

Benitez-Nelson, C. R., Buesseler, K. O., Karl, D. M., & Andrews, J. (2001). A time-series study of particulate matter export in the North Pacific Subtropical Gyre based on ^{234}Th:^{238}U disequilibrium. *Deep-Sea Research I*, *48*(12), 2595–2611. https://doi.org/10.1016/S0967-0637(01)00032-2

Bergquist, B. A., & Boyle, E. A. (2006). Dissolved iron in the tropical and subtropical Atlantic Ocean. *Global Biogeochemical Cycles*, *20*(1), GB1015. https://doi.org/10.1029/2005gb002505

Bergquist, B. A., Wu, J., & Boyle, E. A. (2007). Variability in oceanic dissolved iron is dominated by the colloidal fraction. *Geochimica et Cosmochimica Acta*, *71*(12), 2960–2974. https://doi.org/10.1016/j.gca.2007.03.013

Berman-Frank, I., Bidle, K. D., Haramaty, L., & Falkowski, P. G. (2004). The demise of the marine cyanobacterium, *Trichodesmium* spp., via an autocatalyzed cell death pathway. *Limnology and Oceanography*, *49*(4), 997–1005. https://doi.org/10.4319/lo.2004.49.4.0997

Bindoff, N. L., Cheung, W. W. L., Kairo, J. G., Arístegui, J., Guinder, V. A., Hallberg, R., et al. (2019). Changing ocean, marine ecosystems, and dependent communities. In H.-O. Pörtner, D. C. Roberts, V. Masson-Delmotte, P. Zhai, M. Tignor, E. Poloczanska, et al. (Eds.), *IPCC special report on oceans and cryospheres in a changing climate* (pp. 447–587). Cambridge University Press. https://doi.org/10.1017/9781009157964.007

Bissinger, J. E., Montagnes, D. J. S., Sharples, J., & Atkinson, D. (2008). Predicting marine phytoplankton maximum growth rates from temperature: Improving on the Eppley curve using quantile regression. *Limnology and Oceanography*, *53*(2), 487–493. https://doi.org/10.4319/lo.2008.53.2.0487

Blain, S., Bonnet, S., & Guieu, C. (2008). Dissolved iron distribution in the tropical and sub tropical South Eastern Pacific. *Biogeosciences*, *5*(1), 269–280. https://doi.org/10.5194/bg-5-269-2008

Bombar, D., Paerl, R. W., & Riemann, L. (2016). Marine non-cyanobacterial diazotrophs: Moving beyond molecular detection. *Trends Microbiol*, *24*(11), 916–927. https://doi.org/10.1016/j.tim.2016.07.002

Bonnet, S., Baklouti, M., Gimenez, A., Berthelot, H., & Berman-Frank, I. (2016). Biogeochemical and biological impacts of diazotroph blooms in a low-nutrient, low-chlorophyll ecosystem: Synthesis from the VAHINE mesocosm experiment (New Caledonia). *Biogeosciences*, *13*(15), 4461–4479. https://doi.org/10.5194/bg-13-4461-2016

Bonnet, S., Berthelot, H., Turk-Kubo, K., Cornet-Barthaux, V., Fawcett, S., Berman-Frank, I., et al. (2016). Diazotroph derived nitrogen supports diatom growth in the South West Pacific: A quantitative study using nanoSIMS. *Limnology and Oceanography*, *61*(5), 1549–1562. https://doi.org/10.1002/lno.10300

Bonnet, S., Berthelot, H., Turk-Kubo, K., Fawcett, S., Rahav, E., Helguen, S., & Berman-Frank, I. (2016). Dynamics of N_2 fixation and fate of diazotroph-derived nitrogen in a low-nutrient, low-chlorophyll ecosystem: Results from the VAHINE mesocosm experiment (New Caledonia). *Biogeosciences*, *13*(9), 2653–2673. https://doi.org/10.5194/bg-13-2653-2016

Bonnet, S., Caffin, M., Berthelot, H., Grosso, O., Benavides, M., Helias-Nunige, S., et al. (2018). In-depth characterization of diazotroph activity across the western tropical South Pacific hot spot of N_2 fixation (OUTPACE cruise). *Biogeosciences*, *15*(13), 4215–4232. https://doi.org/10.5194/bg-15-4215-2018

Bonnet, S., Caffin, M., Berthelot, H., & Moutin, T. (2017). Hot spot of N_2 fixation in the western tropical South Pacific pleads for a spatial decoupling between N_2 fixation and denitrification. *Proceedings of the National Academy of Sciences of the United States of America*, *114*(14), E2800–E2801. https://doi.org/10.1073/pnas.1619514114

Böttjer, D., Dore, J. E., Karl, D. M., Letelier, R. M., Mahaffey, C., Wilson, S. T., et al. (2016). Temporal variability of nitrogen fixation and particulate nitrogen export at Station ALOHA. *Limnology and Oceanography*, *62*(1), 200–216. https://doi.org/10.1002/lno.10386

Bouruet-Aubertot, P., Cuypers, Y., Doglioli, A., Caffin, M., Yohia, C., de Verneil, A., et al. (2018). Longitudinal contrast in turbulence along a similar to 19 degrees S section in the Pacific and its consequences for biogeochemical fluxes. *Biogeosciences*, *15*(24), 7485–7504. https://doi.org/10.5194/bg-15-7485-2018

Boyce, D. G., Lewis, M. R., & Worm, B. (2010). Global phytoplankton decline over the past century. *Nature*, *466*(7306), 591–596. https://doi.org/10.1038/nature09268

Boyle, E. A., Bergquist, B. A., Kayser, R. A., & Mahowald, N. (2005). Iron, manganese, and lead at Hawaii Ocean Time-series station ALOHA: Temporal variability and an intermediate water hydrothermal plume. *Geochimica et Cosmochimica Acta*, *69*(4), 933–952. https://doi.org/10.1016/j.gca.2004.07.034

Bronk, D. A. (2002). Dynamics of DON. In D. A. Hansell & C. A. Carlson (Eds.), *Biogeochemistry of marine dissolved organic matter* (1st ed., pp. 153–249). Academic Press. https://doi.org/10.1016/B978-012323841-2/50007-5

Bronk, D. A., See, J. H., Bradley, P., & Killberg, L. (2007). DON as a source of bioavailable nitrogen for phytoplankton. *Biogeosciences*, *4*(3), 283–296. https://doi.org/10.5194/bg-4-283-2007

Brown, M. T., Landing, W. M., & Measures, C. I. (2005). Dissolved and particulate Fe in the western and central North Pacific: Results from the 2002 IOC cruise. *Geochemistry Geophysics Geosystems*, *6*(10), Q10001. https://doi.org/10.1029/2004gc000893

Browning, T. J., Liu, X., Zhang, R., Wen, Z., Liu, J., Zhou, Y., et al. (2022). Nutrient co-limitation in the subtropical Northwest Pacific. *Limnology and Oceanography Letters*, *7*(1), 52–61. https://doi.org/10.1002/lol2.10205

Bruland, K. W., Orians, K. J., & Cowen, J. P. (1994). Reactive trace-metals in the stratified central North Pacific. *Geochimica et Cosmochimica Acta*, *58*(15), 3171–3182. https://doi.org/10.1016/0016-7037(94)90044-2

Buck, C. S., Landing, W. M., & Resing, J. (2013). Pacific Ocean aerosols: Deposition and solubility of iron, aluminum, and other trace elements. *Marine Chemistry*, *157*, 117–130. https://doi.org/10.1016/j.marchem.2013.09.005

Caffin, M., Berthelot, H., Cornet-Barthaux, V., Barani, A., & Bonnet, S. (2018). Transfer of diazotroph-derived nitrogen to the planktonic food web across gradients of N_2 fixation activity and diversity in the western tropical South Pacific Ocean. *Biogeosciences*, *15*(12), 3795–3810. https://doi.org/10.5194/bg-15-3795-2018

Campbell, L., & Vaulot, D. (1993). Photosynthetic picoplankton community structure in the Subtropical North Pacific Ocean near Hawaii (station ALOHA). *Deep-Sea Research I*, *40*(10), 2043–2060. https://doi.org/10.1016/0967-0637(93)90044-4

Capone, D. G., Zehr, J. P., Paerl, H. W., Badger, M. R., & Carpenter, E. J. (1997). *Trichodesmium*, a globally significant marine cyanobacterium. *Science*, *276*(5316), 1221–1229. https://doi.org/10.1126/science.276.5316.1221

Carr, M.-E., Friedrichs, M. A. M., Schmeltz, M., Noguchi Aita, M., Antoine, D., Arrigo, K. R., et al. (2006). A comparison of global estimates of marine primary production from ocean color. *Deep-Sea Research II*, *53*(5–7), 741–770. https://doi.org/10.1016/j.dsr2.2006.01.028

Cavender-Bares, K. K., Karl, D. M., & Chisholm, S. W. (2001). Nutrient gradients in the western North Atlantic Ocean: Relationship to microbial community structure and comparison to patterns in the Pacific Ocean. *Deep-Sea Research I*, *48*(11), 2373–2395. https://doi.org/10.1016/S0967-0637(01)00027-9

Chai, F., Johnson, K. S., Claustre, H., Xing, X., Wang, Y., Boss, E., et al. (2020). Monitoring ocean biogeochemistry with autonomous platforms. *Nature Reviews Earth & Environment*, *1*(6), 315–326. https://doi.org/10.1038/s43017-020-0053-y

Chen, B. Z., Landry, M. R., Huang, B. Q., & Liu, H. B. (2012). Does warming enhance the effect of microzooplankton grazing on marine phytoplankton in the ocean? *Limnology and Oceanography*, *57*(2), 519–526. https://doi.org/10.4319/lo.2012.57.2.0519

Chen, C., Wang, G., Xie, S.-P., & Liu, W. (2019). Why does global warming weaken the Gulf Stream but intensify the Kuroshio? *Journal of Climate*, *32*(21), 7437–7451. https://doi.org/10.1175/JCLI-D-18-0895.1

Chen, Y. L. L., Chen, H. Y., Lin, Y. H., Yong, T. C., Taniuchi, Y., & Tuo, S. H. (2014). The relative contributions of unicellular and filamentous diazotrophs to N_2 fixation in the South China Sea and the upstream Kuroshio. *Deep-Sea Research I*, *85*, 56–71. https://doi.org/10.1016/j.dsr.2013.11.006

Chen, Y. L. L., Chen, H. Y., Tuo, S. H., & Ohki, K. (2008). Seasonal dynamics of new production from *Trichodesmium* N_2 fixation and nitrate uptake in the upstream Kuroshio and South China Sea basin. *Limnology and Oceanography*, *53*(5), 1705–1721. https://doi.org/10.4319/lo.2008.53.5.1705

Cheung, S., Nitanai, R., Tsurumoto, C., Endo, H., Nakaoka, S. I., Cheah, W., et al. (2020). Physical forcing controls the basin-scale occurrence of nitrogen-fixing organisms in the North Pacific Ocean. *Global Biogeochemical Cycles*, *34*(9), e2019GB006452. https://doi.org/10.1029/2019gb006452

Cheung, S., Zehr, J. P., Xia, X., Tsurumoto, C., Endo, H., Nakaoka, S. I., et al. (2021). Gamma4: A genetically versatile Gammaproteobacterial *nifH* phylotype that is widely distributed in the North Pacific Ocean. *Environmental Microbiology*, *23*(8), 4246–4259. https://doi.org/10.1111/1462-2920.15604

Cho, H.-M., Kim, G., Kwon, E. Y., & Han, Y. (2019). Radium tracing cross-shelf fluxes of nutrients in the Northwest Pacific Ocean. *Geophysical Research Letters*, *46*(20), 11321–11328. https://doi.org/10.1029/2019GL084594

Chow, C. H., Cheah, W., & Tai, J. H. (2017). A rare and extensive summer bloom enhanced by ocean eddies in the oligotrophic western North Pacific Subtropical Gyre. *Scientific Reports*, *7*(1), 6199. https://doi.org/10.1038/s41598-017-06584-3

Church, M. J., Björkman, K., Karl, D. M., Saito, M. A., & Zehr, J. P. (2008). Regional distributions of nitrogen-fixing bacteria in the Pacific Ocean. *Limnology and Oceanography*, *53*(1), 63–77. https://doi.org/10.4319/lo.2008.53.1.0063

Church, M. J., Jenkins, B. D., Karl, D. M., & Zehr, J. P. (2005). Vertical distributions of nitrogen fixing phylotypes at Stn ALOHA in the oligotrophic North Pacific Ocean. *Aquatic Microbial Ecology*, *38*(1), 3–14. https://doi.org/10.3354/ame038003

Church, M. J., Mahaffey, C., Letelier, R. M., Lukas, R., Zehr, J. P., & Karl, D. M. (2009). Physical forcing of nitrogen fixation and diazotroph community structure in the North Pacific subtropical gyre. *Global Biogeochemical Cycles*, *23*(2), GB2020. https://doi.org/10.1029/2008gb003418

Cianca, A., Helmke, P., Mourino, B., Rueda, M. J., Llinas, O., & Neuer, S. (2007). Decadal analysis of hydrography and in situ nutrient budgets in the western and eastern North Atlantic subtropical gyre. *Journal of Geophysical Research*, *112*(C7), C07025. https://doi.org/10.1029/2006jc003788

Clarke, G. L., Ewing, G. C., & Lorenzen, C. J. (1970). Spectra of backscattered light from the sea obtained from aircraft as a measure of chlorophyll concentration. *Science*, *167*(3921), 1119–1121. https://doi.org/10.1126/science.167.3921.1119

Claustre, H., Johnson, K. S., & Takeshita, Y. (2020). Observing the global ocean with biogeochemical-Argo. *Annual Review of Marine Science*, *12*(1), 23–48. https://doi.org/10.1146/annurev-marine-010419-010956

Coale, K. H., & Bruland, K. W. (1987). Oceanic stratified euphotic zone as elucidated by ^{234}Th:^{238}U disequilibria. *Limnology and Oceanography*, *32*(1), 189–200. https://doi.org/10.4319/lo.1987.32.1.0189

Conway, H. L., & Harrison, P. J. (1977). Marine diatoms grown in chemostats under silicate or ammonium limitation. IV. Transient response of *Chaetoceros debilis*, *Skeletonema costatum*, and *Thalassiosira gravida* to a single addition of the limiting nutrient. *Marine Biology*, *43*(1), 33–43. https://doi.org/10.1007/BF00392569

Conway, T. M., & John, S. G. (2014). Quantification of dissolved iron sources to the North Atlantic Ocean. *Nature*, *511*(7508), 212–215. https://doi.org/10.1038/nature13482

Corbière, A., Metzl, N., Reverdin, G., Brunet, C., & Takahashi, A. (2007). Interannual and decadal variability of the oceanic carbon sink in the North Atlantic Subpolar Gyre. *Tellus B*, *59*(2), 168–178. https://doi.org/10.1111/j.1600-0889.2006.00232.x

Cornec, M., Claustre, H., Mignot, A., Guidi, L., Lacour, L., Poteau, A., et al. (2021). Deep chlorophyll maxima in the global ocean: Occurrences, drivers and characteristics. *Global Biogeochem Cycles*, *35*(4), e2020GB006759. https://doi.org/10.1029/2020GB006759

Cosca, C. E. (2003). Seasonal and interannual CO_2 fluxes for the central and eastern equatorial Pacific Ocean as determined from fCO_2-SST relationships. *Journal of Geophysical Research*, *108*(C8), 3278. https://doi.org/10.1029/2000jc000677

Cossarini, G., Mariotti, L., Feudale, L., Mignot, A., Salon, S., Taillandier, V., et al. (2019). Towards operational 3D-Var assimilation of chlorophyll biogeochemical-Argo float data into a biogeochemical model of the Mediterranean Sea. *Ocean Modelling*, *133*, 112–128. https://doi.org/10.1016/j.ocemod.2018.11.005

Cullen, J. J. (1982). The deep chlorophyll maximum: Comparing vertical profiles of chlorophyll *a*. *Canadian Journal of Fisheries and Aquatic Sciences*, *39*(5), 791–803. https://doi.org/10.1139/f82-108

Cullen, J. J. (2015). Subsurface chlorophyll maximum layers: Enduring enigma or mystery solved? *Annual Review of Marine Science*, *7*(1), 207–239. https://doi.org/10.1146/annurev-marine-010213-135111

Cutter, G. A., & Bruland, K. W. (2012). Rapid and noncontaminating sampling system for trace elements in global ocean surveys. *Limnology and Oceanography-Methods*, *10*(6), 425–436. https://doi.org/10.4319/lom.2012.10.425

Dave, A. C., Barton, A. D., Lozier, M. S., & McKinley, G. A. (2015). What drives seasonal change in oligotrophic area in the subtropical North Atlantic? *Journal of Geophysical Research: Oceans*, *120*(6), 3958–3969. https://doi.org/10.1002/2015JC010787

Dave, A. C., & Lozier, M. S. (2010). Local stratification control of marine productivity in the subtropical North Pacific. *Journal of Geophysical Research*, *115*(C12), C12032. https://doi.org/10.1029/2010jc006507

Dave, A. C., & Lozier, M. S. (2013). Examining the global record of interannual variability in stratification and marine productivity in the low-latitude and mid-latitude ocean. *Journal of Geophysical Research: Oceans*, *118*(6), 3114–3127. https://doi.org/10.1002/jgrc.20224

Delhez, E. J. M., & Deleersnijder, E. (2010). Residence time and exposure time of sinking phytoplankton in the euphotic layer. *Journal of Theoretical Biology*, *262*(3), 505–516. https://doi.org/10.1016/j.jtbi.2009.10.004

Dentener, F., Drevet, J., Lamarque, J. F., Bey, I., Eickhout, B., Fiore, A. M., et al. (2006). Nitrogen and sulfur deposition on regional and global scales: A multimodel evaluation. *Global Biogeochemical Cycles*, *20*(4), GB4003. https://doi.org/10.1029/2005GB002672

Deutsch, C., Sarmiento, J. L., Sigman, D. M., Gruber, N., & Dunne, J. P. (2007). Spatial coupling of nitrogen inputs and losses in the ocean. *Nature*, *445*(7124), 163–167. https://doi.org/10.1038/nature05392

Doddridge, E. W., & Marshall, D. P. (2018). Implications of eddy cancellation for nutrient distribution within subtropical gyres. *Journal of Geophysical Research: Oceans*, *123*(9), 6720–6735. https://doi.org/10.1029/2018jc013842

Dore, J. E., Brum, J. R., Tupas, L. M., & Karl, D. M. (2002). Seasonal and interannual variability in sources of nitrogen supporting export in the oligotrophic subtropical North Pacific Ocean. *Limnology and Oceanography*, *47*(6), 1595–1607. https://doi.org/10.4319/lo.2002.47.6.1595

Dore, J. E., Letelier, R. M., Church, M. J., Lukas, R., & Karl, D. M. (2008). Summer phytoplankton blooms in the oligotrophic North Pacific Subtropical Gyre: Historical perspective and recent observations. *Progress in Oceanography*, *76*(1), 2–38. https://doi.org/10.1016/j.pocean.2007.10.002

Doty, M. S. (1962). *Proceedings of the conference on primary productivity measurement, marine and freshwater: 1961*. Technical Report Archive & Image Library.

Du, C., He, R., Liu, Z., Huang, T., Wang, L., Yuan, Z., et al. (2021). Climatology of nutrient distributions in the South China Sea based on a large data set derived from a new algorithm. *Progress in Oceanography*, *195*, 102586. https://doi.org/10.1016/j.pocean.2021.102586

Du, C., Liu, Z., Kao, S.-J., & Dai, M. (2017). Diapycnal fluxes of nutrients in an oligotrophic oceanic regime: The South China Sea. *Geophysical Research Letters*, *44*(22), 510–518. https://doi.org/10.1002/2017GL074921

Duarte, C. M., Regaudie-de-Gioux, A., Arrieta, J. M., Delgado-Huertas, A., & Agusti, S. (2013). The oligotrophic ocean is heterotrophic. *Annual Review of Marine Science*, *5*(1), 551–569. https://doi.org/10.1146/annurev-marine-121211-172337

Duce, R. A., LaRoche, J., Altieri, K., Arrigo, K. R., Baker, A. R., Capone, D. G., et al. (2008). Impacts of atmospheric anthropogenic nitrogen on the open ocean. *Science*, *320*(5878), 893–897. https://doi.org/10.1126/science.1150369

Ducklow, H. W., Steinberg, D. K., & Buesseler, K. O. (2001). Upper ocean carbon export and the biological pump. *Oceanography*, *14*(4), 50–58. https://doi.org/10.5670/oceanog.2001.06

Dugdale, R. C. (1967). Nutrient limitation in the sea: Dynamics, identification, and significance. *Limnology and Oceanography*, *12*(4), 685–695. https://doi.org/10.4319/lo.1967.12.4.0685

Dugdale, R. C., & Goering, J. J. (1967). Uptake of new and regenerated forms of nitrogen in primary production. *Limnology and Oceanography*, *12*(2), 196–206. https://doi.org/10.4319/lo.1967.12.2.0196

Dugenne, M., Gradoville, M. R., Church, M. J., Wilson, S. T., Sheyn, U., Harke, M. J., et al. (2023). Nitrogen fixation in mesoscale eddies of the North Pacific Subtropical Gyre: Patterns and mechanisms. *Global Biogeochem. Cycles*, *37*(4), e2022GB007386. https://doi.org/10.1029/2022GB007386

Dugenne, M., Henderikx Freitas, F., Wilson, S. T., Karl, D. M., & White, A. E. (2020). Life and death of *Crocosphaera* sp. in the Pacific Ocean: Fine scale predator–prey dynamics. *Limnology and Oceanography*, *65*(11), 2603–2617. https://doi.org/10.1002/lno.11473

Dutkiewicz, S., Cermeno, P., Jahn, O., Follows, M. J., Hickman, A. E., Taniguchi, D. A. A., & Ward, B. A. (2020). Dimensions of marine phytoplankton diversity. *Biogeosciences*, *17*(3), 609–634. https://doi.org/10.5194/bg-17-609-2020

Dutkiewicz, S., Ward, B. A., Scott, J., & Follows, M. J. (2014). Understanding predicted shifts in diazotroph biogeography using resource competition theory. *Biogeosciences*, *11*(17), 5445–5461. https://doi.org/10.5194/bg-11-5445-2014

Egge, J., & Aksnes, D. (1992). Silicate as regulating nutrient in phytoplankton competition. *Marine Ecology Progress Series*, *83*(2), 281–289. https://doi.org/10.3354/meps083281

Emerson, S. (2014). Annual net community production and the biological carbon flux in the ocean. *Global Biogeochem. Cycles*, *28*(1), 14–28. https://doi.org/10.1002/2013GB004680

Endo, H., Ogata, H., & Suzuki, K. (2018). Contrasting biogeography and diversity patterns between diatoms and haptophytes in the central Pacific Ocean. *Scientific Reports*, *8*(1), 10916. https://doi.org/10.1038/s41598-018-29039-9

Eppley, R. W. (1972). Temperature and phytoplankton growth in the sea. *Fishery Bulletin*, *70*, 1063–1085.

Eppley, R. W., & Peterson, B. J. (1979). Particulate organic matter flux and planktonic new production in the deep ocean. *Nature*, *282*(5740), 677–680. https://doi.org/10.1038/282677a0

Eppley, R. W., Renger, E. H., Venrick, E. L., & Mullin, M. M. (1973). A study of plankton dynamics and nutrient cycling in the central gyre of the North Pacific Ocean. *Limnology and Oceanography*, *18*(4), 534–551. https://doi.org/10.4319/lo.1973.18.4.0534

Falkowski, P. G. (1994). The role of phytoplankton photosynthesis in global biogeochemical cycles. *Photosynthesis Research*, *39*(3), 235–258. https://doi.org/10.1007/BF00014586

Farnelid, H., Turk-Kubo, K., Ploug, H., Ossolinski, J. E., Collins, J. R., van Mooy, B. A. S., & Zehr, J. P. (2019). Diverse diazotrophs are present on sinking particles in the North Pacific Subtropical Gyre. *ISME Journal*, *13*(1), 170–182. https://doi.org/10.1038/s41396-018-0259-x

Fawcett, S. E., Lomas, M., Casey, J. R., Ward, B. B., & Sigman, D. M. (2011). Assimilation of upwelled nitrate by small eukaryotes in the Sargasso Sea. *Nature Geoscience*, *4*(10), 717–722. https://doi.org/10.1038/ngeo1265

Fennel, K., Gehlen, M., Brasseur, P., Brown, C. W., Ciavatta, S., Cossarini, G., et al. (2019). Advancing marine biogeochemical and ecosystem reanalyses and forecasts as tools for monitoring and managing ecosystem health. *Frontiers in Marine Science*, *6*, 89. https://doi.org/10.3389/fmars.2019.00089

Fernandez, I. C., Raimbault, P., Caniaux, G., Garcia, N., & Rimmelin, P. (2005). Influence of mesoscale eddies on nitrate distribution during the POMME program in the northeast Atlantic Ocean. *Journal of Marine Systems*, *55*(3–4), 155–175. https://doi.org/10.1016/j.jmarsys.2004.08.007

Fernandez-Castro, B., Mourino-Carballido, B., Marañón, E., Choucino, P., Gago, J., Ramirez, T., et al. (2015). Importance of salt fingering for new nitrogen supply in the oligotrophic ocean. *Nature Communications*, *6*(1), 8002. https://doi.org/10.1038/ncomms9002

Ferrón, S., Barone, B., Church, M. J., White, A. E., & Karl, D. M. (2021). Euphotic zone metabolism in the North Pacific Subtropical Gyre based on oxygen dynamics. *Global Biogeochemical Cycles*, *35*(3), e2020GB006744. https://doi.org/10.1029/2020GB006744

Feucher, C., Maze, G., & Mercier, H. (2019). Subtropical mode water and permanent pycnocline properties in the world ocean. *Journal of Geophysical Research: Oceans*, *124*(2), 1139–1154. https://doi.org/10.1029/2018jc014526

Fitzsimmons, J. N., Boyle, E. A., & Jenkins, W. J. (2014). Distal transport of dissolved hydrothermal iron in the deep South Pacific Ocean. *Proceedings of the National Academy of Sciences of the United States of America*, *111*(47), 16654–16661. https://doi.org/10.1073/pnas.1418778111

Fitzsimmons, J. N., Hayes, C. T., Al-Subiai, S. N., Zhang, R. F., Morton, P. L., Weisend, R. E., et al. (2015). Daily to decadal variability of size-fractionated iron and iron-binding ligands at the Hawaii Ocean Time-series Station ALOHA. *Geochimica et Cosmochimica Acta*, *171*, 303–324. https://doi.org/10.1016/j.gca.2015.08.012

Flombaum, P., Gallegos, J. L., Gordillo, R. A., Rincon, J., Zabala, L. L., Jiao, N., et al. (2013). Present and future global distributions of the marine Cyanobacteria *Prochlorococcus* and *Synechococcus*. *Proceedings of the National Academy of Sciences of the United States of America*, *110*(24), 9824–9829. https://doi.org/10.1073/pnas.1307701110

Follett, C. L., Dutkiewicz, S., Karl, D. M., Inomura, K., & Follows, M. J. (2018). Seasonal resource conditions favor a summertime increase in North Pacific diatom-diazotroph associations. *ISME Journal*, *12*(6), 1543–1557. https://doi.org/10.1038/s41396-017-0012-x

Fong, A. A., Karl, D. M., Lukas, R., Letelier, R. M., Zehr, J. P., & Church, M. J. (2008). Nitrogen fixation in an anticyclonic eddy in the oligotrophic North Pacific Ocean. *ISME Journal*, *2*(6), 663–676. https://doi.org/10.1038/ismej.2008.22

Friedrich, T., Powell, B. S., Stock, C. A., Hahn-Woernle, L., Dussin, R., & Curchitser, E. N. (2021). Drivers of phytoplankton blooms in Hawaii: A regional model study. *Journal of Geophysical Research: Oceans*, *126*(5), e2020JC017069. https://doi.org/10.1029/2020jc017069

Ganachaud, A., & Wunsch, C. (2002). Oceanic nutrient and oxygen transports and bounds on export production during the World Ocean Circulation Experiment. *Global Biogeochemical Cycles*, *16*(4), 5-1–5-14. https://doi.org/10.1029/2000GB001333

Garcia, H. E., Weathers, K., Paver, C. R., Smolyar, I., Boyer, T. P., Locarnini, R. A., et al. (2019). In A. M. Technical (Ed.), *World Ocean Atlas 2018, volume 4: Dissolved inorganic nutrients (phosphate, nitrate and nitrate+nitrite, silicate)* (Vol. 84, p. 35). NOAA Atlas NESDIS.

Garcia-Corral, L. S., Holding, J. M., Carrillo-de-Albornoz, P., Steckbauer, A., Perez-Lorenzo, M., Navarro, N., et al. (2017). Temperature dependence of plankton community metabolism in the subtropical and tropical oceans. *Global Biogeochemical Cycles*, *31*(7), 1141–1154. https://doi.org/10.1002/2017gb005629

GEOTRACES Intermediate Data Product Group. (2021). *The GEOTRACES intermediate data product 2021 (IDP2021)*. NERC EDS British Oceanographic Data Centre NOC. Retrieved from https://www.geotraces.org/geotraces-intermediate-data-product-2021/

Goldman, J. C. (1984). Oceanic nutrient cycles. In M. J. R. Fasham (Ed.), *Flows of energy and materials in marine ecosystems: Theory and practice* (pp. 137–170). Plenum Press.

Goldthwait, S. A., & Steinberg, D. K. (2008). Elevated biomass of mesozooplankton and enhanced fecal pellet flux in cyclonic and mode-water eddies in the Sargasso Sea. *Deep-Sea Research II*, *55*(10–13), 1360–1377. https://doi.org/10.1016/j.dsr2.2008.01.003

Grabowski, M. N. W., Church, M. J., & Karl, D. M. (2008). Nitrogen fixation rates and controls at Stn ALOHA. *Aquatic Microbial Ecology*, *52*(2), 175–183. https://doi.org/10.3354/ame01209

Gradoville, M. R., Farnelid, H., White, A. E., Turk-Kubo, K. A., Stewart, B., Ribalet, F., et al. (2020). Latitudinal constraints on the abundance and activity of the cyanobacterium UCYN-A and other marine diazotrophs in the North Pacific. *Limnology and Oceanography*, *65*(8), 1858–1875. https://doi.org/10.1002/lno.11423

Graff, J. R., Westberry, T. K., Milligan, A. J., Brown, M. B., Dall'Olmo, G., Dongen-Vogels, V. V., et al. (2015). Analytical phytoplankton carbon measurements spanning diverse ecosystems. *Deep Sea Research Part I: Oceanographic Research Papers*, *102*, 16–25. https://doi.org/10.1016/j.dsr.2015.04.006

Gregg, W. W., & Rousseaux, C. S. (2019). Global ocean primary production trends in the modern ocean color satellite record (1998–2015). *Environmental Research Letters*, *14*(12), 124011. https://doi.org/10.1088/1748-9326/ab4667

Großkopf, T., Mohr, W., Baustian, T., Schunck, H., Gill, D., Kuypers, M. M. M., et al. (2012). Doubling of marine dinitrogen-fixation rates based on direct measurements. *Nature*, *488*(7411), 361–364. https://doi.org/10.1038/nature11338

Gruber, N., Capone, D. G., Bronk, D. A., Mulholland, M. R., & Carpenter, E. J. (2008). The marine nitrogen cycle: Overview and challenges. In D. G. Capone, D. A. Bronk, M. R. Mulholland, & E. J. Carpenter (Eds.), *Nitrogen in the marine environment* (2nd ed., pp. 1–50). Elsevier. https://doi.org/10.1016/b978-0-12-372522-6.00001-3

Gruber, N., & Sarmiento, J. L. (1997). Global patterns of marine nitrogen fixation and denitrification. *Global Biogeochemical Cycles*, *11*(2), 235–266. https://doi.org/10.1029/97GB00077

Guidi, L., Calil, P. H. R., Duhamel, S., Björkman, K. M., Doney, S. C., Jackson, G. A., et al. (2012). Does eddy-eddy interaction control surface phytoplankton distribution and carbon export in the North Pacific Subtropical Gyre? *Journal of Geophysical Research*, *117*(G2), G02024. https://doi.org/10.1029/2012JG001984

Guieu, C., Bonnet, S., Petrenko, A., Menkes, C., Chavagnac, V., Desboeufs, K., et al. (2018). Iron from a submarine source impacts the productive layer of the Western Tropical South Pacific (WTSP). *Scientific Reports*, *8*(1), 9075. https://doi.org/10.1038/s41598-018-27407-z

Guo, X., Zhu, X.-H., Wu, Q.-S., & Huang, D. (2012). The Kuroshio nutrient stream and its temporal variation in the East China Sea. *Journal of Geophysical Research*, *11*(C1), C01026. https://doi.org/10.1029/2011JC007292

Gupta, M., Williams, R. G., Lauderdale, J. M., Jahn, O., Hill, C., Dutkiewicz, S., & Follows, M. J. (2022). A nutrient relay sustains subtropical ocean productivity. *Proceedings of the National Academy of Sciences of the United States of America*, *119*(41), e2206504119. https://doi.org/10.1073/pnas.2206504119

Hashihama, F., Kanda, J., Maeda, Y., Ogawa, H., & Furuya, K. (2014). Selective depressions of surface silicic acid within cyclonic mesoscale eddies in the oligotrophic western North Pacific. *Deep Sea Research I*, *90*, 115–124. https://doi.org/10.1016/j.dsr.2014.05.004

Hashihama, F., Saito, H., Shiozaki, T., Ehama, M., Suwa, S., Sugiyama, T., et al. (2020). Biogeochemical controls of particulate phosphorus distribution across the oligotrophic subtropical Pacific Ocean. *Global Biogeochemical Cycles*, *34*(9), e2020GB006669. https://doi.org/10.1029/2020GB006669

Hashihama, F., Yasuda, I., Kumabe, A., Sato, M., Sasaoka, H., Iida, Y., et al. (2021). Nanomolar phosphate supply and its recycling drive net community production in the subtropical North Pacific. *Nature Communications*, *12*(1), 3462. https://doi.org/10.1038/s41467-021-23837-y

Hawco, N. J., Barone, B., Church, M. J., Babcock-Adams, L., Repeta, D. J., Wear, E. K., et al. (2021). Iron depletion in the deep chlorophyll maximum: Mesoscale eddies as natural iron fertilization experiments. *Global Biogeochemical Cycles*, *35*(12), e2021GB007112. https://doi.org/10.1029/2021GB007112

Hawco, N. J., Yang, S.-C., Foreman, R. K., Funkey, C. P., Dugenne, M., White, A. E., et al. (2020). Metal isotope signatures from lava-seawater interaction during the 2018 eruption of Kīlauea. *Geochimica et Cosmochimica Acta*, *282*, 340–356. https://doi.org/10.1016/j.gca.2020.05.005

Hawco, N. J., Yang, S.-C., Pinedo-González, P., Black, E. E., Kenyon, J., Ferrón, S., et al. (2022). Recycling of dissolved iron in the North Pacific Subtropical Gyre. *Limnology and Oceanography*, *67*(11), 2448–2465. https://doi.org/10.1002/lno.12212

Henderson, G. M. (2016). Ocean trace element cycles. *Philosophical Transactions of the Royal Society A: Mathematical, Physical and Engineering Sciences*, *374*(2081), 20150300. https://doi.org/10.1098/rsta.2015.0300

Henson, S. A., Cael, B. B., Allen, S. R., & Dutkiewicz, S. (2021). Future phytoplankton diversity in a changing climate. *Nature Communications*, *12*(1), 5372. https://doi.org/10.1038/s41467-021-25699-w

Henson, S. A., Sarmiento, J. L., Dunne, J. P., Bopp, L., Lima, I., Doney, S. C., et al. (2010). Detection of anthropogenic climate change in satellite records of ocean chlorophyll and productivity. *Biogeosciences*, *7*(2), 621–640. https://doi.org/10.5194/bg-7-621-2010

Hewson, I., Govil, S. R., Capone, D. G., Carpenter, E. J., & Fuhrman, J. A. (2004). Evidence of Trichodesmium viral lysis and potential significance for biogeochemical cycling in the oligotrophic ocean. *Aquatic Microbial Ecology*, *36*(1), 1–8. https://doi.org/10.3354/ame036001

Hoegh-Guldberg, O., Cai, R., Poloczanska, E. S., Brewer, P. G., Sundby, S., Hilmi, K., et al. (2014). The ocean - Supplementary material. In V. R. Barros, C. B. Field, D. J. Dokken, M. D. Mastrandrea, K. J. Mach, T. E. Bilir, et al. (Eds.), *Climate change 2014: Impacts, adaptation, and vulnerability. Part B: Regional aspects. Contribution of working group II to the fifth assessment report of the intergovernmental panel on climate change*. Retrieved from www.ipcc-wg2.gov/AR5%20and%20www.ipcc.ch

Hofmann, M., Worm, B., Rahmstorf, S., & Schellnhuber, H. J. (2011). Declining ocean chlorophyll under unabated anthropogenic CO_2 emissions. *Environmental Research Letters*, *6*(3), 034035. https://doi.org/10.1088/1748-9326/6/3/034035

Hogle, S. L., Dupont, C. L., Hopkinson, B. M., King, A. L., Buck, K. N., Roe, K. L., et al. (2018). Pervasive iron limitation at subsurface chlorophyll maxima of the California Current. *Proceedings of the National Academy of Sciences of the United States of America*, *115*(52), 13300–13305. https://doi.org/10.1073/pnas.1813192115

Hu, C. M., Lee, Z., & Franz, B. (2012). Chlorophyll *a* algorithms for oligotrophic oceans: A novel approach based on three-band reflectance difference. *Journal of Geophysical Research*, *117*(C1), C01011. https://doi.org/10.1029/2011jc007395

Huang, Y., Tagliabue, A., & Cassar, N. (2022). Data-driven modeling of dissolved iron in the global ocean. *Frontiers in Marine Science*, *9*, 837183. https://doi.org/10.3389/fmars.2022.837183

Hudson, R. J. M., & Morel, F. M. M. (1990). Iron transport in marine phytoplankton: Kinetics of cellular and medium coordination reactions. *Limnology and Oceanography*, *35*(5), 1002–1020. https://doi.org/10.4319/lo.1990.35.5.1002

Hunt, B. P. V., Bonnet, S., Berthelot, H., Conroy, B. J., Foster, R. A., & Pagano, M. (2016). Contribution and pathways of diazotroph-derived nitrogen to zooplankton during the VAHINE mesocosm experiment in the oligotrophic New Caledonia lagoon. *Biogeosciences*, *13*(10), 3131–3145. https://doi.org/10.5194/bg-13-3131-2016

Iida, Y., Kojima, A., Takatani, Y., Nakano, T., Sugimoto, H., Midorikawa, T., & Ishii, M. (2015). Trends in pCO_2 and sea–air CO_2 flux over the global open oceans for the last two decades. *Journal of Oceanography*, *71*(6), 637–661. https://doi.org/10.1007/s10872-015-0306-4

Iida, Y., Takatani, Y., Kojima, A., & Ishii, M. (2021). Global trends of ocean CO_2 sink and ocean acidification: An observation-based reconstruction of surface ocean inorganic carbon variables. *Journal of Oceanography*, *77*(2), 323–358. https://doi.org/10.1007/s10872-020-00571-5

IPCC. (2021). Summary for policymakers. In *Climate change 2021: The physical science basis. Contribution of working group I to the sixth assessment report of the intergovernmental panel on climate change* (pp. 3–32).

Irwin, A. J., & Oliver, M. J. (2009). Are ocean deserts getting larger? *Geophysical Research Letters*, *36*(18), L18609. https://doi.org/10.1029/2009gl039883

Jenkins, W. J., & Doney, S. C. (2003). The subtropical nutrient spiral. *Global Biogeochemical Cycles*, *17*(4), 1110. https://doi.org/10.1029/2003gb002085

Jiang, S., Hashihama, F., & Saito, H. (2021). Phytoplankton growth and grazing mortality through the oligotrophic subtropical North Pacific. *Journal of Oceanography*, *77*(3), 505–521. https://doi.org/10.1007/s10872-020-00580-4

Jickells, T. D., An, Z. S., Andersen, K. K., Baker, A. R., Bergametti, G., Brooks, N., et al. (2005). Global iron connections between desert dust, ocean biogeochemistry, and climate. *Science*, *308*(5718), 67–71. https://doi.org/10.1126/science.1105959

Johnson, K. S., Riser, S. C., & Karl, D. M. (2010). Nitrate supply from deep to near-surface waters of the North Pacific subtropical gyre. *Nature*, *465*(7301), 1062–1065. https://doi.org/10.1038/nature09170

Johnson, Z. I., Zinser, E. R., Coe, A., McNulty, N. P., Woodward, E. M. S., & Chisholm, S. W. (2006). Niche partitioning among *Prochlorococcus* ecotypes along ocean-scale environmental gradients. *Science*, *311*(5768), 1737–1740. https://doi.org/10.1126/science.1118052

Jung, J., Furutani, H., & Uematsu, M. (2011). Atmospheric inorganic nitrogen in marine aerosol and precipitation and its deposition to the North and South Pacific Oceans. *Journal of Atmospheric Chemistry*, *68*(2), 157–181. https://doi.org/10.1007/s10874-012-9218-5

Jung, J., Han, B., Rodriguez, B., Miyazaki, Y., Chung, H. Y., Kim, K., et al. (2019). Atmospheric dry deposition of water-soluble nitrogen to the subarctic western North Pacific Ocean during summer. *Atmosphere*, *10*(7), 351. https://doi.org/10.3390/atmos10070351

Juranek, L. W., White, A. E., Dugenne, M., Henderikx Freitas, F., Dutkiewicz, S., Ribalet, F., et al. (2020). The importance of the phytoplankton "middle class" to ocean net community production. *Global Biogeochemical Cycles*, *34*(12), e2020GB006702. https://doi.org/10.1029/2020GB006702

Karl, D. M. (1999). A sea of change: Biogeochemical variability in the North Pacific Subtropical Gyre. *Ecosystems*, *2*(3), 181–214. https://doi.org/10.1007/s100219900068

Karl, D. M. (2002a). Hidden in a sea of microbes. *Nature*, *415*(6872), 590–591. https://doi.org/10.1038/415590b

Karl, D. M. (2002b). Nutrient dynamics in the deep blue sea. *Trends in Microbiology*, *10*(9), 410–418. https://doi.org/10.1016/s0966-842x(02)02430-7

Karl, D. M., Bates, N. R., Emerson, S., Harrison, P. J., Jeandel, C., Llinâs, O., et al. (2003). Temporal studies of biogeochemical processes determined from ocean time-series observations during the JGOFS Era. In M. J. R. Fasham (Ed.), *Ocean biogeochemistry: The role of the ocean carbon cycle in global change* (pp. 239–267). Springer Berlin Heidelberg. https://doi.org/10.1007/978-3-642-55844-3_11

Karl, D. M., Bidigare, R. R., & Letelier, R. (2007). Sustained and aperiodic variability in organic matter production and phototrophic microbial community structure in the North Pacific Subtropical Gyre. In P. Williams, D. Thomas, & C. Reynolds (Eds.), *Phytoplankton productivity: Carbon assimilation in marine and freshwater ecosystems* (p. 386). Wiley-Blackwell. https://doi.org/10.1002/9780470995204.ch9

Karl, D. M., Bidigare, R. R., & Letelier, R. M. (2001). Long-term changes in plankton community structure and productivity in the North Pacific Subtropical Gyre: The domain shift hypothesis. *Deep-Sea Research II*, *48*(8–9), 1449–1470. https://doi.org/10.1016/S0967-0645(00)00149-1

Karl, D. M., Bidigare, R. R., & Letelier, R. M. (2002). Sustained and aperiodic variability in organic matter production and phototrophic microbial community structure in the North Pacific Subtropical gyre. In P. J. L. B. Williams, D. N. Thomas, & C. S. Reynolds (Eds.), *Phytoplankton productivity: Carbon assimilation in marine and freshwater ecosystems* (pp. 222–264). Blackwell.

Karl, D. M., Björkman, K. M., Dore, J. E., Fujieki, L., Hebel, D. V., Houlihan, T., et al. (2001). Ecological nitrogen-to-phosphorus stoichiometry at station ALOHA. *Deep-Sea Research II*, *48*(8–9), 1529–1566. https://doi.org/10.1016/S0967-0645(00)00152-1

Karl, D. M., & Church, M. J. (2014). Microbial oceanography and the Hawaii Ocean Time-series programme. *Nature Reviews Microbiology*, *12*(10), 699–713. https://doi.org/10.1038/nrmicro3333

Karl, D. M., & Church, M. J. (2017). Ecosystem structure and dynamics in the North Pacific Subtropical Gyre: New views of an old ocean. *Ecosystems*, *20*(3), 433–457. https://doi.org/10.1007/s10021-017-0117-0

Karl, D. M., Church, M. J., Dore, J. E., Letelier, R. M., & Mahaffey, C. (2012). Predictable and efficient carbon sequestration in the North Pacific Ocean supported by symbiotic nitrogen fixation. *Proceedings of the National Academy of Sciences of the United States of America*, *109*(6), 1842–1849. https://doi.org/10.1073/pnas.1120312109

Karl, D. M., & Letelier, R. M. (2008). Nitrogen fixation-enhanced carbon sequestration in low nitrate, low chlorophyll seascapes. *Marine Ecology Progress Series*, *364*, 257–268. https://doi.org/10.3354/meps07547

Karl, D. M., Letelier, R. M., Bidigare, R. R., Björkman, K. M., Church, M. J., Dore, J. E., & White, A. E. (2021). Seasonal-to-decadal scale variability in primary production and particulate matter export at Station ALOHA. *Progress in Oceanography*, *195*, 102563. https://doi.org/10.1016/j.pocean.2021.102563

Karl, D. M., Letelier, R. M., Hebel, D., Tupas, L., Dore, J. E., Christian, J., & Winn, C. (1995). Ecosystem changes in the North Pacific Subtropical Gyre attributed to the 1991–92 El Niño. *Nature*, *373*(6511), 230–234. https://doi.org/10.1038/373230a0

Karl, D. M., & Lukas, R. (1996). The Hawaii Ocean Time-series (HOT) Program: Background, rationale and field implementation. *Deep-Sea Research II*, *43*(2–3), 129–156. https://doi.org/10.1016/0967-0645(96)00005-7

Karl, D. M., & Michaels, A. F. (1996). The Hawaii Ocean Time series (HOT) and the Bermuda Atlantic Time series (BATS). *Deep-Sea Research II*, *43*(2–3), 127–129. https://doi.org/10.1016/S0967-0645(96)90000-4

Karl, D. M., & Tien, G. (1992). MAGIC: A sensitive and precise method for measuring dissolved phosphorus in aquatic environments. *Limnology and Oceanography*, *37*(1), 105–116. https://doi.org/10.4319/lo.1992.37.1.0105

Kavanaugh, M. T., Church, M. J., Davis, C. O., Karl, D. M., Letelier, R. M., & Doney, S. C. (2018). ALOHA from the edge: Reconciling three decades of in situ Eulerian observations and geographic variability in the North Pacific Subtropical Gyre. *Frontiers in Marine Science*, *5*, 130. https://doi.org/10.3389/fmars.2018.00130

Kemp, A. E. S., & Villareal, T. A. (2013). High diatom production and export in stratified waters - A potential negative feedback to global warming. *Progress in Oceanography*, *119*, 4–23. https://doi.org/10.1016/j.pocean.2013.06.004

Kim, I.-N., Lee, K., Gruber, N., Karl, D. M., Bullister, J. L., Yang, S., & Kim, T.-W. (2014). Increasing anthropogenic nitrogen in the North Pacific Ocean. *Science*, *346*(6213), 1102–1106. https://doi.org/10.1126/science.1258396

Kitajima, S., Furuya, K., Hashihama, F., Takeda, S., & Kanda, J. (2009). Latitudinal distribution of diazotrophs and their nitrogen fixation in the tropical and subtropical western North Pacific. *Limnology and Oceanography*, *54*(2), 537–547. https://doi.org/10.4319/lo.2009.54.2.0537

Kletou, D., & Hall-Spencer, J. M. (2012). Threats to ultraoligotrophic marine ecosystems. In A. Cruzado (Ed.), *Marine ecosystems* (pp. 1–34). InTech.

Knap, A., Michaels, A., Close, A., Ducklow, H., & Dickson, A. (Eds.) (1996). JGOFS Rep. 19, JGOFS Core Proj. Off. [Reprint of Intergovernmental Oceanographic Commission Manuals and Guides], *Protocols for the Joint Global Ocean flux study (JGOFS) core measurements* (Vol. 29, p. 170). UNESCO.

Knapp, A. N., Casciotti, K. L., Berelson, W. M., Prokopenko, M. G., & Capone, D. G. (2016). Low rates of nitrogen fixation in eastern tropical South Pacific surface waters. *Proceedings of the National Academy of Sciences of the United States of America*, *113*(16), 4398–4403. https://doi.org/10.1073/pnas.1515641113

Knapp, A. N., Sigman, D. M., & Lipschultz, F. (2005). N isotopic composition of dissolved organic nitrogen and nitrate at the Bermuda Atlantic Time-series study site. *Global Biogeochemical Cycles*, *19*(1), GB1018. https://doi.org/10.1029/2004GB002320

Kobashi, F., & Kubokawa, A. (2012). Review on North Pacific subtropical countercurrents and subtropical fronts: Role of mode waters in ocean circulation and climate. *Journal of Oceanography*, *68*(1), 21–43. https://doi.org/10.1007/s10872-011-0083-7

König, D., Conway, T. M., Hamilton, D. S., & Tagliabue, A. (2022). Surface ocean biogeochemistry regulates the impact of anthropogenic aerosol Fe deposition on the cycling of iron and iron isotopes in the North Pacific. *Geophysical Research Letters*, *49*(13), e2022GL098016. https://doi.org/10.1029/2022GL098016

Konno, U., Tsunogai, U., Komatsu, D. D., Daita, S., Nakagawa, F., Tsuda, A., et al. (2010). Determination of total N_2 fixation rates in the ocean taking into account both the particulate and filtrate fractions. *Biogeosciences*, *7*(8), 2369–2377. https://doi.org/10.5194/bg-7-2369-2010

Krumhardt, K. M., Lovenduski, N. S., Long, M. C., & Lindsay, K. (2017). Avoidable impacts of ocean warming on marine primary production: Insights from the CESM ensembles. *Global Biogeochemical Cycles*, *31*(1), 114–133. https://doi.org/10.1002/2016GB005528

Kurisu, M., Sakata, K., Uematsu, M., Ito, A., & Takahashi, Y. (2021). Contribution of combustion Fe in marine aerosols over the northwestern Pacific estimated by Fe stable isotope ratios. *Atmospheric Chemistry and Physics*, *21*(20), 16027–16050. https://doi.org/10.5194/acp-21-16027-2021

Kwon, Y. O., Alexander, M. A., Bond, N. A., Frankignoul, C., Nakamura, H., Qiu, B., & Thompson, L. (2010). Role of the Gulf Stream and Kuroshio-Oyashio systems in large-scale atmosphere-ocean interaction: A review. *Journal of Climate*, *23*(12), 3249–3281. https://doi.org/10.1175/2010jcli3343.1

Landolfi, A., Prowe, A. E. F., Pahlow, M., Somes, C. J., Chien, C. T., Schartau, M., et al. (2021). Can top-down controls expand the ecological niche of marine N_2 fixers? *Frontiers in Microbiology*, *12*, 690200. https://doi.org/10.3389/fmicb.2021.690200

Landrum, J. P., Altabet, M. A., & Montoya, J. P. (2011). Basin-scale distributions of stable nitrogen isotopes in the subtropical North Atlantic Ocean: Contribution of diazotroph nitrogen to particulate organic matter and mesozooplankton. *Deep-Sea Research I*, *58*(5), 615–625. https://doi.org/10.1016/j.dsr.2011.01.012

Lauvset, S. K., Lange, N., Tanhua, T., Bittig, H. C., Olsen, A., Kozyr, A., et al. (2022). GLODAPv2.2022: The latest version of the global interior ocean biogeochemical data product. *Earth System Science Data*, *14*(12), 5543–5572. https://doi.org/10.5194/essd-14-5543-2022

Laws, E. A., Bidigare, R. R., & Karl, D. M. (2016). Enigmatic relationship between chlorophyll *a* concentrations and photosynthetic rates at Station ALOHA. *Heliyon*, *2*(9), e00156. https://doi.org/10.1016/j.heliyon.2016.e00156

Laws, E. A., DiTullio, G. R., & Redalje, D. G. (1987). High phytoplankton growth and production rates in the North Pacific Subtropical gyre. *Limnology and Oceanography*, *32*(4), 905–918. https://doi.org/10.4319/lo.1987.32.4.0905

Laws, E. A., Karl, D. M., Redalje, D. G., Jurick, R. S., & Winn, C. D. (1983). Variability in ratios of phytoplankton carbon and RNA to ATP and chlorophyll *a* in batch and continuous cultures. *Journal of Phycology*, *19*(4), 439–445. https://doi.org/10.1111/j.0022-3646.1983.00439.x

Lee, K., Karl, D. M., Wanninkhof, R., & Zhang, J.-Z. (2002). Global estimates of net carbon production in the nitrate-depleted tropical and subtropical oceans. *Geophysical Research Letters*, *29*(19), 1907–13-4. https://doi.org/10.1029/2001GL014198

Lee, Z., Lance, V. P., Shang, S., Vaillancourt, R., Freeman, S., Lubac, B., et al. (2011). An assessment of optical properties and primary production derived from remote sensing in the Southern Ocean (SO GasEx). *Journal of Geophysical Research*, *116*, C00F03. https://doi.org/10.1029/2010JC006747

Lee, Z., Marra, J., Perry, M. J., & Kahru, M. (2015). Estimating oceanic primary productivity from ocean color remote sensing: A strategic assessment. *Journal of Marine Systems*, *149*, 50–59. https://doi.org/10.1016/j.jmarsys.2014.11.015

Lee, Z., & Marra, J. F. (2022). The use of VGPM to estimate oceanic primary production: A "tango" difficult to dance. *Journal of Remote Sensing*, *2022*, 9851013. https://doi.org/10.34133/2022/9851013

Lee, Z., Shang, S., Du, K., Wei, J., & Arnone, R. (2014). Usable solar radiation and its attenuation in the upper water column. *Journal of Geophysical Research: Oceans*, *119*(2), 1488–1497. https://doi.org/10.1002/2013jc009507

Lee, Z., Shang, S., Li, Y., Luis, K., Dai, M., & Wang, Y. (2022). Three-dimensional variation in light quality in the upper water column revealed with a single parameter. *IEEE Transactions on Geoscience and Remote Sensing*, *60*, 1–10. https://doi.org/10.1109/TGRS.2021.3093014

Letelier, R. M., Bidigare, R. R., Hebel, D. V., Ondrusek, M., Winn, C. D., & Karl, D. M. (1993). Temporal variability of phytoplankton community structure based on pigment analysis. *Limnology and Oceanography*, *38*(7), 1420–1437. https://doi.org/10.4319/lo.1993.38.7.1420

Letelier, R. M., Björkman, K. M., Church, M. J., Hamilton, D. S., Mahowald, N. M., Scanza, R. A., et al. (2019). Climate-driven oscillation of phosphorus and iron limitation in the North Pacific Subtropical Gyre. *Proceedings of the National Academy of Sciences of the United States of America*, *116*(26), 12720–12728. https://doi.org/10.1073/pnas.1900789116

Letelier, R. M., Dore, J. E., Winn, C. D., & Karl, D. M. (1996). Seasonal and interannual variations in photosynthetic carbon assimilation at station. *Deep-Sea Research II*, *43*(2–3), 467–490. https://doi.org/10.1016/0967-0645(96)00006-9

Letelier, R. M., Karl, D. M., Abbott, M. R., & Bidigare, R. R. (2004). Light driven seasonal patterns of chlorophyll and nitrate in the lower euphotic zone of the North Pacific Subtropical Gyre. *Limnology and Oceanography*, *49*(2), 508–519. https://doi.org/10.4319/lo.2004.49.2.0508

Letscher, R. T., Hansell, D. A., Carlson, C. A., Lumpkin, R., & Knapp, A. N. (2013). Dissolved organic nitrogen in the global surface ocean: Distribution and fate. *Global Biogeochemical Cycles*, *27*(1), 141–153. https://doi.org/10.1029/2012gb004449

Letscher, R. T., Primeau, F., & Moore, J. K. (2016). Nutrient budgets in the subtropical ocean gyres dominated by lateral transport. *Nature Geoscience*, *9*(11), 815–819. https://doi.org/10.1038/Ngeo2812

Letscher, R. T., Wang, W.-L., Liang, Z., & Knapp, A. N. (2022). Regionally variable contribution of dissolved organic phosphorus to marine annual net community production. *Global Biogeochem. Cycles*, *36*(12), e2022GB007354. https://doi.org/10.1029/2022GB007354

Lewis, M. R., Harrison, W. G., Oakey, N. S., Hebert, D., & Platt, T. (1986). Vertical nitrate fluxes in the oligotrophic ocean. *Science*, *234*(4778), 870–873. https://doi.org/10.1126/science.234.4778.87

Li, B., Karl, D. M., Letelier, R. M., Bidigare, R. R., & Church, M. J. (2013). Variability of chromophytic phytoplankton in the North Pacific Subtropical Gyre. *Deep-Sea Research II*, *93*, 84–95. https://doi.org/10.1016/j.dsr2.2013.03.007

Li, C., Chiang, K.-P., Laws, E. A., Liu, X., Chen, J., Huang, Y., et al. (2022). Quasi-antiphase diel patterns of abundance and cell size/biomass of picophytoplankton in the oligotrophic ocean. *Geophysical Research Letters*, *49*(5), e2022GL097753. https://doi.org/10.1029/2022gl097753

Li, H., Xu, F., Zhou, W., Wang, D., Wright, J. S., Liu, Z., & Lin, Y. (2017). Development of a global gridded Argo data set with Barnes successive corrections. *Journal of Geophysical Research: Oceans*, *122*(2), 866–889. https://doi.org/10.1002/2016JC012285

Li, Q. P., & Hansell, D. A. (2008). Intercomparison and coupling of magnesium-induced co-precipitation and long-path liquid-waveguide capillary cell techniques for trace analysis of phosphate in seawater. *Analytica Chimica Acta*, *611*(1), 68–72. https://doi.org/10.1016/j.aca.2008.01.074

Lin, I. I. (2012). Typhoon-induced phytoplankton blooms and primary productivity increase in the western North Pacific subtropical ocean. *Journal of Geophysical Research*, *117*(C3), C03039. https://doi.org/10.1029/2011JC007626

Lipschultz, F., Bates, N. R., Carlson, C. A., & Hansell, D. A. (2002). New production in the Sargasso Sea: History and current status. *Global Biogeochemical Cycles*, *16*(1), 1001–1-17. https://doi.org/10.1029/2000gb001319

Liu, D., Zhou, C., Keesing, J. K., Serrano, O., Werner, A., Fang, Y., et al. (2022). Wildfires enhance phytoplankton production in tropical oceans. *Nature Communications*, *13*(1), 1348. https://doi.org/10.1038/s41467-022-29013-0

Lomas, M. W., & Moran, S. B. (2011). Evidence for aggregation and export of cyanobacteria and nano-eukaryotes from the Sargasso Sea euphotic zone. *Biogeosciences*, *8*(1), 203–216. https://doi.org/10.5194/bg-8-203-2011

Long, Y., Zhu, X.-H., Guo, X., & Huang, H. (2018). Temporal variation of Kuroshio nutrient stream south of Japan. *Journal of Geophysical Research: Oceans*, *123*(11), 7896–7913. https://doi.org/10.1029/2017jc013635

Longhurst, A., Sathyendranath, S., Platt, T., & Caverhill, C. (1995). An estimate of global primary production in the ocean from satellite radiometer data. *Journal of Plankton Research*, *17*(6), 1245–1271. https://doi.org/10.1093/plankt/17.6.1245

Lu, S., Liu, Z., Li, H., Li, Z., Wu, X., Sun, C., & Xu, J. (2020). Manual of global ocean Argo gridded data set (BOA_Argo). (Version 2019) (p. 14).

Lu, Y., Wen, Z., Shi, D., Chen, M., Zhang, Y., Bonnet, S., et al. (2018). Effect of light on N_2 fixation and net nitrogen release of *Trichodesmium* in a field study. *Biogeosciences*, *15*(1), 1–12. https://doi.org/10.5194/bg-15-1-2018

Lu, Y., Wen, Z., Shi, D., Lin, W., Bonnet, S., Dai, M., & Kao, S. J. (2019). Biogeography of N_2 fixation influenced by the western boundary current intrusion in the South China Sea. *Journal of Geophysical Research: Oceans*, *124*(10), 6983–6996. https://doi.org/10.1029/2018jc014781

Luo, E., Leu, A. O., Eppley, J. M., Karl, D. M., & DeLong, E. F. (2022). Diversity and origins of bacterial and archaeal viruses on sinking particles reaching the Abyssal Ocean. *ISME Journal*, *16*(6), 1627–1635. https://doi.org/10.1038/s41396-022-01202-1

Luo, L., Kao, S. J., Bao, H. Y., Xiao, H. Y., Xiao, H. W., Yao, X. H., et al. (2018). Sources of reactive nitrogen in marine aerosol over the Northwest Pacific Ocean in spring. *Atmospheric Chemistry and Physics*, *18*(9), 6207–6222. https://doi.org/10.5194/acp-18-6207-2018

Luo, L., Yao, X. H., Gao, H. W., Hsu, S. C., Li, J. W., & Kao, S. J. (2016). Nitrogen speciation in various types of aerosols in spring over the northwestern Pacific Ocean. *Atmospheric Chemistry and Physics*, *16*(1), 325–341. https://doi.org/10.5194/acp-16-325-2016

Luo, W., Inomura, K., Zhang, H., & Luo, Y.-W. (2022). N_2 fixation in *Trichodesmium* does not require spatial segregation from photosynthesis. *mSystems*, *7*(4), e00538-22. https://doi.org/10.1128/msystems.00538-22

Luo, Y., Liu, Q., & Rothstein, L. M. (2009). Simulated response of North Pacific mode waters to global warming. *Geophysical Research Letters*, *36*(23), L23609. https://doi.org/10.1029/2009gl040906

Luo, Y.-W., Doney, S. C., Anderson, L. A., Benavides, M., Berman-Frank, I., Bode, A., et al. (2012). Database of diazotrophs in global ocean abundance, biomass and nitrogen fixation rates. *Earth System Science Data*, *4*(1), 47–73. https://doi.org/10.5194/essd-4-47-2012

Luo, Y.-W., Ducklow, H. W., Friedrichs, M. A. M., Church, M. J., Karl, D. M., & Doney, S. C. (2012). Interannual variability of primary production and dissolved organic nitrogen storage in the North Pacific Subtropical Gyre. *Journal of Geophysical Research*, *117*(G3), G03019. https://doi.org/10.1029/2011JG001830

Luo, Y.-W., Lima, L. D., Karl, D. M., Deutsch, C., & Doney, S. C. (2014). Data-based assessment of environmental controls on global marine nitrogen fixation. *Biogeosciences*, *11*(3), 691–708. https://doi.org/10.5194/bg-11-691-2014

Ma, Y., Zhou, K., Chen, W., Chen, J., Yang, J.-Y. T., & Dai, M. (2023). Partitioning of carbon export in the euphotic zone of the oligotrophic South China Sea. *Biogeosciences*, *20*(11), 2013–2030. https://doi.org/10.5194/bg-20-2013-2023

Macovei, V. A., Torres-Valdés, S., Hartman, S. E., Schuster, U., Moore, C. M., Brown, P. J., et al. (2019). Temporal variability in the nutrient biogeochemistry of the surface North Atlantic: 15 years of ship of opportunity data. *Global Biogeochemical Cycles*, *33*(12), 1674–1692. https://doi.org/10.1029/2018GB006132

Mahowald, N. M., Engelstaedter, S., Luo, C., Sealy, A., Artaxo, P., Benitez-Nelson, C., et al. (2009). Atmospheric iron deposition: Global distribution, variability, and human perturbations. *Annual Review of Marine Science*, *1*, 245–278. https://doi.org/10.1146/annurev.marine.010908.163727

Mahowald, N. M., Kloster, S., Engelstaedter, S., Moore, J. K., Mukhopadhyay, S., McConnell, J. R., et al. (2010). Observed 20th century desert dust variability: Impact on climate and biogeochemistry. *Atmospheric Chemistry and Physics*, *10*(22), 10875–10893. https://doi.org/10.5194/acp-10-10875-2010

Marañón, E., Behrenfeld, M. J., González, N., Mouriño, B., & Zubkov, M. V. (2003). High variability of primary production in oligotrophic waters of the Atlantic Ocean: Uncoupling from phytoplankton biomass and size structure. *Marine Ecology Progress Series*, *257*, 1–11. https://doi.org/10.3354/meps257001

Marañón, E., Holligan, P. M., Barciela, R., Gonzalez, N., Mourino, B., Pazo, M. J., & Varela, M. (2001). Patterns of phytoplankton size structure and productivity in contrasting open-ocean environments. *Marine Ecology Progress Series*, *216*, 43–56. https://doi.org/10.3354/meps216043

Marconi, D., Sigman, D. M., Casciotti, K. L., Campbell, E. C., Weigand, M. A., Fawcett, S., et al. (2017). Tropical dominance of N_2 fixation in the North Atlantic Ocean. *Global Biogeochemical Cycles*, *31*(10), 1608–1623. https://doi.org/10.1002/2016GB005613

Maritorena, S., Siegel, D. A., & Peterson, A. R. (2002). Optimization of a semianalytical ocean color model for global-scale applications. *Applied Optics*, *41*(15), 2705–2714. https://doi.org/10.1364/AO.41.002705

Marra, J., Ho, C., & Trees, C. (2003). An alternative algorithm for the calculation of primary productivity from remote sensing data. Lamont Doherty Earth Observatory Technical Report (LDEO-2003-1).

Marra, J. F., Lance, V. P., Vaillancourt, R. D., & Hargreaves, B. R. (2014). Resolving the ocean's euphotic zone. *Deep-Sea Research I*, *83*, 45–50. https://doi.org/10.1016/j.dsr.2013.09.005

Marshall, T., Granger, J., Casciotti, K. L., Dähnke, K., Emeis, K.-C., Marconi, D., et al. (2022). The Angola Gyre is a hotspot of dinitrogen fixation in the South Atlantic Ocean. *Communications Earth & Environment*, *3*(1), 151. https://doi.org/10.1038/s43247-022-00474-x

Martin, A. P., & Pondaven, P. (2003). On estimates for the vertical nitrate flux due to eddy pumping. *Journal of Geophysical Research*, *108*(C11), 3359. https://doi.org/10.1029/2003jc001841

Martin-Jézéquel, V., Hildebrand, M., & Brzezinski, M. A. (2000). Silicon metabolism in diatoms: Implications for growth. *Journal of Phycology*, *36*(5), 821–840. https://doi.org/10.1046/j.1529-8817.2000.00019.x

Martino, M., Hamilton, D., Baker, A. R., Jickells, T. D., Bromley, T., Nojiri, Y., et al. (2014). Western Pacific atmospheric nutrient deposition fluxes, their impact on surface ocean productivity. *Global Biogeochemical Cycles*, *28*(7), 712–728. https://doi.org/10.1002/2013GB004794

Martiny, A. C., Lomas, M. W., Fu, W., Boyd, P. W., Chen, Y.-L. L., Cutter, G. A., et al. (2019). Biogeochemical controls of surface ocean phosphate. *Science Advances*, *5*(8), eaax0341. https://doi.org/10.1126/sciadv.aax0341

Masuda, T., Inomura, K., Kodama, T., Shiozaki, T., Kitajima, S., Armin, G., et al. (2022). *Crocosphaera* as a major consumer of fixed nitrogen. *Microbiology Spectrum*, *10*(4), e02177-21. https://doi.org/10.1128/spectrum.02177-21

Mawji, E., Schlitzer, R., Dodas, E. M., Abadie, C., Abouchami, W., Anderson, R. F., et al. (2015). The GEOTRACES intermediate data product 2014. *Marine Chemistry*, *177*, 1–8. https://doi.org/10.1016/j.marchem.2015.04.005

Maximenko, N. A., Bang, B., & Sasaki, H. (2005). Observational evidence of alternating zonal jets in the world ocean. *Geophysical Research Letters*, *32*(12), L12607. https://doi.org/10.1029/2005GL022728

McClain, C. R., Signorini, S. R., & Christian, J. R. (2004). Subtropical gyre variability observed by ocean-color satellites. *Deep-Sea Research II*, *51*(1–3), 281–301. https://doi.org/10.1016/j.dsr2.2003.08.002

McGillicuddy, D. J., Robinson, A. R., Siegel, D. A., Jannasch, H. W., Johnson, R., Dickey, T. D., et al. (1998). Influence of mesoscale eddies on new production in the Sargasso Sea. *Nature*, *394*(6690), 263–266. https://doi.org/10.1038/28367

Mestre, M., Ruiz-González, C., Logares, R., Duarte, C. M., Gasol, J. M., & Sala, M. M. (2018). Sinking particles promote vertical connectivity in the ocean microbiome. *Proceedings of the National Academy of Sciences of the United States of America*, *115*(29), E6799–E6807. https://doi.org/10.1073/pnas.1802470115

Michaels, A. F., Bates, N. R., Buesseler, K. O., Carlson, C. A., & Knap, A. H. (1994). Carbon-cycle imbalances in the Sargasso Sea. *Nature*, *372*(6506), 537–540. https://doi.org/10.1038/372537a0

Mills, M. M., & Arrigo, K. R. (2010). Magnitude of oceanic nitrogen fixation influenced by the nutrient uptake ratio of phytoplankton. *Nature Geoscience*, *3*(6), 412–416. https://doi.org/10.1038/ngeo856

Mohr, W., Grosskopf, T., Wallace, D. W. R., & LaRoche, J. (2010). Methodological underestimation of oceanic nitrogen fixation rates. *PLoS One*, *5*(9), e12583. https://doi.org/10.1371/journal.pone.0012583

Moisander, P. H., Beinart, R. A., Hewson, I., White, A. E., Johnson, K. S., Carlson, C. A., et al. (2010). Unicellular cyanobacterial distributions broaden the oceanic N_2 fixation domain. *Science*, *327*(5972), 1512–1514. https://doi.org/10.1126/science.1185468

Mojica, K. D. A., van de Poll, W. H., Kehoe, M., Huisman, J., Timmermans, K. R., Buma, A. G. J., et al. (2015). Phytoplankton community structure in relation to vertical stratification along a north-south gradient in the Northeast Atlantic Ocean. *Limnology and Oceanography*, *60*(5), 1498–1521. https://doi.org/10.1002/lno.10113

Moore, C. M., Mills, M. M., Achterberg, E. P., Geider, R. J., LaRoche, J., Lucas, M. I., et al. (2009). Large-scale distribution of Atlantic nitrogen fixation controlled by iron availability. *Nature Geoscience*, *2*(12), 867–871. https://doi.org/10.1038/ngeo667

Moore, C. M., Mills, M. M., Arrigo, K. R., Berman-Frank, I., Bopp, L., Boyd, P. W., et al. (2013). Processes and patterns of oceanic nutrient limitation. *Nature Geoscience*, *6*(9), 701–710. https://doi.org/10.1038/ngeo1765

Moore, J. K., Lindsay, K., Doney, S. C., Long, M. C., & Misumi, K. (2013). Marine ecosystem dynamics and biogeochemical cycling in the Community Earth System Model [CESM1(BGC)]: Comparison of the 1990s with the 2090s under the RCP4.5 and RCP8.5 scenarios. *Journal of Climate*, *26*(23), 9291–9312. https://doi.org/10.1175/jcli-d-12-00566.1

Mouriño-Carballido, B., Graña, R., Fernàndez, A., Bode, A., Varela, M., Domínguez, J. F., et al. (2011). Importance of N_2 fixation vs. nitrate eddy diffusion along a latitudinal transect in the Atlantic Ocean. *Limnology and Oceanography*, *56*(3), 999–1007. https://doi.org/10.4319/lo.2011.56.3.0999

Mulholland, M. R. (2007). The fate of nitrogen fixed by diazotrophs in the ocean. *Biogeosciences*, *4*(1), 37–51. https://doi.org/10.5194/bg-4-37-2007

Mulholland, M. R., & Capone, D. G. (2001). Stoichiometry of nitrogen and carbon utilization in cultured populations of *Trichodesmium* IMS101: Implications for growth. *Limnology and Oceanography*, *46*(2), 436–443. https://doi.org/10.4319/lo.2001.46.2.0436

Needoba, J. A., Foster, R. A., Sakamoto, C., Zehr, J. P., & Johnson, K. S. (2007). Nitrogen fixation by unicellular diazotrophic cyanobacteria in the temperate oligotrophic North Pacific Ocean. *Limnology and Oceanography*, *54*(4), 1317–1327. https://doi.org/10.4319/lo.2007.52.4.1317

Nishioka, J., Nakatsuka, T., Watanabe, Y. W., Yasuda, I., Kuma, K., Ogawa, H., et al. (2013). Intensive mixing along an island chain controls oceanic biogeochemical cycles. *Global Biogeochemical Cycles*, *27*(3), 920–929. https://doi.org/10.1002/gbc.20088

Nishioka, J., Obata, H., Ogawa, H., Ono, K., Yamashita, Y., Lee, K., et al. (2020). Subpolar marginal seas fuel the North Pacific through the intermediate water at the termination of the global ocean circulation. *Proceedings of the National Academy of Sciences of the United States of America*, *117*(23), 12665–12673. https://doi.org/10.1073/pnas.2000658117

Nishioka, J., Obata, H., & Tsumune, D. (2013). Evidence of an extensive spread of hydrothermal dissolved iron in the Indian Ocean. *Earth and Planetary Science Letters*, *361*, 26–33. https://doi.org/10.1016/j.epsl.2012.11.040

Noble, A. E., Lamborg, C. H., Ohnemus, D. C., Lam, P. J., Goepfert, T. J., Measures, C. I., et al. (2012). Basin-scale inputs of cobalt, iron, and manganese from the Benguela-Angola front to the South Atlantic Ocean. *Limnology and Oceanography*, *57*(4), 989–1010. https://doi.org/10.4319/lo.2012.57.4.0989

O'Connor, M. I., Piehler, M. F., Leech, D. M., Anton, A., & Bruno, J. F. (2009). Warming and resource availability shift food web structure and metabolism. *Plos Biology*, *7*(8), e1000178. https://doi.org/10.1371/journal.pbio.1000178

O'Neil, J. M., Metzler, P. M., & Glibert, P. M. (1996). Ingestion of $^{15}N_2$-labelled *Trichodesmium* spp and ammonium regeneration by the harpacticoid copepod *Macrosetella gracilis*. *Marine Biology*, *125*(1), 89–96. https://doi.org/10.1007/BF00350763

O'Reilly, J. (2017). *Status and trends in primary productivity and chlorophyll from 1996 to 2014 in large marine ecosystems and the western Pacific warm pool, based on data from satellite ocean colour sensors* (p. 120). Intergovernmental Oceanographic Commission Technical Series.

Owens, S. A., Pike, S., & Buesseler, K. O. (2015). Thorium-234 as a tracer of particle dynamics and upper ocean export in the Atlantic Ocean. *Deep-Sea Research II*, *116*, 42–59. https://doi.org/10.1016/j.dsr2.2014.11.010

Paasche, E. (1973). Silicon and the ecology of marine plankton diatoms. II. Silicate-uptake kinetics in five diatom species. *Marine Biology*, *19*(3), 262–269. https://doi.org/10.1007/BF02097147

Painter, S. C., Patey, M. D., Forryan, A., & Torres-Valdes, S. (2013). Evaluating the balance between vertical diffusive nitrate supply and nitrogen fixation with reference to nitrate uptake in the eastern subtropical North Atlantic Ocean. *Journal of Geophysical Research: Oceans*, *118*(10), 5732–5749. https://doi.org/10.1002/jgrc.20416

Palter, J. B., Lozier, M. S., & Barber, R. T. (2005). The effect of advection on the nutrient reservoir in the North Atlantic Subtropical gyre. *Nature*, *437*(7059), 687–692. https://doi.org/10.1038/nature03969

Palter, J. B., Marinov, I., Sarmiento, J. L., & Gruber, N. (2013). *Large-Scale, persistent nutrient fronts of the world ocean: Impacts on biogeochemistry* (pp. 1–38). Springer. https://doi.org/10.1007/698_2013_241

Partensky, F., Blanchot, J., & Vaulot, D. (1999). Differential distribution and ecology of *Prochlorococcus* and *Synechococcus* in oceanic waters: A review. *Bulletin de l'Institut Oceanographique, Monaco, spec. issue*, *19*, 457–475.

Perez, V., Fernandez, E., Marañón, E., Moran, X. A. G., & Zubkovc, M. V. (2006). Vertical distribution of phytoplankton biomass, production and growth in the Atlantic Subtropical Gyres. *Deep-Sea Research I*, *53*(10), 1616–1634. https://doi.org/10.1016/j.dsr.2006.07.008

Pinedo-González, P., Hawco, N. J., Bundy, R. M., Armbrust, E. V., Follows, M. J., Cael, B. B., et al. (2020). Anthropogenic Asian aerosols provide Fe to the North Pacific Ocean. *Proceedings of the National Academy of Sciences of the United States of America*, *117*(45), 27862–27868. https://doi.org/10.1073/pnas.2010315117

Poff, K. E., Leu, A. O., Eppley, J. M., Karl, D. M., & DeLong, E. F. (2021). Microbial dynamics of elevated carbon flux in the open ocean's abyss. *Proceedings of the National Academy of Sciences of the United States of America*, *118*(4), e2018269118. https://doi.org/10.1073/pnas.2018269118

Polovina, J. J., Dunne, J. P., Woodworth, P. A., & Howell, E. A. (2011). Projected expansion of the subtropical biome and contraction of the temperate and equatorial upwelling biomes in the North Pacific under global warming. *ICES Journal of Marine Science*, *68*(6), 986–995. https://doi.org/10.1093/icesjms/fsq198

Polovina, J. J., Howell, E. A., & Abecassis, M. (2008). Ocean's least productive waters are expanding. *Geophysical Research Letters*, *35*(3), L03618. https://doi.org/10.1029/2007gl031745

Prospero, J. M. (1990). Mineral aerosol transport to the North Atlantic and North Pacific: The impact of African and Asian sources. In A. H. Knap (Ed.), *The long-range atmospheric transport of natural and contaminant substances* (pp. 59–86). Kluwer.

Pujol, M. I., Faugere, Y., Taburet, G., Dupuy, S., Pelloquin, C., Ablain, M., & Picot, N. (2016). DUACS DT2014: The new multi-mission altimeter data set reprocessed over 20 years. *Ocean Science*, *12*(5), 1067–1090. https://doi.org/10.5194/os-12-1067-2016

Pujol, M.-I., Taburet, G., & SL-TAC Team. (2022). *Quality information document: Sea level TAC-DUACS products (CMEMS-SLQUID-008-032-062)* (p. 72). Copernicus Marine Environment Monitoring System. Retrieved from https://catalogue.marine.copernicus.eu/documents/QUID/CMEMS-SL-QUID-008-032-068.pdf

Pulsifer, J., & Laws, E. (2021). Temperature dependence of freshwater phytoplankton growth rates and zooplankton grazing rates. *Water*, *13*(11), 1591. https://doi.org/10.3390/w13111591

Qi, J., Yu, Y., Yao, X., Gang, Y., & Gao, H. (2020). Dry deposition fluxes of inorganic nitrogen and phosphorus in atmospheric aerosols over the Marginal Seas and Northwest Pacific. *Atmospheric Research*, *245*, 105076. https://doi.org/10.1016/j.atmosres.2020.105076

Qiu, B. (1999). Seasonal eddy field modulation of the North Pacific subtropical countercurrent: TOPEX/Poseidon observations and theory. *Journal of Physical Oceanography*, *29*(10), 2471–2486. https://doi.org/10.1175/1520-0485(1999)029<2471:SEFMOT>2.0.CO;2

Qiu, B., & Chen, S. M. (2006). Decadal variability in the formation of the North Pacific subtropical mode water: Oceanic versus atmospheric control. *Journal of Physical Oceanography*, *36*(7), 1365–1380. https://doi.org/10.1175/Jpo2918.1

Quay, P., Emerson, S., & Palevsky, H. (2020). Regional pattern of the ocean's biological pump based on geochemical observations. *Geophysical Research Letters*, *47*(14), e2020GL088098. https://doi.org/10.1029/2020GL088098

Reid, J. L. (1997). On the total geostrophic circulation of the Pacific Ocean: Flow patterns, tracers, and transports. *Progress in Oceanography*, *39*(4), 263–352. https://doi.org/10.1016/S0079-6611(97)00012-8

Reynolds, S., Mahaffey, C., Roussenov, V., & Williams, R. G. (2014). Evidence for production and lateral transport of dissolved organic phosphorus in the eastern subtropical North Atlantic. *Global Biogeochemical Cycles*, *28*(8), 805–824. https://doi.org/10.1002/2013GB004801

Richardson, T. L., & Jackson, G. A. (2007). Small phytoplankton and carbon export from the surface ocean. *Science*, *315*(5813), 838–840. https://doi.org/10.1126/science.1133471

Riche, O. G. J., & Christian, J. R. (2018). Ocean dinitrogen fixation and its potential effects on ocean primary production in Earth system model simulations of anthropogenic warming. *Elementa: Science of the Anthropocene*, *6*, 16. https://doi.org/10.1525/elementa.277

Rii, Y. M., Bidigare, R. R., & Church, M. J. (2018). Differential responses of eukaryotic phytoplankton to nitrogenous nutrients in the North Pacific Subtropical Gyre. *Frontiers in Marine Science*, *5*, 92. https://doi.org/10.3389/fmars.2018.00092

Rii, Y. M., Karl, D. M., & Church, M. J. (2016). Temporal and vertical variability in picophytoplankton primary productivity in the North Pacific Subtropical Gyre. *Marine Ecology Progress Series*, *562*, 1–18. https://doi.org/10.3354/meps11954

Rii, Y. M., Peoples, L. M., Karl, D. M., & Church, M. J. (2022). Seasonality and episodic variation in picoeukaryote diversity and structure reveal community resilience to disturbances in the North Pacific Subtropical Gyre. *Limnology and Oceanography*, *67*(S1), S331–S351. https://doi.org/10.1002/lno.11916

Rose, J. M., & Caron, D. A. (2007). Does low temperature constrain the growth rates of heterotrophic protists? Evidence and implications for algal blooms in cold waters. *Limnology and Oceanography*, *52*(2), 886–895. https://doi.org/10.4319/lo.2007.52.2.0886

Roshan, S., & DeVries, T. (2017). Efficient dissolved organic carbon production and export in the oligotrophic ocean. *Nature Communications*, *8*(1), 2036. https://doi.org/10.1038/s41467-017-02227-3

Rubin, M., Berman-Frank, I., & Shaked, Y. (2011). Dust- and mineral-iron utilization by the marine dinitrogen-fixer *Trichodesmium*. *Nature Geoscience*, *4*(8), 529–534. https://doi.org/10.1038/ngeo1181

Ryther, J. H. (1956). Photosynthesis in the ocean as a function of light intensity. *Limnology and Oceanography*, *1*(1), 61–70. https://doi.org/10.4319/lo.1956.1.1.0061

Saba, V. S., Friedrichs, M. A. M., Antoine, D., Armstrong, R. A., Asanuma, I., Behrenfeld, M. J., et al. (2011). An evaluation of ocean color model estimates of marine primary productivity in coastal and pelagic regions across the globe. *Biogeosciences*, *8*(2), 489–503. https://doi.org/10.5194/bg-8-489-2011

Saito, M. A., Bertrand, E. M., Dutkiewicz, S., Bulygin, V. V., Moran, D. M., Monteiro, F. M., et al. (2011). Iron conservation by reduction of metalloenzyme inventories in the marine diazotroph *Crocosphaera watsonii*. *Proceedings of the National Academy of Sciences of the United States of America*, *108*(6), 2184–2189. https://doi.org/10.1073/pnas.1006943108

Sarmiento, J. L., Gruber, N., Brzezinski, M. A., & Dunne, J. P. (2004). High-latitude controls of thermocline nutrients and low latitude biological productivity. *Nature*, *427*(6969), 56–60. https://doi.org/10.1038/nature02127

Sasai, Y., Yoshikawa, C., Smith, S. L., Hashioka, T., Matsumoto, K., Wakita, M., et al. (2016). Coupled 1-D physical-biological model study of phytoplankton production at two contrasting time-series stations in the western North Pacific. *Journal of Oceanography*, *72*(3), 509–526. https://doi.org/10.1007/s10872-015-0341-1

Sathyendranath, S., Brewin, R. J. W., Brockmann, C., Brotas, V., Calton, B., Chuprin, A., et al. (2019). An ocean-colour time series for use in climate studies: The experience of the Ocean-Colour Climate Change Initiative (OC-CCI). *Sensors*, *19*(19), 4285. https://doi.org/10.3390/s19194285

Sathyendranath, S., & Platt, T. (1989). Computation of aquatic primary production - Extended formalism to include effect of angular and spectral distribution of light. *Limnology and Oceanography*, *34*(1), 188–198. https://doi.org/10.4319/lo.1989.34.1.0188

Sato, M., Shiozaki, T., Hashihama, F., Kodama, T., Ogawa, H., Saito, H., et al. (2022). Relative depths of the subsurface peaks of phytoplankton abundance conserved over ocean provinces. *Limnology and Oceanography*, *67*(11), 2557–2571. https://doi.org/10.1002/lno.12222

Scharek, R., Latasa, M., Karl, D. M., & Bidigare, R. R. (1999). Temporal variations in diatom abundance and downward vertical flux in the oligotrophic North Pacific Gyre. *Deep-Sea Research I*, *46*(6), 1051–1075. https://doi.org/10.1016/S0967-0637(98)00102-2

Scharek, R., Tupas, L. M., & Karl, D. M. (1999). Diatom fluxes to the deep sea in the oligotrophic North Pacific gyre at Station ALOHA. *Marine Ecology Progress Series*, *182*, 55–67. https://doi.org/10.3354/meps182055

Schvarcz, C. R., Wilson, S. T., Caffin, M., Stancheva, R., Li, Q., Turk-Kubo, K. A., et al. (2022). Overlooked and widespread pennate diatom-diazotroph symbioses in the sea. *Nature Communications*, *13*(1), 799. https://doi.org/10.1038/s41467-022-28065-6

Sedwick, P. N., Church, T. M., Bowie, A. R., Marsay, C. M., Ussher, S. J., Achilles, K. M., et al. (2005). Iron in the Sargasso Sea (Bermuda Atlantic Time-series Study region) during summer: Eolian imprint, spatiotemporal variability, and ecological implications. *Global Biogeochemical Cycles*, *19*(4), GB4006. https://doi.org/10.1029/2004gb002445

Seki, M. P., & Polovina, J. J. (2001). Ocean Gyre ecosystems. In J. H. Steele (Ed.), *Encyclopedia of ocean sciences* (pp. 1959–1965). Academic Press. https://doi.org/10.1006/rwos.2001.0296

Seok, M.-W., Kim, D., Park, G.-H., Lee, K., Kim, T.-H., Jung, J., et al. (2021). Atmospheric deposition of inorganic nutrients to the Western North Pacific Ocean. *Science of the Total Environment*, *793*, 148401. https://doi.org/10.1016/j.scitotenv.2021.148401

Shao, Z., & Luo, Y.-W. (2022). Controlling factors on the global distribution of a representative marine non-cyanobacterial diazotroph phylotype (Gamma A). *Biogeosciences*, *19*(11), 2939–2952. https://doi.org/10.5194/bg-19-2939-2022

Shao, Z., Xu, Y., Wang, H., Luo, W., Wang, L., Huang, Y., & Luo, Y. W. (2023). Version 2 of the global oceanic diazotroph database. *Earth System Science Data Discussions*, 1–44. https://doi.org/10.5194/essd-2023-13

Shi, G., Ma, H., Zhu, Z., Hu, Z., Chen, Z., Jiang, S., et al. (2021). Using stable isotopes to distinguish atmospheric nitrate production and its contribution to the surface ocean across hemispheres. *Earth and Planetary Science Letters*, *564*, 116914. https://doi.org/10.1016/j.epsl.2021.116914

Shiozaki, T., Bombar, D., Riemann, L., Hashihama, F., Takeda, S., Yamaguchi, T., et al. (2017). Basin scale variability of active diazotrophs and nitrogen fixation in the North Pacific, from the tropics to the subarctic Bering Sea. *Global Biogeochemical Cycles*, *31*(6), 996–1009. https://doi.org/10.1002/2017gb005681

Shiozaki, T., Bombar, D., Riemann, L., Sato, M., Hashihama, F., Kodama, T., et al. (2018). Linkage between dinitrogen fixation and primary production in the oligotrophic South Pacific Ocean. *Global Biogeochemical Cycles*, *32*(7), 1028–1044. https://doi.org/10.1029/2017gb005869

Shiozaki, T., Chen, Y. L. L., Lin, Y. H., Taniuchi, Y., Sheu, D. S., Furuya, K., & Chen, H. Y. (2014). Seasonal variations of unicellular diazotroph groups A and B, and *Trichodesmium* in the northern South China Sea and neighboring upstream Kuroshio Current. *Continental Shelf Research*, *80*, 20–31. https://doi.org/10.1016/j.csr.2014.02.015

Shiozaki, T., Furuya, K., Kodama, T., Kitajima, S., Takeda, S., Takemura, T., & Kanda, J. (2010). New estimation of N_2 fixation in the western and central Pacific Ocean and its marginal seas. *Global Biogeochemical Cycles*, *24*(1), GB1015. https://doi.org/10.1029/2009gb003620

Siegel, D. A., McGillicuddy, D. J., & Fields, E. A. (1999). Mesoscale eddies, satellite altimetry, and new production in the Sargasso Sea. *Journal of Geophysical Research*, *104*(C6), 13359–13379. https://doi.org/10.1029/1999jc900051

Siegel, D. A., Westberry, T. K., O'Brien, M. C., Nelson, N. B., Michaels, A. F., Morrison, J. R., et al. (2001). Bio-optical modeling of primary production on regional scales: The Bermuda BioOptics project. *Deep-Sea Research II*, *48*(8–9), 1865–1896. https://doi.org/10.1016/S0967-0645(00)00167-3

Signorini, S. R., Franz, B. A., & McClain, C. R. (2015). Chlorophyll variability in the oligotrophic gyres: Mechanisms, seasonality and trends. *Frontiers in Marine Science*, *2*, 1. https://doi.org/10.3389/fmars.2015.00001

Signorini, S. R., & McClain, C. R. (2012). Subtropical gyre variability as seen from satellites. *Remote Sensing Letters*, *3*(6), 471–479. https://doi.org/10.1080/01431161.2011.625053

Small, L. F., Knauer, G. A., & Tuel, M. D. (1987). The role of sinking fecal pellets in stratified euphotic zones. *Deep-Sea Research*, *34*(10), 1705–1712. https://doi.org/10.1016/0198-0149(87)90019-7

Sohm, J. A., Subramaniam, A., Gunderson, T. E., Carpenter, E. J., & Capone, D. G. (2011). Nitrogen fixation by *Trichodesmium* spp. and unicellular diazotrophs in the North Pacific subtropical Gyre. *Journal of Geophysical Research*, *116*(G3), G03002. https://doi.org/10.1029/2010JG001513

Sommer, U., & Lewandowska, A. (2011). Climate change and the phytoplankton spring bloom: Warming and overwintering zooplankton have similar effects on phytoplankton. *Global Change Biology*, *17*(1), 154–162. https://doi.org/10.1111/j.1365-2486.2010.02182.x

Song, L., Lee, Z., Shang, S., Huang, B., Wu, J., Wu, Z., et al. (2023). On the spatial and temporal variations of primary production in the South China Sea. *IEEE Transactions on Geoscience and Remote Sensing*, *61*, 1–14. https://doi.org/10.1109/tgrs.2023.3241209

Steinacher, M., Joos, F., Frölicher, T. L., Bopp, L., Cadule, P., Cocco, V., et al. (2010). Projected 21st century decrease in marine productivity: A multi-model analysis. *Biogeosciences*, *7*(3), 979–1005. https://doi.org/10.5194/bg-7-979-2010

Steinberg, D. K., Carlson, C. A., Bates, N. R., Johnson, R. J., Michaels, A. F., & Knap, A. H. (2001). Overview of the US JGOFS Bermuda Atlantic time-series study (BATS): A decade-scale look at ocean biology and biogeochemistry. *Deep-Sea Research II*, *48*(8–9), 1405–1447. https://doi.org/10.1016/S0967-0645(00)00148-X

Stenegren, M., Caputo, A., Berg, C., Bonnet, S., & Foster, R. A. (2018). Distribution and drivers of symbiotic and free-living diazotrophic cyanobacteria in the western tropical South Pacific. *Biogeosciences*, *15*(5), 1559–1578. https://doi.org/10.5194/bg-15-1559-2018

Stramma, L., Schmidtko, S., Bograd, S. J., Ono, T., Ross, T., Sasano, D., & Whitney, F. A. (2020). Trends and decadal oscillations of oxygen and nutrients at 50 to 300 m depth in the equatorial and North Pacific. *Biogeosciences*, *17*(3), 813–831. https://doi.org/10.5194/bg-17-813-2020

Sverdrup, H. U. (1953). On conditions for the vernal blooming of phytoplankton. *ICES Journal of Marine Science*, *18*(3), 287–295. https://doi.org/10.1093/icesjms/18.3.287

Tagliabue, A., Aumont, O., DeAth, R., Dunne, J. P., Dutkiewicz, S., Galbraith, E., et al. (2016). How well do global ocean biogeochemistry models simulate dissolved iron distributions? *Global Biogeochemical Cycles*, *30*(2), 149–174. https://doi.org/10.1002/2015gb005289

Tagliabue, A., Bowie, A. R., Boyd, P. W., Buck, K. N., Johnson, K. S., & Saito, M. A. (2017). The integral role of iron in ocean biogeochemistry. *Nature*, *543*(7643), 51–59. https://doi.org/10.1038/nature21058

Tagliabue, A., Mtshali, T., Aumont, O., Bowie, A. R., Klunder, M. B., Roychoudhury, A. N., & Swart, S. (2012). A global compilation of dissolved iron measurements: Focus on distributions and processes in the Southern Ocean. *Biogeosciences*, *9*(6), 2333–2349. https://doi.org/10.5194/bg-9-2333-2012

Talley, L. D., Pickard, G. L., Emery, W. J., & Swift, J. H. (2011). *Descriptive physical oceanography: An introduction* (6th ed. ed.). Academic press.

Tang, W., Li, Z., & Cassar, N. (2019). Machine learning estimates of global marine nitrogen fixation. *Journal of Geophysical Research: Biogeosciences*, *124*(3), 717–730. https://doi.org/10.1029/2018JG004828

Tanita, I., Shiozaki, T., Kodama, T., Hashihama, F., Sato, M., Takahashi, K., & Furuya, K. (2021). Regionally variable responses of nitrogen fixation to iron and phosphorus enrichment in the Pacific Ocean. *Journal of Geophysical Research: Biogeosciences*, *126*(9), e2021JG006542. https://doi.org/10.1029/2021jg006542

Taylor, S. P., Patterson, M. O., Lam, A. R., Jones, H., Woodard, S. C., Habicht, M. H., et al. (2022). Expanded North Pacific Subtropical Gyre and heterodyne expression during the mid-Pleistocene. *Paleoceanography and Paleoclimatology*, *37*(5), e2021PA004395. https://doi.org/10.1029/2021PA004395

Teng, Y.-C., Primeau, F. W., Moore, J. K., Lomas, M. W., & Martiny, A. C. (2014). Global-scale variations of the ratios of carbon to phosphorus in exported marine organic matter. *Nature Geoscience*, *7*(12), 895–898. https://doi.org/10.1038/ngeo2303

Thomalla, S., Turnewitsch, R., Lucas, M., & Poulton, A. (2006). Particulate organic carbon export from the North and South Atlantic gyres: The ^{234}Th/^{238}U disequilibrium approach. *Deep Sea Research II*, *53*(14), 1629–1648. https://doi.org/10.1016/j.dsr2.2006.05.018

Torres-Valdés, S., Roussenov, V. M., Sanders, R., Reynolds, S., Pan, X., Mather, R., et al. (2009). Distribution of dissolved organic nutrients and their effect on export production over the Atlantic Ocean. *Global Biogeochemical Cycles*, *23*(4), GB4019. https://doi.org/10.1029/2008GB003389

Tréguer, P., Bowler, C., Moriceau, B., Dutkiewicz, S., Gehlen, M., Aumont, O., et al. (2018). Influence of diatom diversity on the ocean biological carbon pump. *Nature Geoscience*, *11*(1), 27–37. https://doi.org/10.1038/s41561-017-0028-x

Tréguer, P. J., & Rocha, C. L. D. L. (2013). The world ocean silica cycle. *Annual Review of Marine Science*, *5*(1), 477–501. https://doi.org/10.1146/annurev-marine-121211-172346

Tseng, Y. F., Lin, F. J., Chiang, K. P., Kao, S. J., & Shiah, F. K. (2005). Potential impacts of N_2-fixing *Trichodesmium* on heterotrophic bacterioplankton turnover rates and organic carbon transfer efficiency in the subtropical oligotrophic ocean system. *Terrestrial Atmospheric and Oceanic Sciences*, *16*(2), 361–376. https://doi.org/10.3319/TAO.2005.16.2.361(Oc

Turk-Kubo, K. A., Henke, B. A., Gradoville, M. R., Magasin, J. D., Church, M. J., & Zehr, J. P. (2023). Seasonal and spatial patterns in diazotroph community composition at Station ALOHA. *Frontiers in Marine Science*, *10*, 1130158. https://doi.org/10.3389/fmars.2023.1130158

Turk-Kubo, K. A., Mills, M. M., Arrigo, K. R., van Dijken, G., Henke, B. A., Stewart, B., et al. (2021). UCYN-A/haptophyte symbioses dominate N_2 fixation in the Southern California Current System. *ISME Communications*, *1*(1), 42. https://doi.org/10.1038/s43705-021-00039-7

Tyrrell, T. (1999). The relative influences of nitrogen and phosphorus on oceanic primary production. *Nature*, *400*(6744), 525–531. https://doi.org/10.1038/22941

Umhau, B. P., Benitez-Nelson, C. R., Close, H. G., Hannides, C. C. S., Motta, L., Popp, B. N., et al. (2019). Seasonal and spatial changes in carbon and nitrogen fluxes estimated using ^{234}Th:^{238}U disequilibria in the North Pacific tropical and subtropical gyre. *Marine Chemistry*, *217*, 103705. https://doi.org/10.1016/j.marchem.2019.103705

Venrick, E. (1993). Phytoplankton seasonality in the central North Pacific: The endless summer reconsidered. *Limnology and Oceanography*, *38*(6), 1135–1149. https://doi.org/10.4319/lo.1993.38.6.1135

Venrick, E., McGowan, J., Cayan, D., & Hayward, T. (1987). Climate and chlorophyll *a*: Long-term trends in the central North Pacific Ocean. *Science*, *238*(4823), 70–72. https://doi.org/10.1126/science.238.4823.70

Villareal, T. A., Brown, C. G., Brzezinski, M. A., Krause, J. W., & Wilson, C. (2012). Summer diatom blooms in the North Pacific Subtropical Gyre: 2008–2009. *PLoS One*, *7*(4), e33109. https://doi.org/10.1371/journal.pone.0033109

Villareal, T. A., Pilskaln, C. H., Montoya, J. P., & Dennett, M. (2014). Upward nitrate transport by phytoplankton in oceanic waters: Balancing nutrient budgets in oligotrophic seas. *PeerJ*, *2*, e302. https://doi.org/10.7717/peerj.302

Walsby, A. E. (1992). The gas vesicles and buoyancy of. In E. J. Carpenter, D. G. Capone, & J. G. Rueter (Eds.), *Marine pelagic cyanobacteria: Trichodesmium and other diazotrophs* (pp. 141–161). Kluwer Academic Publishers.

Walsh, J. J., & Steidinger, K. A. (2001). Saharan dust and Florida red tides: The cyanophyte connection. *Journal of Geophysical Research*, *106*(C6), 11597–11612. https://doi.org/10.1029/1999jc000123

Wan, X. S., Sheng, H. X., Dai, M., Church, M. J., Zou, W., Li, X., et al. (2021). Phytoplankton-nitrifier interactions control the geographic distribution of nitrite in the upper ocean. *Global Biogeochemical Cycles*, *35*(11), e2021GB007072. https://doi.org/10.1029/2021GB007072

Wan, X. S., Sheng, H. X., Dai, M., Zhang, Y., Shi, D., Trull, T. W., et al. (2018). Ambient nitrate switches the ammonium consumption pathway in the euphotic ocean. *Nature Communications*, *9*(1), 915. https://doi.org/10.1038/s41467-018-03363-0

Wang, H., & Luo, Y.-W. (2022). Top-down control on major groups of global marine diazotrophs. *Acta Oceanologica Sinica*, *41*(8), 111–119. https://doi.org/10.1007/s13131-021-1956-2

Wang, W. L., Moore, J. K., Martiny, A. C., & Primeau, F. W. (2019). Convergent estimates of marine nitrogen fixation. *Nature*, *566*(7743), 205–211. https://doi.org/10.1038/s41586-019-0911-2

Wanninkhof, R., Park, G. H., Takahashi, T., Sweeney, C., Feely, R., Nojiri, Y., et al. (2013). Global ocean carbon uptake: Magnitude, variability and trends. *Biogeosciences*, *10*(3), 1983–2000. https://doi.org/10.5194/bg-10-1983-2013

Ward, B. A., Dutkiewicz, S., Moore, C. M., & Follows, M. J. (2013). Iron, phosphorus, and nitrogen supply ratios define the biogeography of nitrogen fixation. *Limnology and Oceanography*, *58*(6), 2059–2075. https://doi.org/10.4319/lo.2013.58.6.2059

Ward, B. B. (2008). Nitrification in marine systems. In D. G. Capone, D. A. Bronk, M. R. Mulholland, & E. J. Carpenter (Eds.), *Nitrogen in the marine environment* (2nd ed., pp. 199–261). Elsevier.

Weber, T., Cram, J. A., Leung, S. W., DeVries, T., & Deutsch, C. (2016). Deep ocean nutrients imply large latitudinal variation in particle transfer efficiency. *Proceedings of the National Academy of Sciences of the United States of America*, *113*(31), 8606–8611. https://doi.org/10.1073/pnas.1604414113

Wen, Z., Browning, T. J., Cai, Y., Dai, R., Zhang, R., Du, C., et al. (2022). Nutrient regulation of biological nitrogen fixation across the tropical western North Pacific. *Science Advances*, *8*(5), eabl7564. https://doi.org/10.1126/sciadv.abl7564

Wenley, J., Currie, K., Lockwood, S., Thomson, B., Baltar, F., & Morales, S. E. (2021). Seasonal prokaryotic community linkages between surface and deep ocean water. *Frontiers in Marine Science*, *8*, 659641. https://doi.org/10.3389/fmars.2021.659641

Williams, R. G., & Follows, M. J. (1998). The Ekman transfer of nutrients and maintenance of new production over the North Atlantic. *Deep Sea Research I*, *45*(2), 461-489. https://doi.org/10.1016/S0967-0637(97)00094-0

Williams, R. G., & Follows, M. J. (2011). *Ocean dynamics and the carbon cycle: Principles and mechanisms*. Combridge University Press.

Wilson, C., & Coles, V. J. (2005). Global climatological relationships between satellite biological and physical observations and upper ocean properties. *Journal of Geophysical Research*, *110*(C10), C10001. https://doi.org/10.1029/2004jc002724
Winn, C. D., Campbell, L., Christian, J. R., Letelier, R. M., Hebel, D. V., Dore, J. E., et al. (1995). Seasonal variability in the phytoplankton community of the North Pacific Subtropical Gyre. *Global Biogeochemical Cycles*, *9*(4), 605–620. https://doi.org/10.1029/95gb02149
Wirtz, K., Smith, S. L., Mathis, M., & Taucher, J. (2022). Vertically migrating phytoplankton fuel high oceanic primary production. *Nature Climate Change*, *12*(8), 750–756. https://doi.org/10.1038/s41558-022-01430-5
Wohlers, J., Engel, A., Zöllner, E., Breithaupt, P., Jürgens, K., Hoppe, H.-G., et al. (2009). Changes in biogenic carbon flow in response to sea surface warming. *Proceedings of the National Academy of Sciences of the United States of America*, *106*(17), 7067–7072. https://doi.org/10.1073/pnas.0812743106
Worden, A. Z., Nolan, J. K., & Palenik, B. (2004). Assessing the dynamics and ecology of marine picophytoplankton: The importance of the eukaryotic component. *Limnology and Oceanography*, *49*(1), 168–179. https://doi.org/10.4319/lo.2004.49.1.0168
Wu, J., Lee, Z., Xie, Y., Goes, J., Shang, S., Marra, J. F., et al. (2021). Reconciling between optical and biological determinants of the euphotic zone depth. *Journal of Geophysical Research: Oceans*, *126*(5), e2020JC016874. https://doi.org/10.1029/2020jc016874
Wu, J., Sunda, W., Boyle, E. A., & Karl, D. M. (2000). Phosphate depletion in the Western North Atlantic Ocean. *Science*, *289*(5480), 759–762. https://doi.org/10.1126/science.289.5480.759
Xiu, P., & Chai, F. (2012). Spatial and temporal variability in phytoplankton carbon, chlorophyll, and nitrogen in the North Pacific. *Journal of Geophysical Research*, *117*(C11), C11023. https://doi.org/10.1029/2012jc008067
Xiu, P., & Chai, F. (2021). Impact of atmospheric deposition on carbon export to the deep ocean in the Subtropical Northwest Pacific. *Geophysical Research Letters*, *48*(6), e2020GL089640. https://doi.org/10.1029/2020GL089640
Yang, B., Emerson, S. R., & Quay, P. D. (2019). The subtropical ocean's biological carbon pump determined from O_2 and DIC/DI^{13}C tracers. *Geophysical Research Letters*, *46*(10), 5361–5368. https://doi.org/10.1029/2018GL081239
Yang, J.-Y. T., Tang, J.-M., Kang, S., Dai, M., Kao, S.-J., Yan, X., et al. (2022). Comparison of nitrate isotopes between the South China Sea and Western North Pacific Ocean: Insights into biogeochemical signals and water exchange. *Journal of Geophysical Research: Oceans*, *127*(5), e2021JC018304. https://doi.org/10.1029/2021JC018304
Yasunaka, S., Mitsudera, H., Whitney, F., & Nakaoka, S.-I. (2021). Nutrient and dissolved inorganic carbon variability in the North Pacific. *Journal of Oceanography*, *77*(1), 3–16. https://doi.org/10.1007/s10872-020-00561-7
Yasunaka, S., Ono, T., Nojiri, Y., Whitney, F. A., Wada, C., Murata, A., et al. (2016). Long-term variability of surface nutrient concentrations in the North Pacific. *Geophysical Research Letters*, *43*(7), 3389–3397. https://doi.org/10.1002/2016gl068097
Yoder, J. A., Kennelly, M. A., Doney, S. C., & d Lima, I. D. (2010). Are trends in SeaWiFS chlorophyll time-series unusual relative to historic variability. *Acta Oceanologica Sinica*, *29*(2), 1–4. https://doi.org/10.1007/s13131-010-0016-o
Yu, L., Fennel, K., Bertino, L., Gharamti, M. E., & Thompson, K. R. (2018). Insights on multivariate updates of physical and biogeochemical ocean variables using an Ensemble Kalman Filter and an idealized model of upwelling. *Ocean Modelling*, *126*, 13–28. https://doi.org/10.1016/j.ocemod.2018.04.005
Yuan, Z., Browning, T. J., Zhang, R., Wang, C., Du, C., Wang, Y., et al. (2023). Potential drivers and consequences of regional phosphate depletion in the western subtropical North Pacific. *Limnology and Oceanography Letters*, *8*(3), 509–518. https://doi.org/10.1002/lol2.10314
Yun, M. S., Kim, Y., Jeong, Y., Joo, H. T., Jo, Y.-H., Lee, C. H., et al. (2020). Weak response of biological productivity and community structure of phytoplankton to mesoscale eddies in the oligotrophic Philippine Sea. *Journal of Geophysical Research: Oceans*, *125*(12), e2020JC016436. https://doi.org/10.1029/2020JC016436
Zakem, E. J., Al-Haj, A., Church, M. J., van Dijken, G. L., Dutkiewicz, S., Foster, S. Q., et al. (2018). Ecological control of nitrite in the upper ocean. *Nature Communications*, *9*(1), 1206. https://doi.org/10.1038/s41467-018-03553-w
Zehr, J. P. (2015). How single cells work together. *Science*, *349*(6253), 1163–1164. https://doi.org/10.1126/science.aac9752
Zehr, J. P., & Capone, D. G. (2020). Changing perspectives in marine nitrogen fixation. *Science*, *368*(6492), eaay9514. https://doi.org/10.1126/science.aay9514
Zhang, H. R., Wang, Y., Xiu, P., & Chai, F. (2021). Modeling the seasonal variability of phytoplankton in the subarctic northeast Pacific Ocean. *Marine Ecology Progress Series*, *680*, 33–50. https://doi.org/10.3354/meps13914
Zhang, Q., & Luo, Y.-W. (2022). A competitive advantage of middle-sized diatoms from increasing seawater CO_2. *Frontiers in Microbiology*, *13*, 838629. https://doi.org/10.3389/fmicb.2022.838629
Zhang, X., Wang, L., Jiang, X., & Zhu, C. (2017). *Modeling with digital ocean and digital coast*. Springer Press. https://doi.org/10.1007/978-3-319-42710-2
Zhang, Y., Zheng, X., Kong, D., Yan, H., & Liu, Z. (2021). Enhanced North Pacific subtropical gyre circulation during the late Holocene. *Nature Communications*, *12*(1), 5957. https://doi.org/10.1038/s41467-021-26218-7
Zhou, K., Benitez-Nelson, C. R., Huang, J., Xiu, P., Sun, Z., & Dai, M. (2021). Cyclonic eddies modulate temporal and spatial decoupling of particulate carbon, nitrogen, and biogenic silica export in the North Pacific Subtropical Gyre. *Limnology and Oceanography*, *66*(9), 3508–3522. https://doi.org/10.1002/lno.11895

References From the Supporting Information

Bâki Iz, H. (2018). Is the global sea surface temperature rise accelerating? *Geodesy and Geodynamics*, *9*(6), 432–438. https://doi.org/10.1016/j.geog.2018.04.002
Bulgin, C. E., Merchant, C. J., & Ferreira, D. (2020). Tendencies, variability and persistence of sea surface temperature anomalies. *Scientific Reports*, *10*(1), 7986. https://doi.org/10.1038/s41598-020-64785-9
Carton, J. A., & Giese, B. S. (2008). A reanalysis of ocean climate using Simple Ocean Data Assimilation (SODA). *Monthly Weather Review*, *136*(8), 2999–3017. https://doi.org/10.1175/2007MWR1978.1
Cheng, L., Abraham, J., Hausfather, Z., & Trenberth, K. E. (2019). How fast are the oceans warming? *Science*, *363*(6423), 128–129. https://doi.org/10.1126/science.aav7619
Cox, P. M., Betts, R. A., Jones, C. D., Spall, S. A., & Totterdell, I. J. (2000). Acceleration of global warming due to carbon-cycle feedbacks in a coupled climate model. *Nature*, *408*(6809), 184–187. https://doi.org/10.1038/35041539
Deser, C., Phillips, A. S., & Alexander, M. A. (2010). Twentieth century tropical sea surface temperature trends revisited. *Geophysical Research Letters*, *37*(10), L10701. https://doi.org/10.1029/2010GL043321
Durack, P. J., Wijffels, S. E., & Matear, R. J. (2012). Ocean salinities reveal strong global water cycle intensification during 1950 to 2000. *Science*, *336*(6080), 455–458. https://doi.org/10.1126/science.1212222

Gentemann, C. L., Fewings, M. R., & García-Reyes, M. (2017). Satellite sea surface temperatures along the west coast of the United States during the 2014–2016 northeast Pacific marine heat wave. *Geophysical Research Letters*, *44*(1), 312–319. https://doi.org/10.1002/2016GL071039

Jo, A. R., Lee, J.-Y., Timmermann, A., Jin, F.-F., Yamaguchi, R., & Gallego, A. (2022). Future amplification of sea surface temperature seasonality due to enhanced ocean stratification. *Geophysical Research Letters*, *49*(9), e2022GL098607. https://doi.org/10.1029/2022GL098607

Ju, W.-S., Long, S.-M., Xie, S.-P., Wang, G., & Du, Y. (2020). Changes in the North Pacific subtropical gyre under 1.5°C low warming scenario. *Climate Dynamics*, *55*(11), 3117–3131. https://doi.org/10.1007/s00382-020-05436-7

Kawakami, Y., Kitamura, Y., Nakano, T., & Sugimoto, S. (2020). Long-term thermohaline variations in the North Pacific Subtropical Gyre from a repeat hydrographic section along 165°E. *Journal of Geophysical Research: Oceans*, *125*(1), e2019JC015382. https://doi.org/10.1029/2019JC015382

Kim, J., Kim, G., Cho, H.-M., Nam, S., Hwang, J., Park, S., et al. (2022). Decline in the nutrient inventories of the upper subtropical northwest Pacific Ocean. *Geophysical Research Letters*, *49*(9), e2021GL093968. https://doi.org/10.1029/2021GL093968

Koven, C. D., Ringeval, B., Friedlingstein, P., Ciais, P., Cadule, P., Khvorostyanov, D., et al. (2011). Permafrost carbon-climate feedbacks accelerate global warming. *Proceedings of the National Academy of Sciences of the United States of America*, *108*(36), 14769–14774. https://doi.org/10.1073/pnas.1103910108

Li, G., Cheng, L., Zhu, J., Trenberth, K. E., Mann, M. E., & Abraham, J. P. (2020). Increasing ocean stratification over the past half-century. *Nature Climate Change*, *10*(12), 1116–1123. https://doi.org/10.1038/s41558-020-00918-2

Medhaug, I., Stolpe, M. B., Fischer, E. M., & Knutti, R. (2017). Reconciling controversies about the 'global warming hiatus'. *Nature*, *545*(7652), 41–47. https://doi.org/10.1038/nature22315

Melzer, B. A., & Subrahmanyam, B. (2015). Investigating decadal changes in sea surface salinity in oceanic subtropical gyres. *Geophysical Research Letters*, *42*(18), 7631–7638. https://doi.org/10.1002/2015GL065636

Meng, S., Gong, X., Yu, Y., Yao, X., Gong, X., Lu, K., et al. (2021). Strengthened ocean-desert process in the North Pacific over the past two decades. *Environmental Research Letters*, *16*(2), 024034. https://doi.org/10.1088/1748-9326/abd96f

Nakano, T., Kaneko, I., Soga, T., Tsujino, H., Yasuda, T., Ishizaki, H., & Kamachi, M. (2007). Mid-depth freshening in the North Pacific subtropical gyre observed along the JMA repeat and WOCE hydrographic sections. *Geophysical Research Letters*, *34*(23), L23608. https://doi.org/10.1029/2007GL031433

Nishikawa, H., Nishikawa, S., Ishizaki, H., Wakamatsu, T., & Ishikawa, Y. (2020). Detection of the Oyashio and Kuroshio fronts under the projected climate change in the 21st century. *Progress in Earth and Planetary Science*, *7*(1), 29. https://doi.org/10.1186/s40645-020-00342-2

Oka, E., Katsura, S., Inoue, H., Kojima, A., Kitamoto, M., Nakano, T., & Suga, T. (2017). Long-term change and variation of salinity in the western North Pacific Subtropical Gyre revealed by 50-year long observations along 137°E. *Journal of Oceanography*, *73*(4), 479–490. https://doi.org/10.1007/s10872-017-0416-2

Peng, Q., Xie, S.-P., Wang, D., Huang, R. X., Chen, G., Shu, Y., et al. (2022). Surface warming induced global acceleration of upper ocean currents. *Science Advances*, *8*(16), eabj8394. https://doi.org/10.1126/sciadv.abj8394

Sallée, J.-B., Pellichero, V., Akhoudas, C., Pauthenet, E., Vignes, L., Schmidtko, S., et al. (2021). Summertime increases in upper-ocean stratification and mixed-layer depth. *Nature*, *591*(7851), 592–598. https://doi.org/10.1038/s41586-021-03303-x

Skliris, N., Marsh, R., Josey, S. A., Good, S. A., Liu, C., & Allan, R. P. (2014). Salinity changes in the World Ocean since 1950 in relation to changing surface freshwater fluxes. *Climate Dynamics*, *43*(3), 709–736. https://doi.org/10.1007/s00382-014-2131-7

Sugimoto, S. (2022). Decreasing wintertime mixed-layer depth in the northwestern North Pacific Subtropical gyre. *Geophysical Research Letters*, *49*(2), e2021GL095091. https://doi.org/10.1029/2021GL095091

Sugimoto, S., Hanawa, K., Watanabe, T., Suga, T., & Xie, S.-P. (2017). Enhanced warming of the subtropical mode water in the North Pacific and North Atlantic. *Nature Climate Change*, *7*(9), 656–658. https://doi.org/10.1038/nclimate3371

Wang, G., Xie, S.-P., Huang, R. X., & Chen, C. (2015). Robust warming pattern of global subtropical oceans and its mechanism. *Journal of Climate*, *28*(21), 8574–8584. https://doi.org/10.1175/JCLI-D-14-00809.1

Wu, B., Lin, X., & Yu, L. (2021). Poleward shift of the Kuroshio Extension front and its impact on the North Pacific subtropical mode water in the recent decades. *Journal of Physical Oceanography*, *51*(2), 457–474. https://doi.org/10.1175/JPO-D-20-0088.1

Wu, L., Cai, W., Zhang, L., Nakamura, H., Timmermann, A., Joyce, T., et al. (2012). Enhanced warming over the global subtropical western boundary currents. *Nature Climate Change*, *2*(3), 161–166. https://doi.org/10.1038/nclimate1353

Xu, L., Wang, K., & Wu, B. (2022). Weakening and poleward shifting of the North Pacific subtropical fronts from 1980 to 2018. *Journal of Physical Oceanography*, *52*(3), 399–417. https://doi.org/10.1175/JPO-D-21-0170.1

Yang, H., Lohmann, G., Krebs-Kanzow, U., Ionita, M., Shi, X., Sidorenko, D., et al. (2020). Poleward shift of the major ocean gyres detected in a warming climate. *Geophysical Research Letters*, *47*(5), e2019GL085868. https://doi.org/10.1029/2019GL085868

Yang, H., Lohmann, G., Wei, W., Dima, M., Ionita, M., & Liu, J. (2016). Intensification and poleward shift of subtropical western boundary currents in a warming climate. *Journal of Geophysical Research: Oceans*, *121*(7), 4928–4945. https://doi.org/10.1002/2015JC011513

Zhang, X., Church, J. A., Platten, S. M., & Monselesan, D. (2014). Projection of subtropical gyre circulation and associated sea level changes in the Pacific based on CMIP3 climate models. *Climate Dynamics*, *43*(1), 131–144. https://doi.org/10.1007/s00382-013-1902-x

Erratum

In the originally published version of this article, in the author contribution section, contributions of each author as "lead," "equal," or "supporting" has been updated. This may be considered the authoritative version of record.